Negative frequency effects in nonlinear optics

Submitted for the degree of Doctor of Philosophy (PhD) in Physics
by

Cristian Redondo Lourés

Institute of Photonics and Quantum Sciences,
School of Engineering and Physical Sciences,
Heriot-Watt University

October 2016

Abstract

In this thesis we analyse the impact of the new terms that appear in the nonlinear polarisation of the equations relevant to nonlinear $\chi^{(3)}$ optical materials when the slowly varying envelope approximation (SVEA) is not applied. These new terms introduce new nonlinear interactions between the positive and negative frequency parts of the spectrum of an optical pulse, giving rise to novel nonlinear phenomena that were not present in the usual models based in SVEA, like the ubiquitous nonlinear Schrödinger equation (NLSE). The analysis carried out in this thesis is theoretical, with both numerical simulations and analytical results presented. These results predict new frequency generation processes that can have a considerable impact in ultrashort pulse propagation and supercontinuum generation. We also discuss the experimental need for this extended model, as well as some possible signatures of these novel frequency generation processes in recent experiments.

Acknowledgements

The first person I should name in this acknowledgements section is obviously my supervisor, Fabio Biancalana. It was thanks to his guidance that this thesis could be completed in the first place. I owe much of this work to his support and his encouraging me to keep working through difficult times when I was stuck trying to solve some apparently impossible problems; many of those problems transformed into interesting, worthy results once solved.

I would also like to acknowledge the contributions of many other people who, even if not in such a direct way as Fabio, were important in the completion of this job. One of those people was Daniele Faccio, who constantly advised us of any recent experimental developments, and was our go-to person when we wanted to discuss the feasibility and realisability of our simulated results; I have to mention Thomas Roger as well, as he was responsible for an experimental analysis that supports some of the results of this thesis; Andrea Armaroli wrote a code to solve numerically the *Unidirectional Pulse Propagation Equation* (UPPE) that has been extremely useful for me during these years; and Philippe Grelu, with whom I spent a great week in France studying the interesting system that are fibre lasers.

Finally, I would like to thank some people who helped me outside my research work. I will start with LB, who generously proofread my first manuscript and corrected its many mistakes. And I want to close these acknowledgements saying thanks to my family for their help and support through all these years of education of which my working in this thesis was a wonderful culmination.

ACADEMIC REGISTRY

Research Thesis Submission

Name*:*			
School:			
Version: *(i.e. First, Resubmission, Final)*		Degree Sought:	

Declaration

In accordance with the appropriate regulations I hereby submit my thesis and I declare that:

1) the thesis embodies the results of my own work and has been composed by myself
2) where appropriate, I have made acknowledgement of the work of others and have made reference to work carried out in collaboration with other persons
3) the thesis is the correct version of the thesis for submission and is the same version as any electronic versions submitted*.
4) my thesis for the award referred to, deposited in the Heriot-Watt University Library, should be made available for loan or photocopying and be available via the Institutional Repository, subject to such conditions as the Librarian may require
5) I understand that as a student of the University I am required to abide by the Regulations of the University and to conform to its discipline.
6) I confirm that the thesis has been verified against plagiarism via an approved plagiarism detection application e.g. Turnitin.

* *Please note that it is the responsibility of the candidate to ensure that the correct version of the thesis is submitted.*

Signature of Candidate*:*		Date:	

Submission

Submitted By *(name in capitals):*	
Signature of Individual Submitting:	
Date Submitted:	

For Completion in the Student Service Centre (SSC)

Received in the SSC by *(name in capitals):*			
Method of Submission *(Handed in to SSC; posted through internal/external mail):*			
*E-thesis Submitted (**mandatory for final theses)***			
Signature:		Date:	

Please note this form should be bound into the submitted thesis.

List of publications

The research conducted while working on this thesis has led to the publication, or submission, of the following research papers:

Cristian Redondo Loures, Andrea Armaroli, and Fabio Biancalana, "Contribution of third-harmonic and negative-frequency polarization fields to self-phase modulation in nonlinear media", Opt. Lett. **40**, 613 (2015).

Cristian Redondo Loures, Daniele Faccio, and Fabio Biancalana, "Nonlinear cavity and frequency comb radiations induced by negative frequency field effects", Physical Review Letters **115**, 193904 (2015).

Cristian Redondo Loures, Thomas Roger, Daniele Faccio, and Fabio Biancalana, "Super-resonant radiation stimulated by higher harmonics", *submitted*.

Cristian Redondo Loures and Fabio Biancalana, "Consequences of the interaction between positive and negative frequency fields beyond the slowly varying envelope approximation", review paper to be submitted.

Contents

1 Introduction

In this introduction the basic concepts that are necessary for this thesis will be introduced, trying to explain the origin of the relevant equations and physical magnitudes that this work deals with from first principles. Special care is taken in explaining why the work conducted in this thesis is already relevant in the field of ultrashort pulse propagation and might be even more so in the future. At the end of it an outline of the rest of the thesis is presented.

All electromagnetic phenomena can be traced back to Maxwell's equations [1, 2]. In modern notation and using the International System of Units they take a form that is more than well known in the literature [3–5]:

$$\nabla \times \mathbf{E} = -\partial_t \mathbf{B}, \tag{1.1}$$

$$\nabla \times \mathbf{H} = \mathbf{J} + \partial_t \mathbf{D}, \tag{1.2}$$

$$\nabla \cdot \mathbf{D} = \rho_f, \tag{1.3}$$

$$\nabla \cdot \mathbf{B} = 0. \tag{1.4}$$

In these equations, $\mathbf{E}$ and $\mathbf{B}$ are the electric and magnetic field, $\mathbf{D}$ and $\mathbf{H}$ two auxiliary fields (displacement and magnetizing field respectively) that are relevant for fields in media different from the vacuum, $\mathbf{J}$ is the electric current density, and ρ_f is the free electric charge. Assuming a non-magnetic medium, we only need the relation between $\mathbf{E}$ and $\mathbf{D}$ to be able to solve these equations. By definition $\mathbf{D} = \epsilon_0 \mathbf{E} + \mathbf{P}$, where $\mathbf{P}$ is the polarisation induced by the electric field in a medium and ϵ_0 the vacuum permittivity. Therefore, if we have a relation between $\mathbf{E}$ and $\mathbf{P}$ the problem of electromagnetic waves in a medium would be formulated.

Since the vector polarisation $\mathbf{P}$ is induced by a vector electric field $\mathbf{E}$ we can

perform an expansion in a power series of the form

$$\mathbf{P} = \epsilon_0 \left(\chi^{(1)} \cdot \mathbf{E} + \chi^{(2)} \colon \mathbf{EE} + \chi^{(3)} \vdots \mathbf{EEE} + \dots \right), \tag{1.5}$$

where the $\chi^{(i)}$ are in general i-th order tensors with elements that depend on time and the dots represent convolution.

Although the mathematical formulation would be now complete, it is usually impractical to work with the full Maxwell equations, and some approximations are made to reduce them to a simpler form that still manages to precisely reproduce the physics of a system of interest. In particular, for centrosymmetric materials $\chi^{(2)}$ always vanishes, and for the range of intensities of experimental relevance an expansion to orders higher than $\chi^{(3)}$ is not needed. Other further simplifications would include assuming the material is homogeneous (i.e., the value of $\chi^{(i)}$ does not change with the position inside the material), isotropic (the system is rotationally symmetric, which makes $\chi^{(3)}$ a scalar), the nonlinear response instantaneous (which means ignoring the photon-phonon interaction or *Raman effect* [6, 7]), and the polarisation maintained with propagation. With all of these approximations the problem is greatly simplified.

The equation that describes the propagation of optical pulses in an optical $\chi^{(3)}$ material like the one described above has been found to be the famous *nonlinear Schrödinger equation* (NLSE) (see [3] and references therein). If we write our dimensionless electric field, E_d, as $E_d = \mathcal{E} + \mathcal{E}^* = A(\xi, \tau) \exp(-i\mu\tau) + cc$ ($\mu = \omega_0 t_0$ is the dimensionless frequency) then the NLSE for the envelope A of the field reads (in adimensional units):

$$i\partial_\xi A - \frac{1}{2} s \partial_\tau^2 A + |A|^2 A = 0, \tag{1.6}$$

where $\xi = L/L_D$ is the dimensionless space variable, with $L_D = t_0^2/|\beta_2|$ the dispersion length; $\tau = t/t_0$ the scaled time, with t_0 the width of a fundamental soliton of the system; $\beta_2 = \partial_\omega^2 \beta(\omega)|_{\omega_0}$ is the group velocity dispersion ($\beta(\omega)$ is the full dispersion relation and ω_0 the central frequency of the pulse); and s is the sign of the group velocity dispersion of the material at ω_0, $s = 1$ for normal dispersion and $s = -1$ for anomalous dispersion.

The equation describes the changes in the temporal profile of a pulse as it propagates through a nonlinear material. The second term is related to the linear chromatic dispersion, which is here expanded in a Taylor series up to second order, and the last term is the Kerr nonlinearity that modifies the phase of intense pulses. This non-

linearity is the cause of, for example, the spectral broadening of short pulses or the formation of solitons in optical fibres [8, 9]. This formation of optical solitons is one of the most important nonlinear phenomena in optics [9–11], and it is only possible because the Kerr nonlinearity compensates for the chromatic dispersion so that the phase of the pulse is independent of time. Nonlinear terms coming from a $\chi^{(3)}$ coefficient in the expansion of the polarisation (1.5) mediate processes known as *four wave mixing* (FWM), for reasons that will become evident in the next chapter. A general soliton solution of the NLSE will have a $N\text{sech}\,(N\tau)$ profile, where N is a free parameter.

Apart from the ones described above, several other approximations are needed to derive the NLSE from Maxwell's equations. Some of these approximations are completely justified and accurately capture the nature of many experimental setups, for example, the assumption that the propagation inside a material is unidirectional, or that backward waves are negligible compared with forward propagating waves. When we pump a material with a laser source, these two conditions will be satisfied to a very good degree. One key approximation in the reduction of Maxwell equations to the NLSE equation is the so-called *slowly varying envelope approximation* (SVEA), which assumes that the problem has two well separated timescales: one dictated by the frequency of the optical pulse, that will typically be of the order of femtoseconds ($\omega_0 \approx 10^{15}$ Hz for optical pulses), and the other by the temporal width t_0 of the pulse itself, which will be the scale in which changes to the shape of the envelope of the electric field will typically occur. Under this approximation, which can be mathematically expressed as $\Delta\omega \ll \omega_0$, where $\Delta\omega$ is the spectral width of the pulse (proportional to t_0^{-1}), the nonlinear polarisation term of Maxwell equations can be heavily simplified by retaining only the terms with a phase of $\exp(-i\mu\tau)$ (the phase of $\mathcal{E}$). With this we are ignoring terms with phases like $\exp(i\mu\tau)$ or $\exp(-3i\mu\tau)$, which will be justified as long as they oscillate fast enough that their effects will cancel during propagation. The NLSE and some of its most straightforward extensions (for example, generalising the dispersion to include higher orders of its power series expansion), even with the SVEA limitation, have been successfully used to explain and predict many nonlinear phenomena in optical materials [9–15].

However, when the parameter μ is small ($t_0 \approx 1/\omega_0$, the two time scales become similar) the SVEA is not justified any more, and the descriptions based on it might not be able to capture the full physics of the system. We are in a regime in which

the width of the pulse is comparable to the period of the oscillations of the electric field, i.e., the pulse is almost single cycle. In this situation the very definition of an envelope of the electric field becomes problematic.

Recent experimental developments have seen the appearance of new power sources and nonlinear materials, and in parallel to these, new refined theoretical models have arisen [16–25]. In particular, the one described in [25], based on the envelope of the analytic signal of the field, does not rely on SVEA but still retains the shape of an "NLSE-like" equation, meaning that it is easily solved numerically and that it is analytically tractable. For completeness, we will explain the basics of this new model in this introduction following [21–25].

A real function $f(t)$ has a Fourier spectrum that satisfies $\mathcal{F}[f(t)] = F(\omega) = F(-\omega)^*$. Therefore, we can rebuild the original function $f(t)$ if we know the value of its Fourier transform for positive values of the variable ω. Due to this property, our real electric field E is fully characterised by its *analytic signal*. The analytic signal is defined as the field with the same spectrum as the original field for positive ω and 0 for negative ω. Mathematically, $\mathcal{E} = \pi^{-1}\int_0^\infty \mathcal{F}[E]\exp(-i\omega t)d\omega$, the analytic signal is derived by means of the inverse Fourier transform when only the positive frequency part of the spectrum is taken into account. By the property explained above, it is easy to see that the complex conjugate of the analytic signal would be a field in which the positive frequency part has been eliminated, and that therefore contains only negative frequencies. Thanks to the linearity of Fourier transforms, the sum $(\mathcal{E} + \mathcal{E}^*)/2$ will give a field with the same spectrum as the original, since the only-positive-frequency spectrum of $\mathcal{E}$ and the only-negative-frequency spectrum of $\mathcal{E}^*$ will add up to rebuild E_ω, the spectrum of the original electric field.

In terms of $\mathcal{E}$, the product E^3 in the nonlinear polarisation reads $\mathcal{E}^3 + |\mathcal{E}|^2\mathcal{E} + |\mathcal{E}|^2\mathcal{E}^* + (\mathcal{E}^*)^3$. Applying the SVEA to these nonlinear polarisation terms would mean retaining only the second term, which is the one with the same phase as $\mathcal{E}$. By retaining all of them at this stage we can derive a more complete equation that does not rely on this approximation. As is customary, we will not work with the field $\mathcal{E}$ but with its envelope A, defined as

$$A = \mathcal{E}\exp(i\omega_0 t - i\beta_0 z), \tag{1.7}$$

where $\beta_0 = \beta(\omega_0)$ is the linear momentum at the central frequency. Reference [25] shows that with these elements the equation (in dimensionless units) for A takes the

form

$$i\partial_\xi A + \hat{D}(i\partial_\tau)A + \hat{S}(i\partial_\tau)\Big[|A|^2 A + |A|^2 A^* \exp(2i\mu\tau + 2i\kappa\xi) + \frac{1}{3}A^3 \exp(-2i\mu\tau - 2i\kappa\xi)\Big]_+ = 0, \quad (1.8)$$

where ξ, τ are dimensionless space-time variables in the co-moving frame, $\hat{D} \equiv \sum_{m=2}^{\infty} b_m (i\partial_\tau)^m/m!$ the dispersion operator ($b_m = \beta_m/(|\beta_2|t_0^{m-2})$ are the normalised dispersion coefficients), $\hat{S}$ the shock operator, $\kappa = (\beta_1\omega_0 - \beta_0)L_D$ measures the difference between group and phase velocity in the medium, and μ and L_D are as defined above. Note that there is an extra operation, $[]_+$, acting on the nonlinear terms. By definition, and since it is derived from an analytic signal, the spectrum of A cannot have any detunings below μ (which would mean negative frequencies in $\mathcal{E}$). This operation is a filtering operation that kills any spurious contribution to A at detunings from the central frequency smaller than $-\mu$ that might come from the nonlinear mixing between A and A^*, since the latter comes from $\mathcal{E}^*$, which only has negative frequencies. This operation also eliminates the term proportional to $(A^*)^3$ from the equation: the only contribution to this term comes from $\mathcal{E}^*$, which will only affect the negative frequency part that we are eliminating from A, and can thus be ignored. In time domain, $[]_+$ is implemented by making use of the Hilbert transform, $[F(\xi,\tau)]_+ = F(\xi,\tau) - i\mathcal{H}[F(\xi,\tau)]$, with $\mathcal{H}[F(\xi,\tau)] = \pi^{-1}\mathcal{P}\int_{-\infty}^{\infty} d\tau' F(\xi,\tau')/(\tau - \tau')$, and $\mathcal{P}$ means that we are taking the principal value of the integral.

At first sight, this equation resembles a generalised nonlinear Schrödinger equation [26], but, unlike in the usual extension of the NLSE, here there are extra nonlinear coupling terms. Apart from the well-known Kerr nonlinearity, we have the third harmonic generation term (THG) [27], which arises naturally in this formulation, and a completely new term, that has been called *negative Kerr term* due to its resemblance with the Kerr nonlinearity if we substitute the positive frequency field A by the negative frequency one A^*. The appearance of new nonlinear terms in the equation means that there are new couplings between the fields $\mathcal{E}$ and $\mathcal{E}^*$ that cannot be neglected in the limit in which SVEA is not applicable. This means that the propagation in a $\chi^{(3)}$ material will be affected by non-trivial interactions between the positive ($\mathcal{E}$) and negative ($\mathcal{E}^*$) frequency parts of the spectrum of the electric field E. The model based on Equation (1.8) is thus able to explain and predict new physical processes that cannot be found with the more simple models based in SVEA, in which some of these interactions between positive and negative frequency fields are

neglected.

The introduction of this model was mainly motivated by the experiments reported in [28], in which pulses propagating in nonlinear media emitted a new kind of resonant radiation that could not be explained by the usual phase matching conditions derived from the NLSE, see [12–15]. The authors of [28] hint that this radiation could be coming from new interactions between the positive and negative frequency parts of the spectrum (hence its name, *negative resonant radiation* or NRR), and heuristically derive its phase matching condition. The first success of the model based on Equation (1.8) was being able to produce that phase matching condition analytically and explain it as coming from the negative Kerr term [25]. It also predicted the emission of a third type of resonant radiation, the *third harmonic resonant radiation* (THRR), which has probably been recently observed experimentally, as reported in [29] and explained in a later chapter.

The fact that the model could explain the existence of NRR and its position and make the completely new prediction of the existence of THRR was a motivation to further explore the new phenomena that the interactions between positive and negative frequencies that were not present in the NLSE could produce. This thesis presents the results obtained during the last three years of that research.

Before closing the introduction it is worth noting that Equation (1.8) is, in essence, equivalent to a Unidirectional Pulse Propagation Equation (UPPE, [20]) in terms of physical meaning. As we already mentioned, our equation, having a formal similarity to the NLSE, is faster to simulate and easier to treat analytically than this UPPE, which is in essence a forward Maxwell equation for the full electric field. We will however come back to this UPPE in Chapter 3, when analysing how the SPM spectral broadening changes due to the new negative frequency effects.

The structure of the thesis is as follows: Chapter 2 will analyse the model and all of its features with special emphasis on the physical meaning of the two new nonlinear terms. Chapter 3 will show how some nonlinear phenomena that were present in previous models based on SVEA are modified when the full nonlinear polarisation is taken into account. Chapter 4 will be devoted to resonant radiation, since the study of this frequency conversion process in the new framework produced enough interesting new results to deserve a separate chapter. Finally, the conclusions of the work done so far and the possibilities of further research to be done in this topic will

be studied.

2 Characterisation of the model

We will explain in this chapter some of the most important mathematical features of the model based on Equation (1.8).

We can see that, when only second order dispersion is taken into account, and if the nonlinear dispersion is ignored (the shock term $\hat{S}(i\partial_\tau)$ is set to 1), the equation will resemble the NLSE (1.6) with the addition of two new nonlinear terms. In their seminal paper, Conforti *et al* already proved that energy is conserved when both terms are included in the equation, regardless of the filtering operation, but that they do not conserve energy separately [25]. This shows that a deeper relationship exists between the NK and THG terms of Equation (1.8), and since this relationship involves conservation of energy, using a Hamiltonian formalism should be the easiest way to interpret it. An approach to ultrashort pulse propagation equations as a Hamiltonian problem can be found in [30]. Following the ideas of that paper, we want to find a way to write Equation (1.8) as

$$i\partial_\xi \mathcal{E}_\omega + \frac{\delta H}{\delta \mathcal{E}^*_\omega} = 0, \tag{2.1}$$

for some Hamiltonian H, and with $\mathcal{E}_\omega$ the spectral components of the analytic signal $\mathcal{E}$ defined in the introduction. We work in the frequency domain since the dispersion in this case is more easily tractable, being applied by a real dispersion operator $\beta(\omega)$ acting on $\mathcal{E}$, unlike the differential operator we had in frequency domain. Treating the dispersion in the frequency space and then transforming back to time domain is a common procedure that is also used in the derivation of the NLSE, see [3].

In the next two sections we will present the Hamiltonian from which (1.8) is derived, and will also study the equation that small perturbations around the NLSE soliton solution obey. This equation can be written as an eigenvalue problem, see [31], and an analysis of the eigenvalues and eigenfunctions of the problem will show us which first order frequency conversion processes the NK and THG terms mediate.

This will give us a deeper understanding of the meaning of the new nonlinear terms introduced in Equation (1.8).

2.1 Hamiltonian of the equation

If we write the following Hamiltonian

$$H = \beta(\omega)|\mathcal{E}_\omega|^2 + \frac{1}{2}\sum_{\omega_1+\omega_2=\omega_3+\omega_4} \mathcal{E}_{\omega_1}\mathcal{E}_{\omega_2}\mathcal{E}^*_{\omega_3}\mathcal{E}^*_{\omega_4} + \frac{1}{3}\sum_{\omega_1+\omega_2+\omega_3=\omega_4} \mathcal{E}_{\omega_1}\mathcal{E}_{\omega_2}\mathcal{E}_{\omega_3}\mathcal{E}^*_{\omega_4} + \frac{1}{3}\sum_{\omega_1=\omega_2+\omega_3+\omega_4} \mathcal{E}_{\omega_1}\mathcal{E}^*_{\omega_2}\mathcal{E}^*_{\omega_3}\mathcal{E}^*_{\omega_4}, \quad (2.2)$$

we can trivially derive (1.8) applying (2.1), and then doing the inverse Fourier transform. Note that we would get the equation in the $\mathcal{E}$ variable defined in the introduction, and we would need to transform to A using (1.7). $\beta(\omega)$ is the dispersion relation in frequency space, which will become the operator $\hat{D}$ of (1.8) through the inverse Fourier transform if $\beta(\omega)$ is expanded in a Fourier series around β_0. We know that a Hamiltonian ought to be hermitian for energy to be conserved. That is the case of (2.2) only when the last two terms are either both present or absent, but not when we only have one of them. Having both terms absent would mean that the equation of motion derived from (2.2) would be the usual NLSE (which is known to conserve energy), whereas including both terms means including both the NK and THG terms in the equation to recover (1.8). This fact is consistent with the energy conservation found in [25] mentioned before.

Once the equation has been written as a Hamiltonian one, the interpretation of nonlinear terms, like the NK and THG in our case, is straightforward. Although the derivation of (1.8) and (2.2) is completely classical in nature, we can have the second quantization procedure in mind to understand what the given Hamiltonian means. As it can be seen in the quantum physics and quantum field theory literature ([32] gives a comprehensive approach to the subject), nonlinear terms that combine the positive and negative frequency parts of the spectrum of the field (like the ones found in the Hamiltonian (2.2)) are related to the creation and destruction of particles of the theory, with $\mathcal{E}_\omega$ being related to the annihilation of a photon with frequency ω and $\mathcal{E}^*_\omega$ with the creation of the same photon. Therefore, the first nonlinear term (which gives rise to the usual Kerr term) destroys two photons and creates two others, the second term (that gives the THG term) creates a single particle from the destruction of three, and the last one (giving the NK term) creates three particles from a single

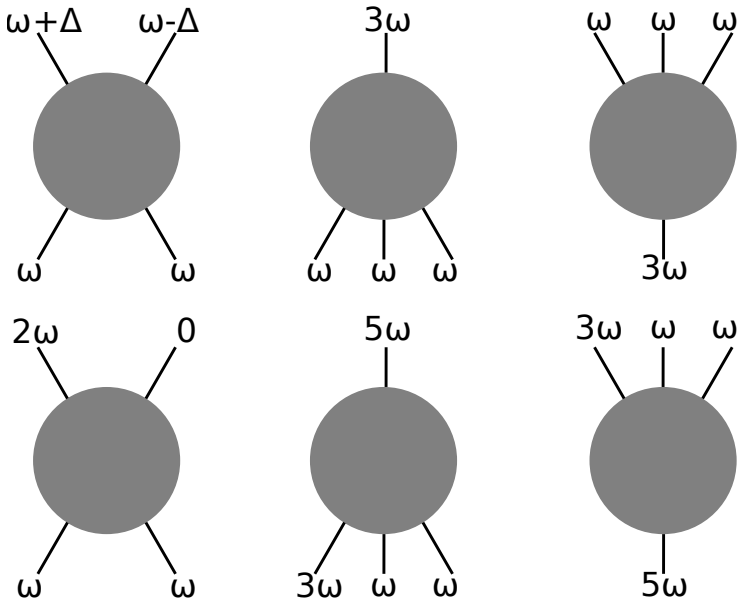

Figure 2.1: Processes mediated by the nonlinear terms of (2.2). Left column: processes mediated by the Kerr term (which already appeared in the NLSE), namely the modulation instability sideband creation (when the momentum conservation allows it) and the TFISH. Middle column: higher odd-harmonic creation due to four wave mixing. These processes are mediated by the third harmonic generation term and in principle would create all odd harmonics of the pump due to cascaded four wave mixing. Right column: " inverse third harmonic" processes mediated by the negative Kerr term. These correspond to the transfer of energy from the higher modes back to the lower ones and is a new feature of the model (1.8).

one. The convolution given by the sum over frequencies in each term can be seen to give the right frequency conservation condition.

The types of processes that these terms allow can be seen in Figure 2.1. The Kerr term conserves the number of photons, and obviously gives rise to phenomena that were already present in the NLSE, namely the modulation instability (responsible of soliton creation) and the TFISH [33] processes. The THG term is responsible for $3 \to 1$ processes, which will create through cascaded FWM all odd harmonics of a pulse propagating in the $\chi^{(3)}$ material. Lastly, the NK term will allow $1 \to 3$ processes, which will break photons of higher harmonics back into a lower one and two photons of the pump. In this sense, the NK term can be interpreted as sort of an "inverse third harmonic" term that tries to send back to the pump the energy that was previously transferred to higher harmonics, which further confirms the physical

connection between the two. We will see this in more detail in the next section.

This Hamiltonian approach also shows that killing off the term $(A^*)^3$ due to the filtering operation in (1.8) is physically sound: for our Hamiltonian to produce that term in the equation of motion we would need to include a term proportional to $(A^*)^4$ (and its Hermitian conjugate A^4) in (2.2), which would have no physical meaning whatsoever, since they would correspond to the creation/annihilation of four particles out of the vacuum state.

Although interesting and physically coherent, the results of this section are heuristic in nature. Our aim now is to take a more mathematical approach to the problem of new frequency generation in a system governed by Equation (1.8), trying to show that the new nonlinear processes due to negative frequency effects shown in Figure 2.1 are indeed present in the theory. The next section will deal with this problem using perturbation theory.

2.2 Frequency conversion: A first order perturbative treatment

We have already presented the two new terms of the nonlinear polarisation in our model and have heuristically explained their meaning in the previous section. In this section a more formal approach to new frequency generation due to the NK and THG terms will be presented. To this end we will do the following: the first step is to write a linearised equation for the small perturbations around a solution of Equation (1.8). We will then write this as an eigenvalue problem for a certain operator L. Analysing that eigenvalue problem will tell us which new frequencies are excited by the pulse. A similar derivation can be found in [31] to study the stability of extensions of the NLSE with nonlinear terms of the form $F(|A|^2)A$, where $F(|A|^2)$ is a generic function of $|A|^2$. This is an elegant way to derive the Vakhitov-Kolokolov stability criterion [34]. Note however that in our case the new nonlinear terms are not of the form $F(|A|^2)A$, and therefore we need to modify this derivation. In fact, the formal procedure of finding the unstable frequencies by studying the eigenvalues of the operator L is not an approach that can be easily applied here, since L will have an explicit spatio-temporal dependence due to the exponentials in the NK and THG terms. We therefore take a more subtle route to the solution: decomposing the operator L in two parts, one associated with the NLSE equation (which we will call L_0) and another one with the NK and THG terms (L_I), which will be treated

as a perturbation. We will then proceed to compute the matrix elements of the perturbation operator L_I between the relevant eigenfunctions of the unperturbed operator L_0 to find which frequencies are excited by the two new nonlinear terms.

The first step is assuming that we know a solution $A = A_0 \exp(i\phi_0)$ of the usual NLSE (1.6) and analyse how small, arbitrary perturbations around this solution evolve due to the presence of the extra terms in (1.8). To this end we write a field $A = (A_0 + u)\exp(i\phi)$, where u is much smaller than A_0. For convenience we rewrite the NLSE as

$$i\partial_\xi A + \frac{1}{2}N^2\partial_\tau^2 A + N^2|A|^2A = 0, \tag{2.3}$$

since for the equation written this way the most general soliton solution is $A = \text{sech}\,(\tau)\exp\left(i\frac{N^2}{2}\xi\right)$. Adding the NK and THG terms the equation would become

$$i\partial_\xi A + N^2\partial_\tau^2 A + N^2\Bigg(|A|^2A + |A|^2A^*\exp(2i\mu\tau + 2i\kappa\xi) + \frac{1}{3}A^3\exp(-2i\mu\tau - 2i\kappa\xi)\Bigg) = 0, \tag{2.4}$$

where we have dropped the filtering operation to simplify the notation. If we now add the small perturbation u to the unperturbed solution, so that our field reads $A = (\text{sech}\,(\tau) + u(\xi,\tau))\exp\left(i\frac{1}{2}N^2\xi\right)$, we can introduce it in (2.4) and linearise in the small perturbation u:

$$i\partial_\xi u - \frac{1}{2}N^2u + \frac{1}{2}N^2u_{\tau\tau} + 2N^2\text{sech}\,(\tau)^2\,u + N^2\text{sech}\,(\tau)^2\,u^* + N^2\text{sech}\,(\tau)^2\,(2u^* + u)\exp(2i\phi) + N^2\text{sech}\,(\tau)^2\,u\exp(-2i\phi) = 0, \tag{2.5}$$

where we defined a phase ϕ as $\phi = \mu\tau + (\kappa - N^2/2)\xi$.

Our next step will be decomposing the perturbation u so that the dependence on the space variable ξ is explicitly separated from the τ dependence. We have that $u = f(\tau)\exp(i\lambda\xi) + g^*(\tau)\exp(-i\lambda^*\xi)$ leads to

$$\begin{aligned}-\lambda f\exp(i\lambda\xi) + \lambda^* g^*\exp(-i\lambda^*\xi) + {}& \\ \frac{1}{2}N^2(\partial_\tau^2 - 1)\,(f\exp(i\lambda\xi) + g^*\exp(-i\lambda^*\xi)) + {}& \\ 2N^2\text{sech}\,(\tau)^2\,(f\exp(i\lambda\xi) + g^*\exp(-i\lambda^*\xi)) + {}& \\ N^2\text{sech}\,(\tau)^2\,(f^*\exp(-i\lambda^*\xi) + g\exp(i\lambda\xi)) + {}& \\ \exp(2i\phi)\text{sech}\,(\tau)^2\,((f+2g)\exp(i\lambda\xi) + (g^* + 2f^*)\exp(-i\lambda^*\xi)) + {}& \\ \exp(-2i\phi)\text{sech}\,(\tau)^2\,(f\exp(i\lambda\xi + g^*\exp(-i\lambda^*\xi))) = 0 & \end{aligned} \tag{2.6}$$

This equation can be separated in two simultaneous equations that must be satisfied independently by taking the coefficients accompanying the two exponentials $\exp(i\lambda\xi)$ and $\exp(-i\lambda\xi)$. These equations are

$$-\lambda f - \frac{1}{2}N^2 f + \frac{1}{2}N^2\partial_\tau^2 f + 2N^2\text{sech}\,(\tau)^2 f + N^2\text{sech}\,(\tau)^2 g + \exp(2i\phi)N^2\text{sech}\,(\tau)^2 (f+2g) + \exp(-2i\phi)N^2\text{sech}\,(\tau)^2 f = 0, \quad (2.7)$$

$$\lambda g - \frac{1}{2}N^2 g + \frac{1}{2}N^2\partial_\tau^2 g + 2N^2\text{sech}\,(\tau)^2 g + N^2\text{sech}\,(\tau)^2 f \exp(-2i\phi)N^2\text{sech}\,(\tau)^2 (g+2f) + \exp(2i\phi)N^2\text{sech}\,(\tau)^2 g = 0. \quad (2.8)$$

The last step is changing the variables from f and g to two other variables v and w through the relations $f = v + w$ and $g = v - w$ (or conversely, $f + g = 2v$ and $f - g = 2w$). Adding equations (2.7) and (2.8) we would get

$$-\lambda(f-g) - \frac{1}{2}N^2(f+g) + \frac{1}{2}N^2\partial_\tau^2(f+g) + 3N^2\text{sech}\,(\tau)^2 (f+g) \exp(2i\phi)N^2\text{sech}\,(\tau)^2 (f+3g) + \exp(-2i\phi)N^2\text{sech}\,(\tau)^2 (g+3f) = 0, \quad (2.9)$$

while subtracting (2.8) from (2.7) yields

$$-\lambda(f+g) - \frac{1}{2}N^2(f-g) + \frac{1}{2}N^2\partial_\tau^2(f-g) + N^2\text{sech}\,(\tau)^2 (f-g) \exp(2i\phi)N^2\text{sech}\left(\tau^2\right) (f+g) - \exp(-2i\phi)N^2\text{sech}\,(\tau)^2 (f+g) = 0. \quad (2.10)$$

And applying the change of variables proposed before, taking into account that $f + 3g = 2(f+g) - (f-g)$ and $3f + g = 2(f+g) + (f-g)$, we get to our final coupled equations

$$-2\lambda w - N^2 v + N^2\partial_\tau^2 v + 6N^2\text{sech}\,(\tau)^2 v + 4vN^2\text{sech}\,(\tau)^2 (\exp(2i\phi) + \exp(-2i\phi)) - 2wN^2\text{sech}\,(\tau)^2 (\exp(2i\phi) - \exp(2i\phi)) = 0, \quad (2.11)$$

$$-2\lambda v - N^2 w + N^2\partial_\tau^2 w + 2N^2\text{sech}\,(\tau)^2 w + 2vN^2\text{sech}\,(\tau)^2 (\exp(2i\phi) - \exp(-2i\phi)) = 0. \quad (2.12)$$

Although complicated when written in this form, it is easy to see that the previous equations can be cast in the desired form of an eigenvalue problem for the column vector with components v and w,

$$L_0 \begin{pmatrix} v \\ w \end{pmatrix} + L_I \begin{pmatrix} v \\ w \end{pmatrix} - \Omega \begin{pmatrix} v \\ w \end{pmatrix} = 0, \tag{2.13}$$

where

$$L_0 = \begin{pmatrix} 0 & \partial_\tau^2 - 1 + 2\mathrm{sech}\,(\tau)^2 \\ \partial_\tau^2 - 1 + 6\mathrm{sech}\,(\tau)^2 & 0 \end{pmatrix}, \tag{2.14}$$

$$L_I = \begin{pmatrix} 2\mathrm{sech}\,(\tau)^2 \left(e^{2i\phi} - e^{-2i\phi}\right) & 0 \\ 4\mathrm{sech}\,(\tau)^2 \left(e^{2i\phi} + e^{-2i\phi}\right) & -2\mathrm{sech}\,(\tau)^2 \left(e^{2i\phi} - e^{-2i\phi}\right) \end{pmatrix}, \tag{2.15}$$

$$\Omega = \frac{2\lambda}{N^2}. \tag{2.16}$$

If $L_I = 0$ the problem (2.13) is known to allow only real eigenvalues [35], which means that all solutions of the form $A = \mathrm{sech}\,(\tau) \exp\left(i\frac{N^2}{2}\xi\right)$ are stable for any value of N (i.e., no perturbations will grow since Ω is always real and the amplitude of the perturbation u does not change with ξ). This result is just the well-known stability of the NLSE soliton solutions. In particular, these real eigenvalues are two degenerate discrete eigenvalues $\Omega = 0$ and a continuous spectrum for $|\Omega| > 1$, with two branches for both possible signs of Ω. From [31] and [36] we can write the normalised eigenfunctions for both the discrete and the continuous states. For the discrete states we have:

$$|\Psi_1\rangle = \frac{1}{\sqrt{2}} \begin{pmatrix} 0 \\ \mathrm{sech}\,(\tau) \end{pmatrix} = \begin{pmatrix} 0 \\ \psi_1 \end{pmatrix}, \tag{2.17}$$

$$|\Psi_2\rangle = \frac{1}{\sqrt{2}} \begin{pmatrix} \partial_\tau(\mathrm{sech}\,(\tau)) \\ 0 \end{pmatrix} = \begin{pmatrix} \psi_2 \\ 0 \end{pmatrix}. \tag{2.18}$$

And for the continuum:

$$\langle Z_{1,k}| = \exp(ik\tau) \left(\tfrac{1}{2} - \tfrac{ike^{-\tau}}{(k+i)^2}\mathrm{sech}\,(\tau)\,, \quad \tfrac{1}{2} - \tfrac{ike^{-\tau}}{(k+i)^2}\mathrm{sech}\,(\tau) + \tfrac{\mathrm{sech}(\tau)^2}{(k+i)^2} \right) = (\zeta_{1,k}, \zeta_{2,k}), \tag{2.19}$$

$$\langle Z_{2,k}| = \exp(ik\tau)\left(-\tfrac{1}{2} + \tfrac{ike^{-\tau}}{(k+i)^2}\mathrm{sech}\,(\tau)\,,\quad \tfrac{1}{2} - \tfrac{ike^{-\tau}}{(k+i)^2}\mathrm{sech}\,(\tau) + \tfrac{\mathrm{sech}(\tau)^2}{(k+i)^2}\right) = (-\zeta_{1,k}, \zeta_{2,k}), \quad (2.20)$$

where we have defined a parameter $k = \sqrt{\pm\Omega - 1}$, with the negative sign inside of the square root for $\langle Z_{1,k}|$ (negative eigenvalue Ω branch) and the positive sign for $\langle Z_{2,k}|$ (positive eigenvalue Ω branch), which is a frequency for the small perturbation mode associated with the eigenvalue Ω (and physically means detuning from the pump, which is the mode at zero frequency of (2.3)). Note that, for a given value of Ω, two values of k that only differ in their sign are allowed. We can see that both discrete states are heavily localised in the time variable τ, while the continuum ones are not. It can also be easily proved that all these modes are orthonormal.

Now we have the following picture: a soliton, being a collective state, will be formed by many individual photons. Each of the photons travelling inside a NLSE-like soliton will see a potential created by all other photons in the pulse that traps it in one of the discrete states of the unperturbed operator (or a linear combination of both). Small continuous waves propagating around the soliton, on the other hand, will be described by the continuous eigenstates of L_0. Since these eigenstates describing individual photons are orthogonal, any matrix element of the form $\langle Z_{i,k}|L_0|\Psi_j\rangle$ will be zero, which means a photon inside the pulse cannot be emitted to the continuum, hence the stability of the solitons of Equation (1.6). However, we have proven that our extended equation (1.8) produces an additional perturbation L_I which will allow some photons to escape from the pulse to the continuum. We would expect the rate of emission to be proportional to the square amplitude of the matrix elements $\langle Z_{i,k}|L_I|\Psi_j\rangle \neq 0$ [37–39]. Calculating these matrix elements and checking for which frequencies they have a non-zero value will tell us which new frequencies the NK and THG terms create in a first order approximation.

We expect the photons to leave the soliton in pairs, one to a state with $\Omega < 0$ and another one to a state $\Omega > 0$, so that the total eigenvalue is conserved (remember $\Omega = 0$ in the discrete states). Therefore we are interested in the matrix elements in which the final state will be $\langle Z_{1,k} + Z_{2,k}|$ or $\langle Z_{1,k} - Z_{2,k}|$, which we will label $\langle +, k|$ and $\langle -, k|$ respectively. We can see that $\langle +, k| = (0, 2\zeta_{2,k})$ and $\langle -, k| = (2\zeta_{1,k}, 0)$.

Naming the four components of the interaction operator (2.15) as

$$L_I = \begin{pmatrix} A_1 & 0 \\ A_2 & A_3 \end{pmatrix}, \tag{2.21}$$

the matrix elements take the following values:

$$\langle +, k|L_I|\Psi_1\rangle = 2\int d\tau A_2\psi_1\zeta_{2,k} \equiv m_1, \tag{2.22}$$

$$\langle +, k|L_I|\Psi_2\rangle = 2\int d\tau A_3\psi_2\zeta_{2,k} \equiv m_2, \tag{2.23}$$

$$\langle -, k|L_I|\Psi_1\rangle = 2\int d\tau A_1\psi_1\zeta_{1,k} \equiv m_3, \tag{2.24}$$

$$\langle -, k|L_I|\Psi_2\rangle = 0. \tag{2.25}$$

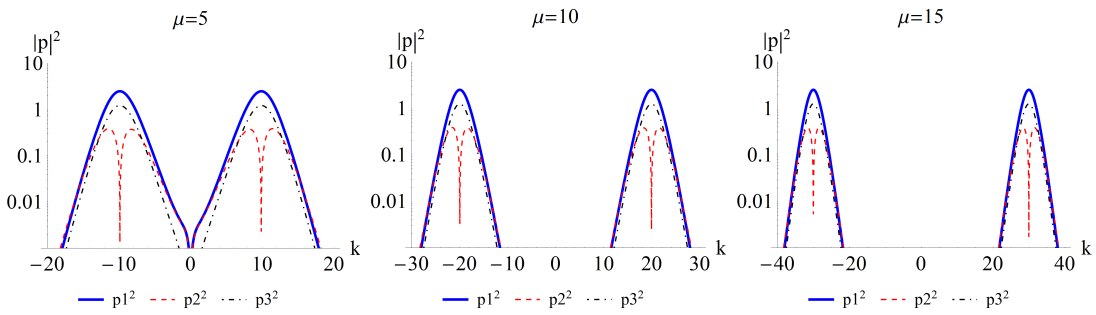

Figure 2.2: Plot of the square of the absolute value of the matrix element for a dimensionless frequency of the pulse of $\mu = 5$ (left), $\mu = 10$ (centre) and $\mu = 15$ (right). The three lines correspond to the first (Equation (2.22), solid blue), second (Equation (2.23),dashed red), and third (Equation (2.24), dot-dashed black) matrix elements.

The matrix elements include a ξ dependence through the phase ϕ of the elements of the interaction terms A_i. However, this dependence is a phase that will not affect the value of their modulus square, and therefore the rate of transition of photons to the continuum. These matrix elements can be written analytically, but the expressions are extremely cumbersome and their physical meaning completely obscure, so we just give them as the integrals (2.22-2.25). Instead of writing that analytical form, we will define a magnitude $p_i = |m_i|^2$, the square of the absolute value of the matrix elements, and plot it against k. This way we can see the detuning with respect to the pump of the continuum modes that will be excited by the NK and THG perturbation. These plots can be seen in Figure 2.2 for three values of the frequency of the pump μ.

As we see, when a soliton of the NLSE is propagated using Equation (1.8) all three non-vanishing matrix elements will make part of its energy escape to continuous modes. These modes are detuned by twice the frequency of the pump with respect to it, and appear at both sides of the spectrum. This means that the frequency of the photons leaving the pump would be 3μ and $-\mu$. It is here that we have to take into account the filtering operation in (1.8) that kills all the modes with negative frequency. A mode will obviously have negative frequency if it is redshifted by an amount superior to μ with respect to the soliton. For this reason, the red detuned peak we see in Figure 2.2 is not physical, and only appears in our calculations because we dropped the filtering operation in (2.4). Therefore, the soliton will only transfer energy to its third harmonic wave, in a process like the one in the top middle diagram of Figure 2.1.

The first order perturbative approach ends here. However, although a full mathematical derivation is not available, we can discuss some of the features we would expect to find at higher orders of perturbation. The fact that two peaks are created at each side of the pump with a detuning of 2μ is due to the fact that the elements A_i of the perturbation operator L_I have a time dependence of the form $a\exp(2i\mu\tau) + b\exp(-2i\mu\tau)$. Higher order transition probabilities will be mediated by products of the A_i elements, which will have exponentials with a time dependence of up to $\exp((2n)i\mu\tau)$ for an n-th order transition. This corresponds to a total frequency of $(2n+1)\mu$, i.e., all odd harmonics are created in a cascade due to higher order processes. This kind of cascaded, four-wave mixing mediated, higher harmonic creation is due to processes like the one in the bottom middle diagram in Figure 2.1.

It is also when we consider higher order processes that the exponentials with a phase $\exp(-2i\mu\tau)$ come into play. Once the spectrum has frequencies of 3μ or higher, processes that decrease the frequency by 2μ no longer produce states with negative frequency and are therefore allowed in our model. These processes are, for example, the two pictures shown in the left column of Figure 2.1. Photons of the higher harmonic waves that were previously created during propagation split in two photons of the pump and a photon of the immediately inferior odd harmonic. These processes, that act as a sort of anti third harmonic that gives energy back to lower frequency modes, are a new feature of this model.

The successful explanation of the generation of new frequencies in Equation (1.8) thanks to our matrix element approach allows for the possibility of exploring fre-

quency generation in a novel way. In principle, if we can write the problem of small perturbations around a stable solution of any equation as an eigenvalue problem similar to (2.13), we could analyse the effect of any general perturbation on the system by choosing the perturbation operator L_I appropriately.

Summing up, in this chapter we have presented the mathematical features of our model for the nonlinear propagation of light. We have written a Hamiltonian from which we can derive the equation including all negative frequency effects, and analysed the first order frequency generation processes in perturbation theory. In the next chapter we will start analysing how common nonlinear phenomena change due to the presence of the NK and THG terms in Equation (1.8).

3 Modification of nonlinear phenomena

In this chapter we will start the analysis of nonlinear phenomena arising from negative frequency effects induced by the NK and THG terms of Equation (1.8). We will do an exhaustive analysis of two of the main nonlinear phenomena that appear in the NLSE: the *self-phase modulation* (SPM) broadening of the spectrum and the soliton self frequency shift due to the Raman scattering.

3.1 Self-phase modulation (SPM) spectral broadening

Self-phase modulation (SPM) is responsible for many important effects in nonlinear optics. Due to the cubic term in the polarisation, any pulse will gain a phase during propagation proportional to its own intensity. This extra nonlinear phase will obviously be negligible for small intensities, but it is responsible for most nonlinear phenomena when intense light propagates in a nonlinear material. One of the main consequences of this nonlinear phase is a spectral broadening of intense pulses when the nonlinearity dominates over the chromatic dispersion [8, 40–42].

This section will start with a review of this SPM-induced broadening in the NLSE, with a full explanation of the mathematical tools needed to study the new frequencies generated. We will extend this formalism afterwards to include the effects of the NK and THG terms, so that we can see how this broadening is modified by the inclusion of these new nonlinear interactions. This work can be found in [43].

3.1.1 SPM in the NLSE

In the usual NLSE (1.6) the SPM creates lobes in the spectrum with a detuning with respect to the central pump frequency increasing linearly with propagation. The formation of this lobes is very well understood theoretically, and it is due only to the Kerr term of the equation [3, 8, 41].

To develop a mathematical theory of SPM broadening in the NLSE the first step is to ignore the chromatic dispersion $\beta(\omega)$ assuming it is linear, which means $s = 0$. This can only be done if the nonlinear length $L_{NL} = (\gamma P)^{-1}$ (P the power of the pulse) is much smaller than the dispersion length $L_D = t_0^2/|\beta_2|$, meaning that nonlinear effects will take place before dispersion has had time to play any role in the pulse evolution. In this case, and when the shock operator does not play a relevant role in the propagation, the NLSE is vastly simplified, since it becomes an ordinary differential equation

$$\partial_\xi A = i|A|^2 A. \tag{3.1}$$

Equation (3.1) can be solved straight away by writing the complex field A as a modulus and a (nonlinear) phase, $A = V(\xi, \tau)\exp(i\phi_{NL}(\xi, \tau))$. The equation then reads

$$\partial_\xi V + iV\partial_\xi \phi_{NL} = iV^3. \tag{3.2}$$

Separating this into real and imaginary part yields

$$\partial_\xi V = 0, \tag{3.3}$$

$$\partial_\xi \phi_{NL} = V^2. \tag{3.4}$$

The first equation shows that the shape of the envelope will not change with propagation, $V = V(\tau)$, and that the only effect of the nonlinearity will be the appearance of a nonlinear phase $\phi_{NL}(\tau, \xi) = V^2(\tau)\xi$. As this phase evolves according to the temporal profile of the pulse $V(\tau)$ it will have a time dependence which will be the origin of the spectral broadening. Knowing the (constant) shape of the input pulse $V(\tau)$ means that we can calculate explicitly the functional form of $\phi_{NL}(\xi, \tau)$.

A phase like the one coming from (3.4), i.e., a phase with a temporal dependence means that there are instantaneous frequencies across the pulse that differ from the central frequency ω_0 [3]. The way to calculate the detuning between these frequencies and ω_0, which we will call $\Delta\omega$, is computing the derivative

$$\Delta\omega = -\partial_\tau \phi_{NL} = -\xi\partial_\tau V^2. \tag{3.5}$$

Two results come immediately from this equation: first of all, the maximum detuning grows linearly with the propagation distance ξ; and secondly, the spectral broadening can change dramatically with the shape of the pulse $V(\tau)^2$, since it depends on its derivative.

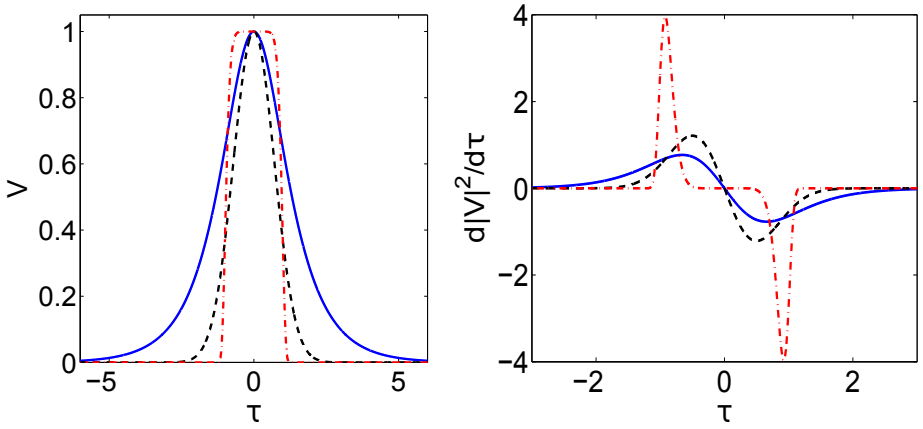

Figure 3.1: Shape V of the pulses and derivatives of their square amplitude $|V|^2$ for a sech (τ) pulse (solid blue), $\exp(-\tau^2)$ (Gaussian, dashed black) pulse and $\exp(-\tau^{10})$ (m=5 Supergaussian, dot-dashed red) pulse. We see that both the Gaussian and the sech (τ) pulses have similar derivatives, and therefore we expect a similar SPM broadening. However, a qualitatively different behaviour should be found in the Supergaussian pulse due to its completely different derivative.

Nothing else can be said about the spectral broadening without assuming a pulse shape. For completeness, Figure 3.1 shows how the derivate of V^2 for sech (τ), $\exp(-\tau^2)$ (Gaussian), and $\exp(-\tau^{10})$ (m=5 Supergaussian) pulses, and Figure 3.2 the final spectra of those same pulses after a propagation of $\xi = 25$ (top row), as well as a plot of the ξ evolution of the spectrum (bottom row). Note that, since we are ignoring the dispersion, $L_D = \infty$ and the distance has to be normalised using the nonlinear length defined above, $\xi = L/L_{NL}$. These spectra are computed by applying the Fourier transform to the field $A(\xi, \tau)$ calculated analytically for different values of ξ.

What the figures show is in perfect agreement with the interpretation given above. Since the derivative of the Supergaussian pulse is only nonzero in a narrow region around the edges of the pulse, new frequencies are only generated in a short window of τ values, meaning that a big fraction of the energy of the pulse stays at the pump frequency, therefore a peak can be seen in the middle of the spectrum. However, the slope of the edges of a Supergaussian pulse is much bigger than those of a sech (τ) or Gaussian pulse, so new frequencies are created further detuned for this type of pulse. On the other hand, the derivatives of the sech (τ) and Gaussian pulse are nonzero in a

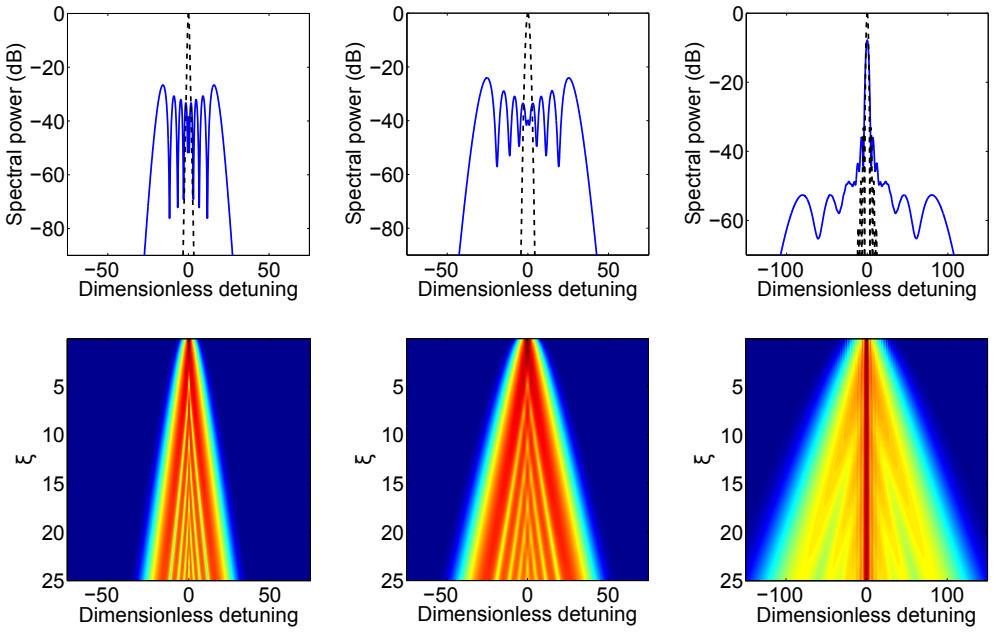

Figure 3.2: Final spectra (top) and SPM broadening evolution (bottom) for different pulses and a propagation of $\xi = 25$. Left column: sech (τ) pulse. Middle column: Gaussian pulse. Right column: m=5 Supergaussian pulse. The initial spectrum (black dashed line) is included for comparison. We see the clear differences between the first two cases and the Supergaussian pulse, as explained in the text. Note the different scale in the axes for this last case.

wider τ region, so the generation of new frequencies happens all over the pulse. This is the reason why the sidebands generated have bigger amplitude for these pulses, but since the maximum value of the derivatives is smaller than for a Supergaussian, the furthest detuned new frequency is closer to the central pump frequency. No central peak above the oscillating pattern can be seen for these pulses. From now on, we will restrict ourselves to the analysis of SPM for Gaussian pulses, since they experience a bigger broadening than sech (τ) pulses for the same propagation, allowing us to see SPM effects with less time-consuming dynamical simulations, while Supergaussian pulses do not have such an efficient energy transfer to the SPM lobes. The maximum detuning of the SPM lobes for a Gaussian pulse, which can be found by calculating the maximum and minimum value of the time derivative of the nonlinear phase it produces, is known to be [44]:

$$\Delta\omega_{max}(\xi) = \pm\frac{2}{\sqrt{e}}V_0^2\xi. \tag{3.6}$$

Note that a factor of $\sqrt{2}$ has to be included with respect to the literature because we

chose a profile $\exp(-\tau^2)$ rather than the most usual $\exp(-\tau^2/2)$, due to the broadening happening faster precisely by that factor with our choice. It is important to note that it is this choice of the specific pulse parameters that causes the Gaussian pulse to broaden faster than the $\operatorname{sech}(\tau)$ pulse, and not the nature of the pulse profiles themselves.

This process of spectral broadening can be understood in terms of the processes seen in Chapter 2 as the annihilation of two photons at the pump frequency and the creation of two new ones symmetrically detuned from the central frequency [45]. In that same paper, though, the authors show experimental results in which the lobes are not completely symmetric due to third- and higher-order dispersion (see also [3]).

We expect the negative frequency effects mediated by the NK and THG nonlinear terms to modify the way these lobes appear in the spectrum. We will explore this in the next two sections, and close with a realistic analysis of some nonlinear materials to see how the asymmetry related to the dispersion affects these new sidebands.

3.1.2 Coupled SPM equations of the new model

The starting point of the discussion of SPM broadening in the new model will be an equation equivalent to 3.1 when the negative frequency terms are taken into account. This equation reads

$$\partial_\xi A = i\left(|A|^2 A + |A|^2 A^* \exp(2i(\kappa\xi + \mu\tau)) + \frac{1}{3}A^3 \exp(-2i(\kappa\xi + \mu\tau))\right). \tag{3.7}$$

From here, we can again decompose the field in amplitude and phase and find two equations equivalent to (3.3) and (3.4). These equations are, defining $\phi = \kappa\xi + \mu\tau$

$$\partial_\xi V = \frac{1}{3}(\alpha_{THG} - 3\alpha_{NK})V^3 \sin[2(\phi - \phi_{NL})], \tag{3.8}$$

$$\partial_\xi \phi_{NL} = V^2\left\{1 + \left(\alpha_{NK} + \frac{1}{3}\alpha_{THG}\right)\cos[2(\phi - \phi_{NL})]\right\}, \tag{3.9}$$

where α_{NK} and α_{THG} are 0 or 1 depending on whether we take into account the NK and THG terms in Equation (3.7). We wrote our equations using these parameters to show the separate contribution of each of the new terms to SPM broadening, but, as we proved in the previous section, our model needs $\alpha_{THG} = \alpha_{NK}$ for our model to come from an hermitian Hamiltonian. Since setting both to 0 reduces our equations to the ones for the SVEA case, in the following we will always assume that both α_{NK} and α_{THG} take a value of 1.

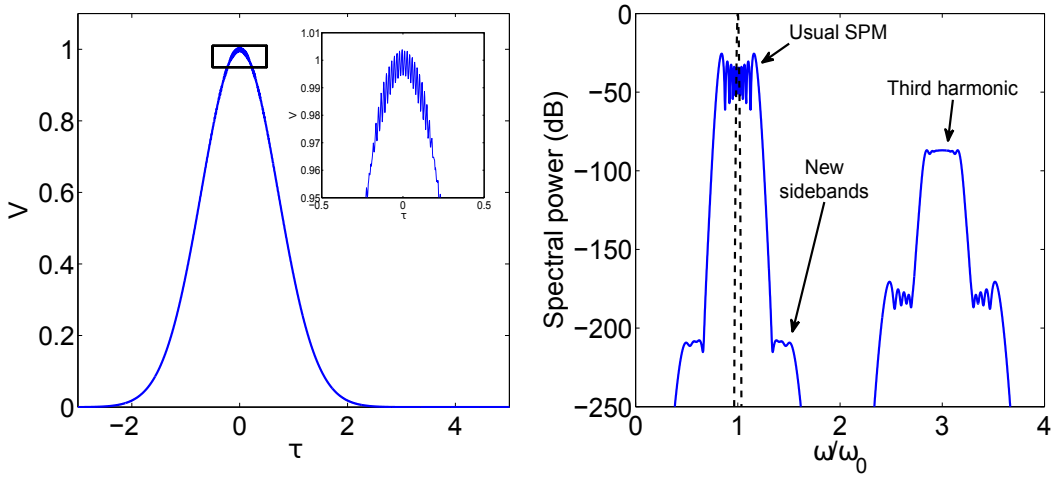

Figure 3.3: Temporal profile (left) and spectrum (right) of a Gaussian pulse after a propagation of $\xi = 30$ for a value of the parameters $\kappa = 100$ and $\mu = 200$. We can see that the temporal profile is not constant and that small oscillations appear atop the pulse (inset), although the modification is small. However, the combination of these small oscillations of the pulse profile and the different evolution of the phase generate a very different spectrum after propagation, with new sidebands appearing at the sides of the pump and the presence of the odd harmonics generated by cascaded third harmonic generation.

In this case the pulse profile is not constant any more (which can be understood easily, as the THG term will create waves with a frequency three times that of the pump and this will make small oscillations appear in the temporal profile of the pulse), which means we have to solve both equations simultaneously. Unfortunately, (3.8) and (3.9) are coupled nonlinear ordinary differential equations, and to the best of the author's knowledge no analytical solution is known for a system like this. Therefore the only option we have is solving them numerically. To this end we use a 4th order Runge-Kutta method [46]. Once we have found the value of V and ϕ_{NL} for a certain propagation we can proceed as before and plot the spectrum of the full field A.

The results for a Gaussian pulse $\exp(-\tau^2)$ can be seen in Figure 3.3. We have propagated the pulse for a distance of $\xi = 30$, with $\kappa = 100$ and $\mu = 200$. Note that by giving a value to μ, which is indispensable to solve equations (3.8) and (3.9), we are fixing the product $\omega_0 t_0$, i.e, for a given value of the frequency of the input pulse we choose a certain pulse width. For example, if the input pulse had a wavelength of 1064 nm, our choice of μ means that the pulse duration would be slightly over 100

fs. In the SVEA case, and since the frequency of the pulse did not appear explicitly in Equation (3.4), we had the freedom to choose both the frequency and duration of the pulse independently if we desired to convert back to dimensional units.

The left panel of Figure 3.3 shows how the pulse profile is not perfectly constant any more, with small oscillations developing around the Gaussian profile. However, the amplitude of these oscillations is small compared with the amplitude of the full pulse (in fact they cannot be appreciated in a graph showing the full profile and we need to focus on the top of the pulse). This will motivate the constant profile approximation that we will apply in the next section. We can also see that, apart from the usual SPM sidebands that appeared when only the Kerr effect was taken into account, new frequencies are generated further detuned than before with a smaller spectral power. These new sidebands were not present in the NLSE formalism, and are a completely novel feature of the model based on Equation (1.8).

The presence of the third harmonic generation term also means that some energy is transferred to a frequency three times that of the pump. We see this as a clear second peak in the spectrum, that has also suffered SPM broadening, showing both the presence of the usual lobes and the new *plateaus* appearing when we use the full polarisation.

Although this model based on the coupled equations (3.8) and (3.9) has been useful to find how the spectral broadening changes due to the new terms of the nonlinear polarisation, no analytical results can be derived from it. Thus, we need to further simplify the system before we can treat it mathematically beyond a simple numerical analysis that, although able to find the new phenomenology, cannot give us a satisfactory explanation for it.

3.1.3 Constant temporal profile approximation and analytic results

To find a way to extract analytical results from the system (3.8)-(3.9), we can make the following approximation: we assume the temporal profile of the pulse V to be constant. As we saw in Figure 3.3, V changes with propagation as oscillations appear on top of the pulse, but the amplitude of these oscillations is small when compared with the pulse itself and its shape is not greatly modified. Therefore the approximation of V constant seems to be justified, and, as we will show later, numerical simulations of the equations show that the results we get in this case are in good agreement with

the ones we saw in the last section if we are only interested in the detuning of the sidebands.

When the approximation of V constant is made (i.e., we reduce Equation (3.8) to $\partial_\xi V = 0$) we can integrate Equation (3.9) analytically. We start by performing a change of variables $X = \mu\tau + \kappa\xi - \phi_{NL}$, so that

$$\partial_\xi X = \kappa - \partial_\xi \phi_{NL}. \tag{3.10}$$

From here, plugging (3.9) into the previous equation we have

$$\partial_\xi X = \kappa - V^2 \left[(1+\alpha)\cos(2X)\right]. \tag{3.11}$$

We have used a new quantity $\alpha = \alpha_{NK} + \alpha_{THG}/3$, so that it takes values of 0 when the new nonlinear terms are ignored and 4/3 when they are taken into account. This equation can be easily integrated using separation of variables. We have

$$\int_{\mu\tau}^{\mu\tau+\kappa\xi-\phi_{NL}} \frac{dX}{\kappa - V^2 - V^2\alpha\cos(2X)} = \int_0^\xi d\xi'. \tag{3.12}$$

The integral in the left hand side of (3.12) can be found elsewhere in the literature (see [47] for example). That result leads us to the equation

$$\frac{\arctan\left[\frac{(V^2(\alpha-1)+\kappa)\tan(\mu\tau+\kappa\xi-\phi_{NL})}{\sqrt{(V^2-\kappa)^2-(V^2\alpha)^2}}\right] - \arctan\left[\frac{(V^2(\alpha-1)+\kappa)\tan(\mu\tau)}{\sqrt{(V^2-\kappa)^2-(V^2\alpha)^2}}\right]}{\sqrt{(V^2-\kappa)^2-(V^2\alpha)^2}} = \xi, \tag{3.13}$$

from where we can solve $\phi_{NL}(\xi,\tau)$. This way we get to our final result

$$\phi_{NL}(\xi,\tau) = \mu\tau + \kappa\xi - \arctan\left\{\frac{\Gamma\,\tan\left(\Gamma\xi + \arctan\left[\frac{\rho\,\tan(\mu\tau)}{\Gamma}\right]\right)}{\rho}\right\}, \tag{3.14}$$

where $\rho = V^2(\alpha-1)+\kappa$ and $\Gamma = \sqrt{(V^2-\kappa)^2-(V^2\alpha)^2}$. Note that, to make sure that our nonlinear phase ϕ_{NL} is real, we should work in a regime in which $\kappa \gg V$, so that both Γ and ρ remain real. This is the case for most nonlinear materials at the relevant range of frequencies and intensities for realistic physical systems. This nonlinear phase (3.14) was first written in [43] in a different but equivalent way. Note that expanding ϕ_{NL} as a series in α to the first order we get

$$\phi_{NL} \approx V^2\xi - \alpha C(\xi,\tau), \tag{3.15}$$

where $C(\xi,\tau)$ is a function of the space time variables and all the constants of the problem. This means that, as convoluted as (3.14) might look, it still reduces to the

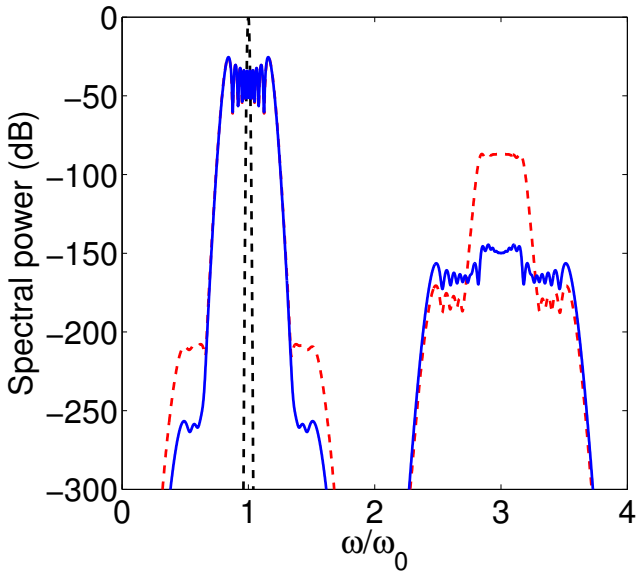

Figure 3.4: Final spectrum of a Gaussian pulse after a propagation of $\xi = 30$ with $\kappa = 100$ and $\mu = 200$. The black dashed line is the initial spectrum of the pulse, and the red dashed line the spectrum as calculated for Figure 3.3 using the coupled equation model. The blue line represents the spectrum calculated making use of the analytical solution for the nonlinear phase (3.14). We see that, despite having very different amplitudes, there is a good agreement between the two models when it comes to the maximum detuning of the sidebands.

usual expression $\phi_{NL} = V^2\xi$ for $\alpha = 0$, i.e., when neither the NK nor the THG terms are taken into account.

Now that we have an analytic expression for the nonlinear phase we can proceed as we did in the Kerr-only case: we can plot the Fourier transform of the field $A = V\exp(i\phi_{NL}(\xi,\tau))$ and see how it evolves with propagation. We will start by plotting the results for the pulse we analysed with the coupled equations (3.8)-(3.9), now calculated with the phase (3.14). We will show how these results compare with the full results obtained in the previous section, and whether or not the final spectra are similar. This will be a proof of the validity of the approximation of constant V profile.

In Figure 3.4 we see the final spectrum of a Gaussian pulse after a propagation of $\xi = 30$ with $\kappa = 100$ and $\mu = 200$, as before. For comparison, we also include here the spectrum calculated with the coupled equations (3.8)-(3.9) and shown in Figure 3.3. This is the red dashed line. The blue line is the one calculated using (3.14).

We can see that there is a rather important difference in the amplitude of the new sidebands, but the maximum detuning between the new frequencies and the pump is the same in both cases. This justifies the approximation of V constant as long as we want to analyse which frequencies are excited and we are not interested in the amount of energy transferred to these modes.

As a matter of fact, it is understandable that restricting the pulse to having a constant profile will reduce the impact of the phenomena mediated by the NK and THG terms, since the generation of new frequencies by these two terms does indeed modify the temporal profile of the pulse. In fact it is more surprising that a third harmonic still appears when the oscillations of the pulse are ignored. This means that higher harmonics are not only generated via oscillations in the temporal profile, but as an effect associated simply with the chirp of the pulse. It is also worth noting that the usual SPM lobes, due to the Kerr term and therefore created solely due to the pulse chirp, are exactly equal in both cases. This is further proof that the new *plateaus* come from the presence of nonlinear terms that are ignored when using SVEA, and therefore a model that relies on this approximation would not be able to capture the physics responsible for the generation of the new frequencies. For the remainder of this section we will focus on the study of the detuning between pump and sidebands, which means we can work with results obtained from the analytical phase without going back to the coupled equations of the previous section.

The next step would be finding the maximum value of the frequencies generated by computing the derivative of the phase (3.14), as we did in the NLSE case. However, we find a surprising result. If we try to analyse the frequencies generated this way, and as seen in Figure 3.5, the behaviour of the derivative is extremely similar to the one where only the Kerr effect was taken into account. Maximising this derivative, which is the procedure we followed to find the maximum frequency generated in the previous case, would give us approximately the same result we obtained in the SVEA case. This means that whichever is the process responsible for the creation of the new *plateaus* observed in both the numerical simulation of the coupled equations and in the analytical calculations, and also for the creation of the higher odd harmonics, it can be captured in the nonlinear phase (3.14) but not explained properly in terms of the generation of instantaneous frequencies. Albeit strange, it is not unsound that the derivatives of the nonlinear phase cannot give us a maximum value for the frequency generated. Since this phase is able to show the creation of odd harmonics

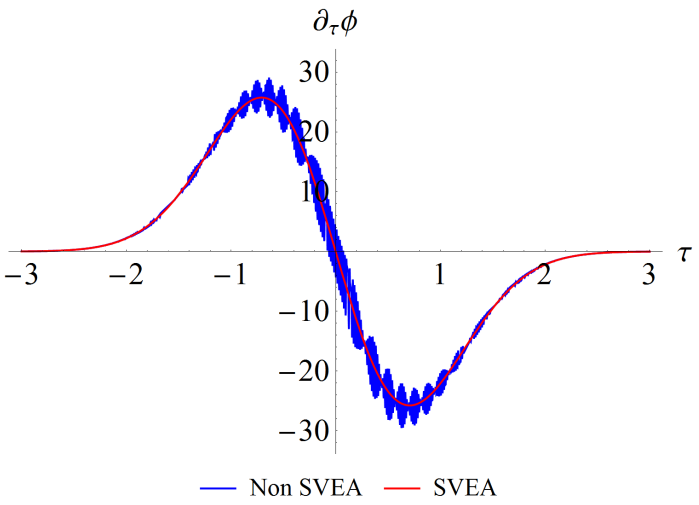

Figure 3.5: Time derivative of the full nonlinear phase for $\xi = 30$ when a Gaussian pulse is considered (blue line). In red, the same for the nonlinear phase $\phi_{NL} = V^2\xi$ of the SVEA case, shown for comparison. We see that the NK and THG terms induce some oscillations in the derivative, but no qualitative changes in its behaviour can be seen.

of the pump, there is in fact no maximum value of the frequency that can appear due to this phase, since all harmonics will be excited during propagation. It is yet another hint that the physics of processes involving the NK and THG terms needs to be studied taking into account the modification of the pulse shape if we want to extract exact analytical results.

We can nevertheless make an exhaustive numerical analysis of the detuning of the new lobes generated and compare them with the maximum detuning of the usual NLSE lobes. Since, as we saw, the maximum detuning of the new sidebands is predicted with a good accuracy by the nonlinear phase calculated in the constant profile approximation, we can quickly compute the spectra for different propagation lengths without having to use time consuming dynamical simulations. The result is shown in Figure 3.6. In this figure we plot the maximum detuning of the lobes at the top of the final spectrum of the pulse after a certain propagation (traditional lobes of the NLSE, blue dots) and the maximum detuning achieved by the extra sidebands (red dots). The blue line is the prediction for the NLSE sidebands given by (3.6). We see that the ratio between the detuning of the usual SPM lobes and the extra *plateaus* is approximately 3 (the red line is calculated as three times the expected detuning for the regular sidebands) irregardless of the parameters chosen. This has

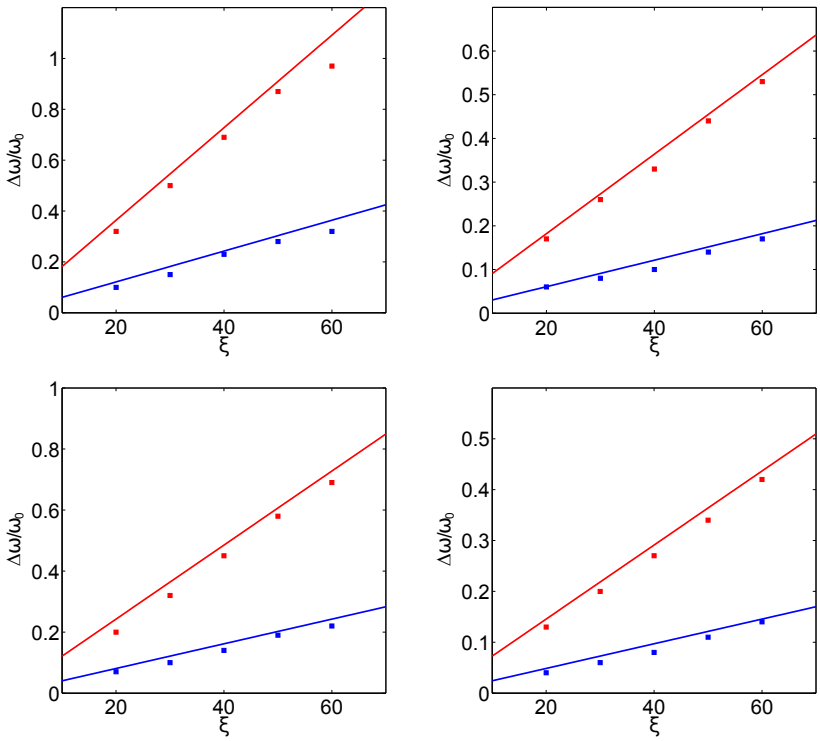

Figure 3.6: Numerically calculated maximum detuning of the sidebands created through SPM for a Gaussian pulse. The red dots represent the detuning of the new sidebands that appear beyond SVEA, while the blue dots represent the usual SPM sidebands. The lines are the predictions given by (3.6) for the traditional lobes (blue), and three times that prediction (red), which gives a good approximation of the detuning of the new *plateaus*. The parameters are: $\kappa = 100$, $\mu = 200$ (top left); $\kappa = 100$, $\mu = 400$ (top right); $\kappa = 1000$, $\mu = 300$ (bottom left); $\kappa = 300$, $\mu = 500$ (bottom right).

been justified in [43] as due to the fact that, coming from a third harmonic generation term, the new sidebands would be created by a phase three times that of the usual sidebands (the Kerr term has the phase of A whereas the THG term has the phase of A^3), therefore there is a ratio of 3 between the two detunings. Although heuristical in nature and derived from the numerics, this derivation of a formula for the detuning of the new sidebands seems to work perfectly for a wide range of parameters, as can be seen in Figure 3.6.

A more detailed analysis of the agreement between this formula for the detuning of the new *plateaus* and the numerical results can be seen in Figure 3.7. It shows the spectra of a Gaussian pulse after different propagation lengths, as well as a contour

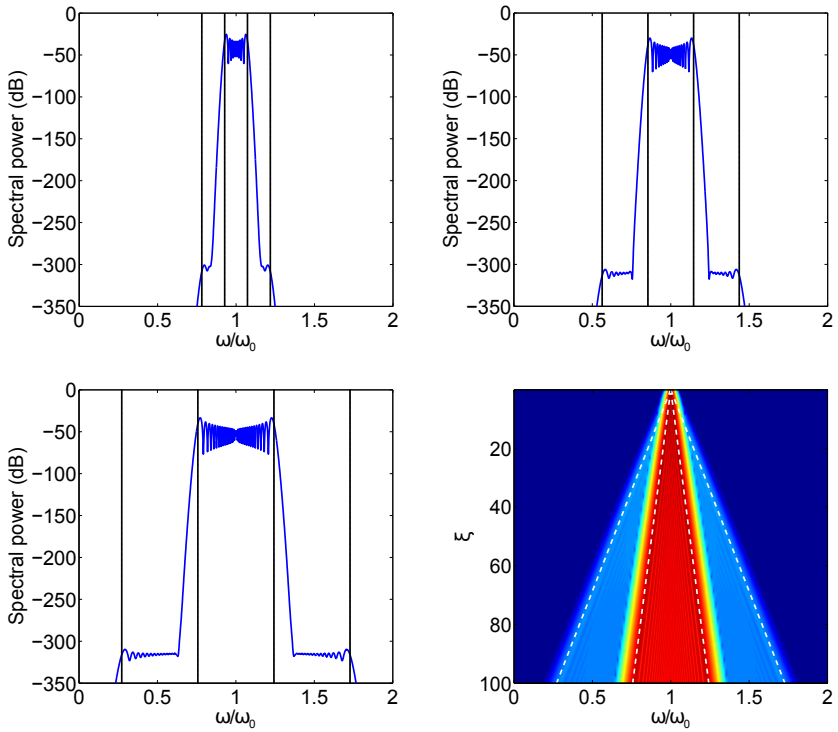

Figure 3.7: Evolution of the detuning of the lobes with propagation for a Gaussian pulse when $\mu = 500$, $\kappa = 300$. The first three panels show the spectrum after a propagation of $\xi = 30$ (top left), $\xi = 60$ (top right), and $\xi = 100$ (bottom left). The black lines are the predicted maximum detunings of the traditional and the new sidebands. The bottom right panel shows a contour plot of the evolution of the spectrum during a propagation of $\xi = 100$. Apart from a broadening of the central peak similar to the one shown for the Gaussian pulse in Figure 3.2, we see the formation of the two extra sidebands. The white dashed lines mark the theoretical prediction for the detunings. We find a very good agreement between theory and numerics.

plot of its evolution. For each spectrum the prediction for the maximum detuning of both the previously known and new SPM lobes is marked by vertical black lines. In the contour plot, the white dashed lines show how the prediction of the maximum detuning for each type of sideband matches perfectly the results of the numerical model for the whole propagation distance. It is therefore confirmed that the new sidebands are generated with a detuning of up to three times that of the ones present in the NLSE.

Until now we have used a very simple model which completely ignored chromatic dispersion and all other effects to treat this SPM broadening. In the next section we

will explore numerically the consequences of both linear and nonlinear dispersion in the formation of the SPM sidebands, since in general these effects cannot be ignored in experimentally realistic scenarios.

3.1.4 Comparison with more complex models

The first step will be introducing the chromatic dispersion $\beta(\omega)$. We know that the consequence of a second order dispersion, be it normal or anomalous, is reducing the rate of SPM broadening without significantly altering the qualitative shape of the spectrum [45, 48–51]. Therefore we will assume that we are working near the zero dispersion wavelength of the system and consider that only a third order dispersion parameter b_3 will affect the propagation of our pulse. As for the nonlinear dispersion, it is introduced by the shock term. Usually the approximation $\hat{S}(i\partial_\tau) = (i + i\partial_\tau/\mu)$ is enough to reproduce the behaviour of a system in which self steepening is important. We will use that form of $\hat{S}$ in our simulations.

When effects other than nonlinearity are taken into account, a system of ordinary equations equivalent to (3.8) and (3.9) cannot be found. We have to solve the full Equation (1.8) instead using the split step Fourier method as described in Appendix B.

The results are shown in Figure 3.8. In this figure, we show the result of solving (1.8) for a Gaussian pulse that propagates for a distance of $\xi = 10$ with $\mu = 300$ and $\kappa = 100$. In the top left panel the simulation is done without including any higher order effects. This is completely equivalent to solving the coupled equations (3.8)-(3.9). The two vertical dotted lines show the theoretical predictions for the maximum detuning due to the usual SPM and the new broadening, and as we can see, both mark with good accuracy the position of some feature that is starting to develop in the pulse. If we continued propagating for a longer distance we would find results similar to the ones in Figure 3.3.

In the top right panel we see what happens when the shock term is considered. The shock term is related to a self steepening in the pulse, which would make the edge of the soliton sharper, and therefore increase the maximum detuning achieved through SPM. It is well known that this term creates a blueshift on the pulse [52]. The blueshift is not too obvious in the "normal" sidebands for our short propagation but is extremely visible in the new *plateaus*, which are much further detuned than

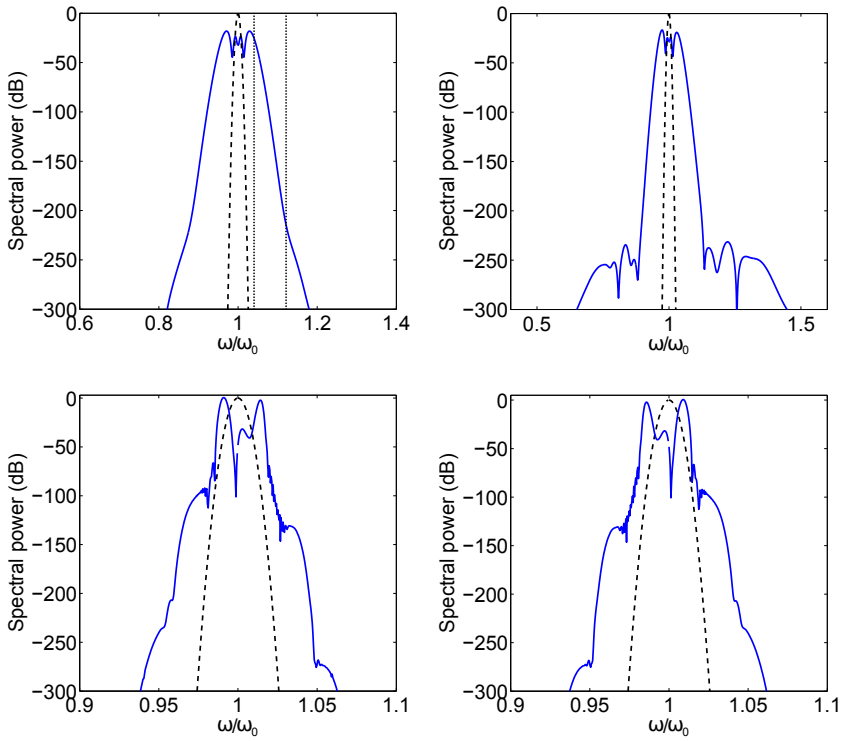

Figure 3.8: Final spectra of a Gaussian pulse after a propagation of $\xi = 10$ using Equation (1.8) when all higher order effects are ignored (top left), the shock term is considered (top right), there is a positive third order dispersion $b_3 = 0.1$ (bottom left), and there is a negative third order dispersion $b_3 = -0.1$. The initial spectra are also shown in all cases. In the top left figure the theoretical predictions for the sidebands are marked by the vertical dotted lines. Note the different scale of the x axis for each figure.

in the previous case after the same propagation. This means that the new SPM broadening described here is heavily enhanced by the shock term, which in principle would be beneficial for any experimental search of this phenomenon that might be conducted in the future.

In the two bottom panels we have the results of the simulation when a third order dispersion $b_3 = \pm 0.1$ is considered, with the positive sign for the plot on the left and the negative sign for the one on the right. We can see that the SPM broadening is much smaller than in the no dispersive case (notice the difference in the scale of the frequency axis). In this case chromatic dispersion makes the pulse disperse in time domain, reducing both the peak power and the slope of the edges of the field, the consequence of that being that nonlinear effects are less visible than in the

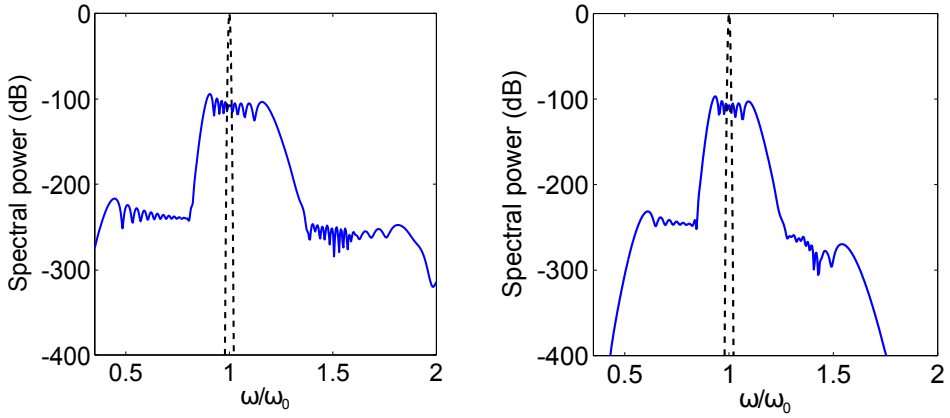

Figure 3.9: Initial and final spectra after a propagation of $z = 2$ mm calculated solving the UPPE for diamond (left) and silica (right) pumped with an intensity of $I = 10$ TW/cm^2. The pulse duration is $t_0 = 200$ fs and the pump wavelength $\lambda = 1550$ nm. We can see that the new sidebands are generated in these realistic simulations in a similar fashion to the ones that appeared in our previous numerical analysis of the coupled equations and the full model (1.8). The code used in these simulations was written by A. Armaroli.

non-dispersive limit. For odd order chromatic dispersion terms an asymmetry in the spectrum develops, that depends on the sign of the relevant parameter. Although some features can be seen in the spectrum around the central broadening, both their detuning and their power are not those typical of the new SPM lobes studied here. A simple simulation of the equation taking into account only the Kerr term while ignoring the NK and THG ones shows that those features develop regardless of the presence of these new nonlinearities. Thus dispersion, unlike the shock term, will make the new SPM lobes more difficult to find in experiments. This means that the ideal experimental setup would be one in which the dispersion relation is as close to a straight line as possible, minimising β_2 and all of its higher orders as much as possible without affecting the nonlinear coefficient of the medium.

Before closing this study of SPM broadening, we present one last numerical result. In this case we simulate a completely realistic system solving the UPPE [20], which, as explained in the introduction, is physically equivalent to our Equation (1.8). The main difference is that in this case we consider the full dispersion profile of the material, instead of the first few terms of a series expansion. The code used for this purpose was written by Andrea Armaroli, who kindly shared it with us, and includes all

conjugate field effects, shock term, and the aforementioned full realistic treatment of chromatic dispersion. With this code we can simulate experimental setups with amazing accuracy.

In Figure 3.9 we can see how the spectrum of a Gaussian pulse with an intensity of $I = 10$ TW/cm^2 changes after a propagation of $z = 2$ mm in bulk diamond (left panel) and bulk silica (right panel). The wavelength of the pump was $\lambda = 1550$ nm, which corresponds to normal dispersion in diamond and anomalous dispersion in silica. We see that, in both cases, the spectrum looks very similar, with asymmetric SPM broadening in the top of the pulse due to the shock term (compare with the oscillations on top of the pulse in the top right panel of Figure 3.8) and the two new sidebands evolving in an asymmetric fashion due to the combination of self-steepening and higher order dispersion effects.

The order of magnitude of the power transferred to the sidebands matches perfectly our simulations of (1.8). The detunings are compatible to the ones found in our numerical results. The fact that we have managed to cross-check our results with those generated by a different model is a proof of validity of the theory of SPM developed in this section, while we wait for experiments that are able to detect the signature of the extra spectral broadening we have predicted. In principle, the main challenge from an experimental point of view would be detecting a signal that is hundreds of dBs smaller than the pump. However, the fact that the maximum detuning of the sideband generated can reach almost as far as the second harmonic of the pump could help concieve an experiment that is able to study this phenomenon.

3.2 Raman self frequency shift

Raman scattering is a very well known process by which photons interact with phonons in a certain material [53, 54]. Although the Raman scattering includes both processes in which a photon gains energy by absorbing a phonon and processes in which a photon gives energy to the material by exciting phonons, we are only interested in the latter. When a soliton propagates in a nonlinear material the photons that form that soliton will lose energy through Raman scattering. As a consequence, photons in the high energy modes of the soliton will be transferred to low energy modes, and thus the spectrum of the soliton will shift continuously towards longer wavelengths with propagation [55–59].

As with the previous analysis of SPM broadening, we will start with a short review of the Raman self frequency shift of solitons in the framework of SVEA, specially emphasising the mathematical tools needed to analyse it. This mathematical formalism will be later extended beyond SVEA, and we will compare the results obtained with and without this approximation.

3.2.1 The Raman effect in the NLSE

The Raman effect can be included in the NLSE (1.6) by means of a delayed nonlinearity. This means that, instead of having only the usual instantaneous response coming from the Kerr term, the material that reacted to the presence of the pulse (hence creating the nonlinear response) will take some finite time to relax to its previous state [60–62]. This means that the NLSE for a material with anomalous dispersion extended to take into account the Raman scattering would be

$$i\partial_\xi A(\xi,\tau) + \frac{1}{2}\partial_\tau^2 A(\xi,\tau) + A(\xi,\tau)\int_0^\infty R(\tau')|A(\xi,\tau-\tau')|^2 d\tau' = 0. \tag{3.16}$$

The function $R(\tau)$ is the response function that characterises the time dependent response of the nonlinear material to the presence of an electric field. It is easy to see from the form of the equation that indeed the role of the response function R is including a delayed nonlinear interaction. If $R(\tau)$ is nonzero for $\tau > 0$, then the field $A(\tau)$ will be affected by its own value at a previous time $A(\tau - \tau')$. The assumption that the medium response is instantaneous (that is, the only relevant nonlinear effect is the Kerr nonlinearity) corresponds to $R(\tau) = \delta(\tau)$. In this case, the integral in the nonlinear term of Equation (3.16) reduces to a convolution of the field with a Dirac delta function, and we recover Equation (1.6). In fact, we can split the response function of the medium into an instantaneous and a delayed response, $R(\tau) = (1 - f_R)\delta(\tau) + f_R h(\tau)$, so that the Kerr and the Raman effects are explicitely separated in the equation:

$$i\partial_\xi A + \frac{1}{2}\partial_\tau^2 A + (1-f_R)|A|^2 A + f_R A\int_0^\infty h(\tau')|A(\xi,\tau-\tau')|^2 d\tau' = 0, \tag{3.17}$$

where the fields whose dependence is not written explicitly are simply functions of (ξ,τ), and $h(\tau)$ is the delayed response function that accounts only for the Raman nonlinearity (f_R is a material dependent constant that measures the relative weight between the two effects). The Raman response function $h(\tau)$ can obviously be extremely different for different materials, since it is created by the collective modes (vibrational, rotational, etc.) that can be excited by the pulse. If we assume that there

is only one vibrational frequency responsible for the Raman effect we can write an explicit expression for $h(\tau)$, which will be the inverse Fourier transform of a Lorentzian profile [59]:

$$h(\tau) = (\tau_1^{-2} + \tau_2^{-2})\tau_1 \exp(-\tau/\tau_2)\sin(\tau/\tau_1), \tag{3.18}$$

where τ_1 and τ_2 are material dependent constants that are related to parameters of the Lorentzian profile we assumed the response function had in frequency space.

Although this convolution term models perfectly the expected resdhift for solitons of the NLSE, it is not easy to perform theoretical calculations using an equation with an integral nonlinear term. It is for this reason that an approximation should be made to simplify Equation (3.17) and write it in a form that is analytically tractable. This approximation is expanding the modulus squared of the field inside the integral in a Taylor series of τ' [3]:

$$|A(\xi, \tau - \tau')|^2 = |A(\xi, \tau)|^2 - \tau' \partial_\tau |A(\xi, \tau)|^2 + \mathcal{O}(\tau'^2). \tag{3.19}$$

Obviously this approximation is only valid for small τ'. To see what this means in terms of the response function, using that $h(\tau)$ is normalised so that $\int_0^\infty h(\tau) = 1$ we have

$$f_R A \int_0^\infty h(\tau')|A(\xi, \tau - \tau')|^2 d\tau' = \\ f_R \left(|A|^2 A + \partial_\tau |A|^2 \int_0^\infty \tau' h(\tau') d\tau' + \mathcal{O}(\tau'^2) \right). \tag{3.20}$$

The first term on the right hand side is a Kerr effect term, and it will add up with the $(1 - f_R)|A|^2 A$ term in (3.17) to form the usual Kerr nonlinearity. The non-trivial term coming from our approximation and that will give us the Raman effect is the second one: we have an integral in τ' with ∞ as the upper limit. To make this compatible with an approximation that needs τ' to be small, we have to make sure the contribution to the integral of big values of τ' is small. This happens if, and only if, $h(\tau')$ given by (3.18) decays fast enough with τ'.

Physically, our approximation (3.19) means that we are assuming the temporal shape of the pulse to be a straight line. This is only a good approximation if the delayed interaction happens between points in the pulse that are not too separated in time. For this to happen, the response, although delayed, has to show its effects only for times much shorter than the typical timescale of the pulse shape, which would

be approximately the width of the pulse. Therefore, in this context, "fast enough" decay for $h(\tau)$ means that the exponential decay has to happen in a timescale smaller that the width of the pulse, i.e., $\tau_2 \ll 1$. If this is the case, the perturbation created by the pulse as it moves through the material will last for a short enough time to affect only the immediate vicinity of the part of the pulse creating it. That way, the assumption that the amplitude square of the pulse varies as a straight line is justified. On the other hand, we cannot choose τ_2 to be too small, since in the limit $\tau_2 \to 0$ the response given by $h(\tau)$ would become instantaneous and we would not have Raman scattering.

These limitations in τ_2 also give us information about τ_1. For small τ the $\sin(\tau/\tau_1)$ term will dominate over the exponential. If τ_1 is too big, by the time this sine term starts growing the exponential controlled by τ_2 will have decreased too much, and no delayed response whatsoever will be seen. However, if τ_1 is very small the sine term will oscillate many times and this will cause its effect to average to zero. We therefore need τ_1 to be comparable to to τ_2 if we want a non-negligible Raman frequency redshift of solitons.

In silica, for example, and in dimensional units $t_1 = 12.2$ fs and $t_2 = 32$ fs [59]. Our dimensionless parameters are $\tau_1 = t_1/t_0$ and $\tau_2 = t_2/t_0$, with t_0 the width of the pulse. We can see that τ_1 will always be smaller than τ_2 regardless of pulse duration. For long pulses of ns or hundreds of ps we would have that τ_2 would be of the order of 10^{-5}, and due to its smallness the approximation that the nonlinear response of the medium is instantaneous holds (Kerr nonlinearity only). For shorter pulses of a few ps, τ_2 grows and the Raman effect starts playing an important role in the propagation of pulses, which can be understood using the approximation (3.19). However, for fs pulses, τ_2 becomes too big and that approximation does not hold any more, as explained above. That is why the full formalism is needed and computing the convolution of Equation (3.16) is the only way to treat Raman effect for ultrashort pulses in silica. But, as already mentioned, the convolution term is not analytically tractable, so we will keep studying the model that results from the approximation described above, and choose convenient values of τ_1 and τ_2 for the regime studied.

We can now define $\tau_R = f_R \int_0^\infty \tau h(\tau) d\tau$ to get the final equation including Raman effect with the approximation of τ_2 small:

$$i\partial_\xi A + \frac{1}{2}\partial_\tau^2 A + |A|^2 A - \tau_R A \partial_\tau |A|^2 = 0. \tag{3.21}$$

This is the usual NLSE equation with an extra term creating the redshift of solitons. We can study the effect of this new term in Equation (3.21) using a soliton perturbation method [63, 64]. If we write the soliton solution of the NLSE as

$$A(\xi,\tau) = A_0(\xi)\text{sech}\left(A_0(\xi)(\tau - \tau_c(\xi))\right)\exp\left(i\phi(\xi) - i\delta(\xi)\tau\right), \tag{3.22}$$

where we let the amplitude A_0, delay τ_c, phase ϕ and detuning δ of the soliton evolve with propagation ξ, a set of equations can be derived that give the evolution of those four soliton parameters. If we can write our perturbed NLSE as

$$i\partial_\xi A + \frac{1}{2}\partial_\tau^2 A + |A|^2 A - i\epsilon(\xi,\tau) = 0, \tag{3.23}$$

then the equations are [3, 63, 64]:

$$\partial_\xi A_0 = \text{Re}\left[\int_{-\infty}^{\infty} \epsilon A^* d\tau\right], \tag{3.24}$$

$$\partial_\xi \delta = -\text{Im}\left[\int_{-\infty}^{\infty} \epsilon \tanh\left(A_0(\tau - \tau_c)\right) A^* d\tau\right], \tag{3.25}$$

$$\partial_\xi \tau_c = -\delta + \frac{1}{A_0^2}\text{Re}\left[\int_{-\infty}^{\infty} \epsilon(\tau - \tau_c) A^* d\tau\right], \tag{3.26}$$

$$\begin{aligned}\partial_\xi \phi = \text{Im}\left[\int_{-\infty}^{\infty} \epsilon\left(\frac{1}{A_0} - (\tau - \tau_c)\tanh(A_0(\tau - \tau_c))\right) A^* d\tau\right] \\ + \frac{1}{2}(A_0^2 - \delta^2) + \tau_c \partial_\xi \delta.\end{aligned} \tag{3.27}$$

The last two equations give the full evolution of the delay and the phase, since they can change due to more effects than just the perturbation. It is easy to see that in our case the perturbation is $\epsilon = -i\tau_R A \partial_\tau |A|^2$. Because of this form of the perturbation, our integrals will always have terms like $\approx i|A|^2\partial_\tau|A|^2$, which is purely imaginary. This means that $\partial_\xi A_0 = 0$ and $\partial_\xi \tau_c = -\delta$. For the detuning we have:

$$\partial_\xi \delta = \tau_R \int_{-\infty}^{\infty} |A|^2 \partial_\tau |A|^2 \tanh\left(A_0(\tau - \tau_c)\right) d\tau. \tag{3.28}$$

Substituting the expression for $A(\xi)$ given by (3.22) in the previous equation gives

$$\partial_\xi \delta = -2A_0^5 \tau_R \int_{-\infty}^{\infty} \text{sech}\left(A_0(\tau - \tau_c)\right)^4 \tanh\left(A_0(\tau - \tau_c)\right)^2 d\tau, \tag{3.29}$$

and performing the integral we get as a final result

$$\partial_\xi \delta = -\tau_R \frac{8A_0^4}{15}. \tag{3.30}$$

We see that the detuning accumulated by the pulse is always negative, i.e., we have a *redshift*. This is in line with our expectations. This redshift will depend not only on the parameter τ_R that depends on the response function, but also increases as a fourth power of the pulse amplitude. This means that Raman frequency shift will be more visible the more intense the light is in the material.

Now that we have seen how the Raman effect appears in the SVEA case and have shown its mathematical treatment, we are ready to extend it to the non-SVEA regime.

3.2.2 Raman effect beyond SVEA

The first step will be deriving an equation that extends (1.8) to account for the Raman effect, starting with the convolution with the full response function in the nonlinear term and then reducing it in the small τ_2 case. This derivation, as well as the application of the perturbative analysis explained before to the new perturbation terms, are extremely cumbersome and left for an appendix (Appendix A). Here, it suffices to say that the equation that includes both Raman and negative frequency effects is:

$$i\partial_\xi A + \frac{1}{2}\partial_\tau^2 A + \Big[A|A|^2 + A^*|A|^2\exp(2i\kappa\xi + 2i\mu\tau) + \frac{1}{3}A^3\exp(-2i\kappa\xi - 2i\mu\tau) - \tau_R A\partial_\tau|A|^2 - \tau_R A^*\exp(2i\kappa\xi + 2i\mu\tau)\partial_\tau|A|^2\Big]_+ = 0. \quad (3.31)$$

The appearance of new terms in the nonlinear polarisation with a delayed response changes the expected evolution of δ, A_0 and τ_c. We can use the new perturbation term, that is, the last nonlinear term in Equation (3.31), and make the perturbation analysis as explained before to find how this new Raman-like term affects the propagation of solitons. Adding this contribution to the one coming from the usual Raman perturbation term will give us the full evolution of the parameters. Again, we will

only show the formulas here, since a careful derivation is shown in Appendix A:

$$\partial_\xi A_0 = -\tau_R \mathrm{Re}\Bigg[\frac{4\pi}{3}\exp[2i(\kappa\xi-\phi)](A_0^2+(\delta+\mu)^2)(\delta+\mu)^2 \operatorname{csech}\left[\frac{\pi(\delta+\mu)}{A_0}\right]\exp[2i(\delta+\mu)\tau_c]\Bigg], \tag{3.32}$$

$$\partial_\xi \delta = -\tau_R\frac{8A_0^4}{15} - \tau_R\mathrm{Re}\Bigg[\exp[2i(\kappa\xi-\phi)]\left(\frac{8\pi A_0^3}{15}(\delta+\mu)-\frac{8\pi}{15A_0}(\delta+\mu)^5\right) \operatorname{csech}\left(\frac{\pi(\delta+\mu)}{A_0}\right)\exp[2i(\delta+\mu)\tau_c]\Bigg], \tag{3.33}$$

$$\partial_\xi \tau_c = -\delta + \tau_R\mathrm{Re}\left[2iA_0^2\exp[2i(\kappa\xi-\phi)]\exp[2i(\delta+\mu)\tau_c]f_\tau\left(\frac{2(\delta+\mu)}{A_0}\right)\right], \tag{3.34}$$

where the function $f_\tau(x)$ is defined as

$$f_\tau(x) = -\frac{1}{48}\sqrt{\frac{\pi}{2}}x\left(-8(2+x^2)+\pi x(4+x^2)\mathrm{ctanh}\left(\frac{\pi x}{2}\right)\right)\operatorname{csech}\left(\frac{\pi x}{2}\right). \tag{3.35}$$

Note that in this beyond-SVEA case the evolution of these three parameters has an explicit dependence on ϕ, which means we need to find its explicit evolution as well. Again, a full derivation of this equation is done in Appendix A, and we just show here the final result:

$$\partial_\xi\phi = \frac{1}{2}(A_0^2-\delta^2)+\tau_c\partial_\xi\delta+ \tau_R\mathrm{Im}\Bigg[2iA_0^3\exp[2i(\delta+\mu)\tau_c]\exp[2i(\kappa\xi-\phi)] \left(\phi_1\left(\frac{2(\delta+\mu)}{A_0}\right)-\phi_2\left(\frac{2(\delta+\mu)}{A_0}\right)\right)\Bigg], \tag{3.36}$$

with the functions $\phi_1(x)$ and $\phi_2(x)$ defined as

$$\phi_1(x) = \frac{i}{24}\sqrt{\frac{\pi}{2}}x^2(4+x^2)\operatorname{csech}\left(\frac{\pi x}{2}\right), \tag{3.37}$$

$$\phi_2(x) = -\frac{i}{240}\sqrt{\frac{\pi}{2}}\left(32-10x^4+\pi x(x^4-16)\mathrm{ctanh}\left(\frac{\pi x}{2}\right)\right)\operatorname{csech}\left(\frac{\pi x}{2}\right). \tag{3.38}$$

The new contributions to the evolution equations coming from the non-SVEA term of Equation (3.31) all have a $\operatorname{csech}(2(\delta+\mu)/A_0)$ factor, which means they will be negligible when the dimensionless frequency of the pulse, which is originally μ before suffering a detuning of δ, is bigger than a few units, due to the exponential decay of the hyperbolic cosecant function. They are also the real (or imaginary for ϕ)

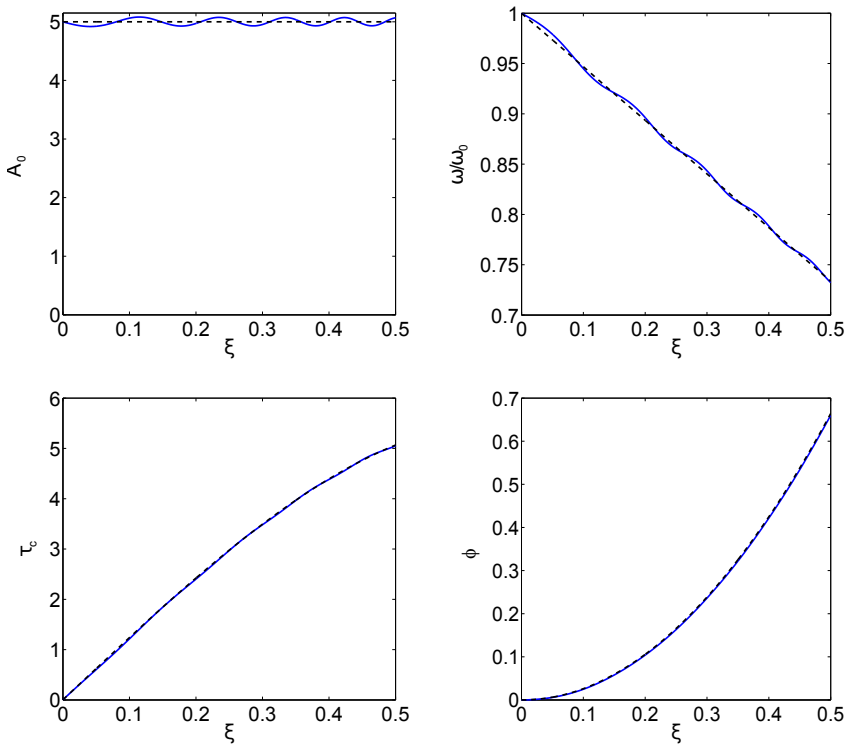

Figure 3.10: Evolution of the parameters of the solution when treating the Raman effect as a perturbation in the SVEA framework (black dashed lines) and beyond SVEA (blue thick line). We see that the difference is minimal for all of them. See text for information about the parameters used.

part of a function that depends on the exponential $\exp(2i(\kappa\xi - \phi))$, so the contribution of these terms will change sign with propagation and average to zero if κ is too big. There is an oscillating term in $\delta + \mu$ as well, which imposes the condition of small frequency too. These conditions of μ and κ small are the expected limit in which negative frequency effects show up, and as expected we recover the SVEA limit when those parameters are big.

The equations for the evolution of the four parameters of the soliton are incredibly complex from an analytical point of view, being four differential equations coupled in an extremely non-trivial way. However, being all of them first order differential equations, it is easy to integrate them numerically. We will now proceed to do this, and compare the predicted evolution of the parameters of the solitonic solution (3.22) in the SVEA and non-SVEA cases.

In Figure 3.10 we plot how the four parameters A_0, δ (as $\delta/\mu+1$), τ_c, and ϕ change

during propagation for a reasonable value of the parameters of the problem (namely $\mu = 10$, $\kappa = 30$, $\tau_1 = 0.1$, $\tau_2 = 0.2$, and $f_R = 0.2$), according to the formulas derived in the previous section for the usual Raman effect (black dashed) and the ones shown before for the Raman effect beyond SVEA (blue thick). The propagation distance is $\xi = 0.5$, and the input pulse is chosen to be $A_{in} = 5\,\mathrm{sech}\,(5\tau)$. We see that for parameters like these ones the effect of the new terms is practically negligible, and only small oscillations around the SVEA value can be seen in the case of the amplitude and the frequency shift of the soliton, while the delay and the phase stay practically the same. These changes are too small to be visible in any dynamical simulations.

Our choice of parameters for Figure 3.10 was already problematic: a value of $\mu = 10$ for the frequency means that the pulse duration of the order of 10 fs if we work at the $\lambda = 1.55\mu m$ wavelength. This would mean that, if we assume the value of t_1 and t_2 for silica written above, we would have $\tau_1 \approx 1$ and $\tau_2 \approx 3$ instead of the ones we used. This means that, for a realistic response function, the approximation of τ_2 small would be completely broken, and we would be forced to either use longer pulses, which would in turn increase the value of μ and make the non-SVEA effects even smaller, or find a material with a different value of t_1 and t_2. Since even the functional form we chose for the response function is particular for silica and might not be a good way to model Raman scattering in other materials, it can prove to be a great challenge to find a system in which the parameters used in Figure 3.10 are experimentally sound, and even then the beyond SVEA effects would not be visible.

We must therefore conclude that it seems unlikely that the new negative frequency effects included in Equation (3.31) will ever be found to have a big impact on the redshift of solitons due to Raman scattering, at least for materials with a delayed response similar to the one shown by fused silica. In fact, and since the timescales of the material modes that create Raman scattering and the pulses that experience non-SVEA effects are so different, it will probably not be possible to design an experiment for which both effects are important simultaneously.

4 New resonant radiations

This chapter will focus on the phenomenon of *resonant radiation* (RR) emission. The emission of RR by solitons of the NLSE has been well known for years [12–15]. It happens because, when a third or higher order dispersion term is included in (1.6), the linear momentum $\beta(\omega_r)$ of a continuous wave with a certain frequency ω_r is equal to the total momentum of the soliton. When that condition, known as *phase matching condition*, is satisfied, the soliton cedes energy resonantly to the continuous mode. This means, in frequency domain, that a sharp peak will appear in the spectrum at the frequency ω_r [65, 66].

In fact, the emission of radiation because of a phase matching between a pump and a continuous wave is much more general than the effect seen in solitons, and has been found in many other physical systems, for example three dimensional light bullets [67–69], dispersive shock waves [70], passive resonators [71–75], and even extremely complex scenarios mixing the effects of more than one of the previous systems [76]. In particular, as mentioned in the introduction, it was the emission of a new, unexplainable kind of RR that gave rise to Equation (1.8) as an extension of the NLSE for regimes where SVEA cannot be applied any more [25, 28]. The analysis of the new kinds of RR arising due to the NK and THG terms of the nonlinear polarisation has been very fruitful, and the main results of this research will be presented in this chapter.

The outline of the chapter is similar to the previous sections: we will start with a review of the phenomenon of RR in the literature and then proceed to extend that formalism to new systems where the resonant radiation associated with the NK and THG terms had not been studied before.

4.1 Basics of resonant radiation

This section will work as a short review of the basic concepts of RR emission. We will start by explaining how RR works for solitons inside the SVEA formalism, i.e., using extensions of the NLSE. After this, we will carefully study the emission of NRR that was the origin of the model studied in this thesis. We will explain the tools that are necessary to find the new kinds of RR that appear beyond SVEA, since these will be the ones we will apply to different systems in the following sections.

4.1.1 Resonant radiation in the NLSE

An intense pulse propagating in a nonlinear material will gain an extra phase during propagation due to self-phase modulation. It is this extra phase, proportional to ξ, that acts as an extra momentum for the pump (the nonlinear momentum). With the scaling we chose in (1.6), in which we have chosen both the nonlinear coefficient of the nonlinear material γ and the power of the pulse P to be $\gamma = P = 1$, the nonlinear momentum of a fundamental soliton of the NLSE is $1/2$ (in dimensional units it would be $\gamma P/2$; for a discussion about unit conversions see [3] and Appendix B). In the co-moving frame this is the only contribution to the momentum of the soliton. In the case where only β_2 is present, the linear momentum of continuous waves around the pump frequency will always be negative (since $\beta_2 < 0$ is a requirement for the existence of solitons in the NLSE). Therefore, when only second order dispersion is taken into account there is no radiation emitted, and the soliton is perfectly stable, as expected.

The situation changes dramatically when higher order dispersion is taken into account. When third order dispersion is present, for example, the linear momentum of waves with a large positive (negative) detuning with respect to the central frequency of the soliton will be positive for $\beta_3 > 0$ ($\beta_3 < 0$). This means that the condition $b_2\Delta^2/2 + b_3\Delta^3/6 = 1/2$ (phase matching condition, Δ is the pump-CW detuning and we are using the dimensionless dispersion coefficients b_i defined in the introduction) will be satisfied for a frequency $\mu_r = \mu + \Delta$ of the CW. Therefore the soliton propagating under the effect of third order dispersion will shed radiation continuously and will not be stable any more. The picture is similar when higher orders of the dispersion are taken into account: as long as the phase matching condition

$$\sum_{n>2} \frac{b_n \Delta^n}{n!} = \frac{1}{2} \tag{4.1}$$

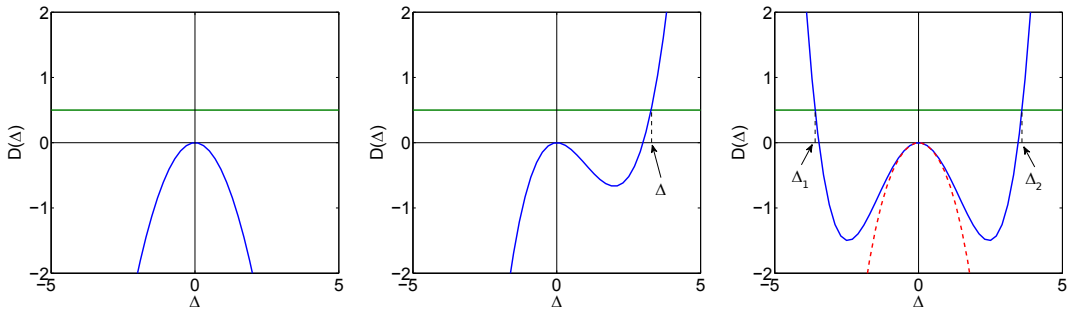

Figure 4.1: Phase matching curves in the NLSE for three different cases. $b_2 = -1$ (anomalous dispersion) in all of them. The green line represents the nonlinear momentum of the pump. For the left panel no higher order dispersion terms are present, so the phase matching condition (4.1) has no solutions and the soliton propagates unperturbed. In the central panel we include a third order dispersion $b_3 = 1$, creating one resonant frequency with detuning Δ with respect to the pump. In the right panel we set $b_4 = \pm 1$. When choosing the negative sign (red dashed curve) there is no phase matching between soliton and radiation. With the positive sign two frequencies, at detunigs Δ_1 and Δ_2, become resonant with the pump.

can be satisfied for some values of the detuning Δ_m, the soliton will emit radiation with the frequencies given by $\mu_{r_m} = \mu + \Delta_m$.

Figure 4.1 shows the phase matching curves, plots of $D(\Delta)$ against Δ that give us graphical solutions of the phase matching condition. In these plots we draw the curve given by the dispersion relation on the left hand side of Equation (4.1), and the crossing(s) with the horizontal line, which is the constant on the right hand side, gives us the values of the frequency for which phase matching is achieved. In this figure we show the phase matching for the cases $b_{n>2} = 0$, $b_{n>3} = 0$, and $b_{3,n>4} = 0$. As expected, no crossings between the nonlinear momentum of the soliton (green line) and the linear momentum of continuous waves (blue curve) exist for the case with b_2 only, since this is the integrable case. When a third order dispersion term is included there will be one crossing at a value of the detuning Δ, which will be either positive or negative depending on the sign of b_3. For a fourth order dispersion, we will have either two or none solutions. If $b_4 < 0$ (red dashed line), the linear momentum of CW solutions will be always negative, even more so than in the b_2 only case; but if b_4 is positive there will be two solutions for the detuning of CWs resonant with the pump, which will satisfy $\Delta_1 = -\Delta_2$ if no third order dispersion is considered.

We will now show the results of solving (1.6) with higher order dispersion with a

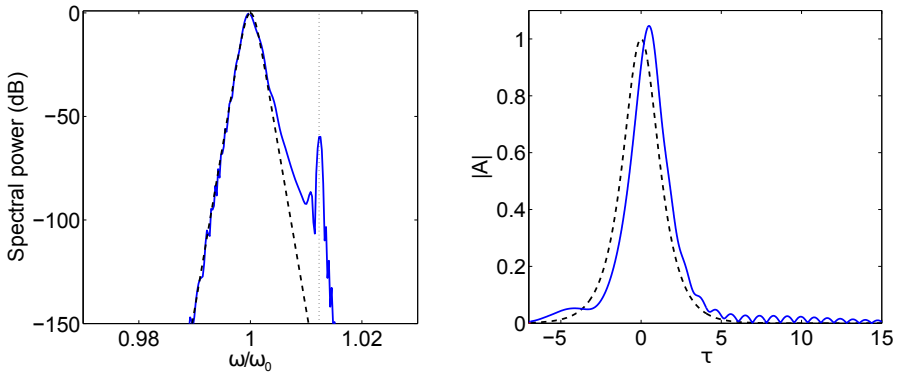

Figure 4.2: Spectrum (left) and temporal profile (right) of a sech (τ) pulse after propagating for a distance of $\xi = 5$ with a third order dispersion term $b_3 = 0.5$. The initial spectrum and profile are shown in black for comparison. We see a clear peak in the spectrum in the position predicted by the phase matching conditions, which is marked by the dotted line. In time domain, the radiation appears as oscillations that leave the pulse, in this case, through its trailing edge.

sech (τ) initial pulse. We choose this shape for the input because this is the soliton of the NLSE, and we would expect the spectrum not to suffer any changes with propagation if only second order dispersion was considered. Any spectral features that might be developed during propagation will be due solely to the emission of resonant radiation, therefore making its identification very easy.

In Figure 4.2 we can see what happens when the sech (τ) soliton is perturbed by third order dispersion. The propagation distance is $\xi = 5$, $b_3 = 0.5$ and the dimensionless frequency $\mu = 500$ (it does not enter our equations but it is used to normalise the x axis of the plot of the spectrum). In the left panel we see that, as expected, a sharp peak appears at the frequency predicted by the phase matching condition (4.1), marked by the dotted vertical black line. This spectral peak means that a continuous wave is originating in the system, and the signature of this in time domain is the characteristic oscillation in the pulse's trailing edge. We can also see that the peak of the soliton has moved from the point $\tau = 0$, which means it has accumulated a certain delay during propagation due to the dispersion. We ought to be careful with this, since a delay, i.e., a change in group velocity of the pump, would modify the phase matching conditions for the system, introducing a linear term in Δ in Equation (4.1). However, in this case, this modification of the velocity is small, and its effect over the phase matching conditions negligible, as proven by the agreement

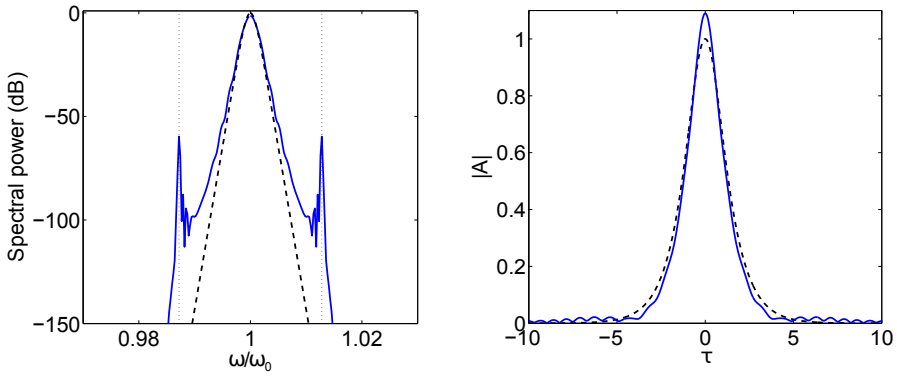

Figure 4.3: Spectrum (left) and temporal profile (right) of a sech (τ) pulse after propagating for a distance of $\xi = 5$ with a fourth order dispersion term $b_4 = 0.3$. The initial spectrum and profile are shown in black for comparison. We see the predicted symmetrical peaks in the spectrum exactly at the position given by the phase matching (dotted black line). For this case, we see that one of the radiations is faster than the soliton and the other one slower, so that oscillations appear in both the trailing and leading edges of the pulse.

between the predicted and numerically obtained position of the RR spectral peak. We will ignore this phenomenon for the remainder of this section, but will come back to it when we analyse other systems in which this effect needs to be taken into account to obtain the precise phase matched frequency.

The result for the case with fourth order dispersion is shown in Figure 4.3. The propagation distance is $\xi = 5$ again, and we choose a value of $b_4 = 0.3$. The frequency is the same as in the previous case, $\mu = 500$. As expected, two radiation peaks appear with symmetrical detunings with respect to the pump. The agreement between the position of the peaks in our simulation and the one predicted by the phase matching conditions is perfect. In time domain, one of the CWs generated will move faster and the other one slower than the soliton. This means that there are oscillations in both the trailing and leading edges of the pulse, and that the peak of the amplitude remains at its original position $\tau = 0$.

With these simulations we have finished our introduction to RR in the SVEA framework. We will now try to extend the concepts we have just explained to more general physical systems using Equation (1.8).

4.1.2 Resonant radiation beyond SVEA: Negative resonant radiation

When SVEA is broken the previous picture is incomplete. The phase matching condition (4.1) for the emission of RR comes exclusively from the presence of the Kerr term in the equation. However, (1.8) contains two other nonlinear terms from which we expect two new phase matching conditions to appear. As it was explained in the introduction, one of these new phase matching conditions was proven to create a RR peak experimentally, and the successful explanation of this phenomenon using this model was the reason why the research contained in this thesis was conducted. We will therefore carefully explain this work in the present section, work that was conducted prior to the beginning of this research project and published in [25].

The phenomenon of resonant radiation emission due to the NK and THG terms can be explained in terms of phase matching conditions, as we did with the RR due to the Kerr term described in the SVEA case. But in this occasion we need to find three resonance conditions for the radiation, one for each of the nonlinear terms present in (1.8). To this end we take another approach to the derivation of the phase matching conditions. This method is outlined in [77]. What we will do is assume that we know a solution of Equation (1.6) when no extra terms or higher order effects are present, $A(\xi,\tau) = V\exp(iq\xi)$. We will add a small perturbation $u(\xi,\tau)$ to this solution and introduce the resulting field in Equation (1.8) to find the evolution of the perturbation field u. The result is (ignoring the shock term for simplicity):

$$i\partial_\xi A + \frac{1}{2}\partial_\tau^2 A + |A|^2 A + \left(\hat{D} - \frac{1}{2}\partial_\tau^2\right) A + i\partial_\xi u + \hat{D}u + \\ |A|^2 A^* \exp(2i\mu\tau + 2i\kappa\xi) + \frac{1}{3}A^3\exp(-2i\mu\tau - 2i\kappa\xi) = 0. \quad (4.2)$$

We have ignored nonlinear terms of the form $\sim A^2 u$ following the guidelines set in [77]. Since we assumed that A was a solution of the NLSE the first three terms will be equal to zero. This means that the resulting equation for the evolution of u, with A of the form given above, would be:

$$i\left(\partial_\xi - i\hat{D}\right)u = -\left(\hat{D} - \frac{1}{2}\partial_\tau^2\right)V\exp(iq\xi) - \\ V^3\exp(2i\mu\tau + 2i\kappa\xi - iq\xi) - \frac{1}{3}V^3\exp(-2i\mu\tau - 2i\kappa\xi + 3iq\xi). \quad (4.3)$$

This is the equation of a wave u being driven by three external terms, which are the ones on the right hand side of (4.3). We now try a CW solution for u of the form $u = u_0\exp(iD(\Delta)\xi - i\Delta\tau)$, where Δ is the detuning between the radiation mode and

the pump. The phase between the radiation field u and the driving terms will be matched if:

$$D(\Delta) = q, \tag{4.4}$$

$$D(\Delta) = 2\kappa - q, \tag{4.5}$$

$$D(\Delta) = -2\kappa + 3q, \tag{4.6}$$

where the first equation comes from matching the phase of u with that of the first driving term on the right hand side, the second equation from the phase matching with the second driving term, and the third equation from the matching with the third term. In these equations q is the nonlinear momentum of the pump which, as explained in Appendix B, is always normalised to $q = 1/2$ for a $\mathrm{sech}\,(\tau)$ pulse in our units.

The first term on the right hand side of (4.3) comes from the extra dispersion terms acting on the field A, and has nothing to do with the new nonlinear terms of our Equation (1.8). A term like this would therefore be present in a SVEA based approach as well, so it is not a surprise that the phase matching condition we derived from it is the well-known condition for RR of the NLSE solitons [12–14], Equation (4.1). It is interesting to note, as it will become relevant for some of the systems studied later in this work, that since the driving term responsible for this phase matching condition comes from the dispersion acting on the unperturbed solution, we do not expect the resonant radiation associated with condition (4.4) to be visible when the initial pulse is a monochromatic CW state, while for the other two it is the amplitude of the solution that feeds the associated resonant radiation, which could potentially appear even for CW states.

The second driving term comes from the NK term of (1.8), and therefore the resonant radiation emitted when the condition (4.5) is satisfied has been called *negative resonant radiation* (NRR) in the literature. This is the phase matching condition that was heuristically derived in [28] to explain the experimental results found when studying the propagation of very intense and steep pulses in crystals and photonic crystal fibres. In this formalism the creation of this radiation is explained as a natural consequence of including all the nonlinear terms that contribute to nonlinear propagation of light in this regime of very intense and extremely short pulses, in which SVEA no longer holds.

Lastly, the third driving term, that comes from the THG term of (1.8), causes

a new kind of resonant radiation that was called *third harmonic resonant radiation* (THRR) due to the origin of its phase matching condition, Equation (4.6). It was a theoretical prediction of this model that, to the best of the author's knowledge, had never been described before the publication of reference [25]. Even in that paper, the numerical simulations performed for bulk silica did not show this new resonant mode, since the phase matched frequency was in the deep infrared and the energy transfer to such a low frequency mode was not efficient enough. However, a recent publication has shown that this kind of radiation could be the most important of the new nonlinear effects, giving rise to a huge energy transfer between the pump and a resonant CW mode [29]. We will analyse the theoretical and experimental evidences of this *super resonant radiation* in one of the following sections.

As a side note, we will mention that the three phase matching conditions can be written as a single equation:

$$D(\Delta) = 2m\kappa + (1 - 2m)q, \tag{4.7}$$

where $m = 1$ in the NRR, $m = 0$ for the RR, and $m = -1$ for the THRR. This way of writing the phase matching conditions (4.4)-(4.6) shows that the two new constants to which the linear dispersion of the CW must be equal to excite the novel resonant modes are equidistant with the one associated with the usual RR. In the special case $\kappa = q$ all three converge and there is only one radiation frequency that is resonant with all three driving terms in the right hand side of (4.3).

Since RR was already studied in the previous section, and THRR will be the object of a thorough analysis in a coming one, we will show here the formation of NRR in a simple system. In the left panel of Figure 4.4 we plot the phase matching curve for values of the parameters $\mu = 20$, $\kappa = 30$, and $b_3 = 0.4$. The three horizontal lines are the conditions for the RR, NRR, and THRR, right hand side of the equations (4.4)-(4.6). The three dotted vertical lines represent the frequencies at which we expect the three phase matching conditions to be satisfied. The right panel of the same figures shows the initial and final spectrum of a $\mathrm{sech}\,(\tau)$ pulse after a propagation of $\xi = 170$. The three vertical dotted lines mark the frequencies at which the phase matching conditions are satisfied, as per the phase matching curve in the left panel. We see that the system clearly develops RR and NRR peaks at the exact positions predicted by the theory. At the position where THRR should appear, however, we cannot see a well defined feature that is a clear signature of resonant radiation. This is in accordance with the numerical results reported in [25].

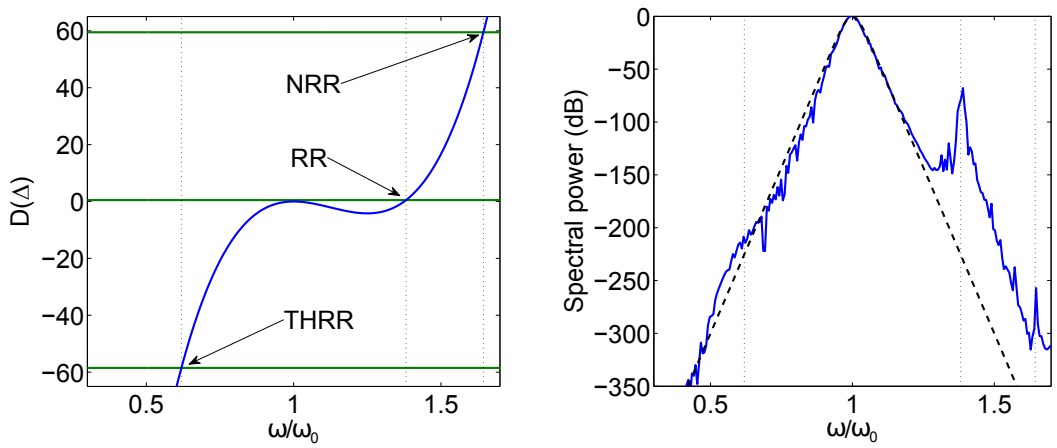

Figure 4.4: Phase matching curve (left) and spectrum (right) showing the formation of NRR in a system governed by (1.8) when pumped with a sech (τ) pulse. The parameters used are $\mu = 20$, $\kappa = 30$, and $b_3 = 0.4$. The propagation distance for the right panel is $\xi = 170$. The vertical dotted lines mark the position of the three radiations as given by the phase matching conditions. We clearly see two peaks appearing at the positions where RR and NRR are predicted to occur, while for the THRR frequency there is no clear spectral feature.

We should remark that for this numerical simulation we have included the shock term of Equation (1.8), which was discarded in the derivation of the phase matching conditions. The good agreement between between the theoretical and numerical position of the resonant emissions despite our including $\hat{S}$ or not means that for sech (τ) pulses in anomalous dispersion the resonant radiation is not affected by self steepening. This is however not true in general, and, as we will see in a later section, for some systems the phase matching conditions must be derived taking into account the nonlinear dispersion if we want an accurate prediction of the resonant frequencies.

4.2 New resonant radiations in Kerr Frequency Combs (KFCs)

The first new system which will be studied is the passive cavity. Our analysis will be quite general and relevant for any system that can be described by a Lugiato-Lefever equation (LLE), from microring cavities to fibre loops or the whispering gallery modes of small spherical resonators.

4.2.1 Theoretical modeling of the externally driven passive cavity and the Lugiato-Lefever equation

In this kind of systems light recirculates around a closed circuit, thus imposing periodic boundary conditions that mean only certain frequencies can be excited. One of the most simple ways in which we can picture this system is thinking about light circulating in a cavity formed by four mirrors, three of which are perfect and one semi-transparent. Light will circulate in a closed loop, but in every roundtrip, when it reaches the semi-transparent mirror, there will be some loss. We can also use the transmittance of this mirror to pump energy into the system by means of a laser, which might have a certain detuning with respect to the frequencies supported by the system. We can also fill the cavity with a nonlinear material if we are interested in studying nonlinear phenomena in these systems. In practice, two of the most common ways in which we can realise a system like this is using fibre loops and microresonators.

Fibre loops are optical fibres arranged in a coil-like shape, coupled to another fibre with which the first one exchanges part of its energy in every loop. If we let a pump propagate through this second fibre, it will act as a seed for the loop, and both the absorption on the loop and the energy lost to the second fibre through the coupling act as a loss for the field inside the loop.

The simplest microresonator is a small glass sphere, in which a so-called whispering gallery mode (WGM) is excited. The most remarkable characteristic of these modes is that the light is confined in all three spherical coordinates, i.e., the light in the sphere is propagating only in a circle around its equator near the surface, and heavily confined in the angle ϕ of this circumference. Again, coupling this with an external waveguide gives an energy pump and provides an additional source of loss, apart from the intrinsic loss of the glass.

These devices show some extremely complex physics, and have been studied in detail over the years due to their massive importance in fields like metrology, spectroscopy, or attosecond pulse generation [78–80]. We will explain here some of the phenomena linked to these systems that are necessary in order to understand the following parts, which deal with resonant radiation.

First of all, we must stress that there are different (albeit equivalent) approaches to this system. On one hand, we have models that rely on the discrete nature of

the spectrum, using a system of coupled ordinary differential equations, one for each mode that we need to take into account [81–83]. In these approaches the electric field inside a microresonator is written in spherical coordinates (r, θ, ϕ), and the angular part as a function related to the spherical harmonics $Y_l^m(\theta, \phi)$. If the modes fulfil the condition $l = m \gg 0$ then the field will be spatially confined to a ring (the shape of a resonator or fibre loop). After doing these substitutions in the Maxwell equations and some cumbersome algebra (see [81] for details) the following equations are derived:

$$\frac{d\mathcal{A}_l}{dt} = -\frac{1}{2}\Delta\omega_l\mathcal{A}_l + \frac{1}{2}\Delta\omega_l\mathcal{F}_0\exp(i\sigma t)\delta(l-l_0)$$
$$- ig_0\sum_{l_m,l_n,l_p}\mathcal{A}_{l_m}\mathcal{A}^*_{l_n}\mathcal{A}_{l_p}\exp[i(\omega_{l_m}-\omega_{l_n}+\omega_{l_p}-\omega_l)t]\Lambda_l^{l_m l_n l_p}\delta(l_m-l_n+l_p-l), \quad (4.8)$$

where t is a slow time over which the modal amplitudes evolve, $\mathcal{A}_l$ is normalised so that $|\mathcal{A}_l|^2$ is the number of photons in a mode with angular momentum l and frequency ω_l, $\Delta\omega_l$ is the bandwidth of the modes, $\mathcal{F}_0$ is the amplitude of the external pump and σ its detuning with the closest cavity mode, g_0 and the operator Λ are related to the nonlinear coupling coefficient and its dispersion, and $\delta(x)$ is the usual Dirac delta function. It is easy to see that the pumping term will act over the central mode mode with $l = l_0$, so that only this mode, with frequency similar to that of the pump (which means σ has to be small), will be fed by the external driving. The rest of the modes will be excited through the four wave mixing process described by the last term once the energy in the pumped mode has grown enough.

On the other hand we can use any version of the ubiquitous NLSE to propagate the field for the length of the cavity and then apply the boundary conditions of pumping/loss to find the new input field for the next roundtrip (Ikeda map, [84–87]):

$$\mathcal{A}_{n+1}(0,t) = T\mathcal{A}_{in}(t) + R\exp(-i\phi_0)\mathcal{A}_n(L,t), \quad (4.9)$$
$$i\partial_z\mathcal{A}_n + i\frac{\alpha}{2}\mathcal{A}_n + \hat{D}(i\partial_t)\mathcal{A}_n + \hat{S}(i\partial_t)p_{nl}[\mathcal{A}_n] = 0, \quad (4.10)$$

with t the fast time that describes the temporal profile of the pulse, $z \in [0, L]$ is the propagation variable for a roundtrip (L is the length of the cavity) $\mathcal{A}_n(z,t)$ the envelope of the pulse propagating in the cavity after n roundtrips, T the transmission coefficient at the pump/cavity junction and R the reflection coefficient at the same point ($R^2 + T^2 = 1$), ϕ_0 the relative phase between the pump $\mathcal{A}_{in}$ and the intracavity field $\phi_0 = \sigma - 2\pi n$, with σ as before, α is the intrinsic material loss, and $\hat{D}$ and $\hat{S}$ are the dispersion and shock operators. $p_{nl}[\mathcal{A}_n]$ stands for the nonlinear polarisation term, and we can include here as general a polarisation as we desire. Usually only

the Kerr nonlinearity is taken into account, but it is completely straightforward to generalise our beyond SVEA model to resonators by including the NK and THG terms into this polarisation.

Although different in nature, both approaches can capture the physics of the passive, externally driven cavity, but they also present some difficulties: first of all, their complexity from an analytical point of view, which means only numerical results can be extracted from them; and even a numerical treatment can be extremely inefficient. For the models based on coupled equations a huge amount of ODEs needs to be solved simultaneously when the pulse duration is short (and therefore the spectrum is wide enough to encompass more that a few modes). If we work with the Ikeda map instead we will find that it is very slow for small cavities (because we cannot make the integration step longer to the cavity itself due to the necessity of imposing the pump/loss boundary conditions at the end of every roundtrip); since typically the pulse shape will not change much in every roundtrip it would be better to find a model that does not force us to stop and apply any discrete boundary conditions.

It is due to these problems that a different approach is usually taken to deal with the passive cavity: the use of the *Lugiato-Lefever equation* (LLE). This equation is a damped-driven NLSE in which a detuning between the pumping frequency and the central frequency of the pulse is allowed. In dimensionless units, and when the full linear and nonlinear dispersions are taken into account, it reads [88–90]:

$$i\partial_\xi A + \hat{D}(i\partial_\tau)A + i(\Gamma + i\delta)A + \hat{S}(i\partial_\tau)|A|^2 A - iA_{in} = 0, \tag{4.11}$$

where Γ and δ are the normalised averaged loss and detuning respectively (losses scale as an inverse distance and detunings are frequencies), A_{in} the normalised pumping field, and the rest of the parameters are as defined for (1.8).

It is not trivial understanding how this Lugiato-Lefever equation relates to the two models described previously. We will try to explain briefly the procedures that let us derive the LLE starting from the modal expansion approach and from the Ikeda map, and the approximations needed to this end.

In the case of the multimode approaches the following approximations are needed [91]: first of all, we need to assume that the overlap between the modes that play a relevant role in the pulse propagation is approximately 1. In principle this will be justified as long as we assume that the light is highly concentrated in a part of the

resonator (very big angular momentum l of the associated modes) and that significant four wave mixing will only occur between neighbouring or almost neighbouring modes. We also need to assume that the bandwidths of all the resonant modes are equal, which is again an approximation that might limit the bandwidth of the pulses that the LLE can model correctly. With these assumptions we can write the spatiotemporal evolution of a pulse with a discrete spectrum that we would calculate through the set of ODEs of the model:

$$\mathcal{A}(\phi, t) = \sum_l \mathcal{A}_l(t) \exp\left(i(\omega_l - \omega_{l_0})t - i(l - l_0)\phi\right), \tag{4.12}$$

where l is the angular momentum of the modes, l_0 is the angular momentum of the pumped mode, and ϕ is the azimuthal angle in the cavity. This angle plays the role of time τ in our usual equations, since we are analysing how the profile of the light inside the cavity as a function of ϕ evolves. The evolution variable, that plays the role usually reserved to ξ in our models, is t. It is trivial to prove that

$$\partial_t \mathcal{A} = \sum_l \left[\partial_t \mathcal{A}_l + i(\omega_l - \omega_{l_0})\mathcal{A}_l\right] \exp\left(i(\omega_l - \omega_{l_0})t - i(l - l_0)\phi\right), \tag{4.13}$$

$$i^n \partial_\phi^n = \sum_l (l - l_0^n)\mathcal{A}_l \exp\left(i(\omega_l - \omega_{l_0})t - i(l - l_0)\phi\right). \tag{4.14}$$

And inserting equations (4.8) and (4.14) in (4.13) with $\Lambda = 1$ (which corresponds to ignoring the shock term), and after some minor alterations (that are specified in [91] in very good detail) we find

$$\partial_t \psi = -(\Gamma + i\alpha)\psi + i|\psi|^2\psi - i\frac{\beta}{2}\partial_\phi^2\psi + F \tag{4.15}$$

Where ψ is the envelope of the field after certain scaling, α is the scaled detuning, the loss has been set to Γ, β gives the second order dispersion and F is the pump. With this we have successfully derived an equation in the form of (4.11) for the fields and variables of the multimode model equation (4.8).

If we choose the Ikeda map as our starting point, we can derive the Lugiato-Lefever equation through an averaging procedure [87]. In the LLE, being a continuous model, the pumping and loss happen continuously during propagation, whereas in the Ikeda map the more realistic approach of energy exchange happening at discrete points during propagations is taken. However, if the modification of the pulse shape after every roundtrip is small, and therefore many roundtrips are necessary to analyse the evolution of a pulse in the cavity, discrete and continuous energy exchange become

indistinguishable. It is in this limit that the Ikeda map formalism can be reduced to the LLE. Typically, if we are interested in solitonic pulses, changes to their profiles will occur in a length scale of $\xi = L_D = L_{NL}$. If we define a parameter x as the ratio between this scale and that given by the length of the cavity, L, $x = L_D/L$, when $x \gg 1$ the averaging procedure is as follows: First of all, we have to change from n fields labelled by the roundtrip and restricted to $z \in [0, L]$, $\mathcal{A}_n(z,t)$, to a continuous field $\mathcal{A}(z,t)$ where $z \in [0, \infty]$. The relation between the two fields will trivially be given by:

$$\mathcal{A}_n(z,t) = \mathcal{A}(nL + z, t). \tag{4.16}$$

If L is small we can approximate this field by its first order expansion, and then:

$$\mathcal{A}_{n+1} - \mathcal{A}_n = L\partial_z \mathcal{A}(z,t). \tag{4.17}$$

Here is where the assumption that the field does not change significantly in one single roundtrip comes into play. We can calculate the difference between the field at the beginning of two consecutive roundtrips by integrating Equation (4.10) between 0 and L, and then applying the conditions (4.9). For the first step, i.e., the integration of the propagation equation, we have to assume that the field $\mathcal{A}_n$ remains almost constant, so that we can take all the evolution terms to be also constant:

$$\int_0^L \mathcal{A}_n dz = \mathcal{A}_n(L,t) - \mathcal{A}_n(0,t) = -L\left(\frac{\alpha}{2}\mathcal{A} - i\hat{D}(i\partial_t)\mathcal{A} - i\hat{S}(i\partial_t)|\mathcal{A}|^2\mathcal{A}\right), \tag{4.18}$$

where we have assumed the only contribution to the nonlinear polarisation is the Kerr term, since we want to derive an equation of the form of (4.11). Now we have to go back to (4.9) and write the relation between the fields at the end of a roundtrip and the beginning of the next one. First of all, the phase detuning has to be changed, since in that equation we are giving to the field at the beginning of the roundtrip the phase of $\mathcal{A}_{in}$ and assuming the final field of the previous roundtrip was detuned, which does not make sense in a continuous field formulation. That means that the phase ϕ_0 has to be moved from the field $\mathcal{A}_n$ to the pump. Secondly, if the transmission coefficient T is small enough, we can approximate $R = \sqrt{1-T^2} \approx 1 - T^2/2$. Using these, we find

$$\mathcal{A}_n(L,t) = \mathcal{A}_{n+1}(0,t) - T\mathcal{A}_{in}\exp(i\phi_0) + \frac{T^2}{2}\mathcal{A}_n(L,t). \tag{4.19}$$

We have chosen to separate the third term in the right hand side since it will be the one giving us the loss due to the coupling with the pump. To do this, we need to assume once again that the pulse shape will not change significantly in a single

roundtrip or due to the boundary conditions, $\mathcal{A}_{n+1}(0,t) \approx \mathcal{A}_n(L,t) \approx \mathcal{A}_n(0,t)$. We can now plug (4.19) in (4.18) to get

$$\mathcal{A}_{n+1}(0,t) - \mathcal{A}_n(0,t) = -L(\frac{\alpha}{2}\mathcal{A} - i\hat{D}(i\partial_t)\mathcal{A} - i\hat{S}(i\partial_t)|\mathcal{A}|^2\mathcal{A}) + T\mathcal{A}_{in}\exp(i\phi_0) - \frac{T^2}{2}\mathcal{A}_n(L,t). \quad (4.20)$$

The left hand side is the same as in (4.17), which means we can equate the two right hand sides of both equations. Doing the transformation $\mathcal{A} \to \mathcal{A}\exp(i\sigma z)$ to remove the phase from the pumping term we find our final result:

$$i\partial_z\mathcal{A}(z,t) + \hat{D}(i\partial_t)\mathcal{A} + \hat{S}(i\partial_t)|\mathcal{A}|^2\mathcal{A} + i\left(\frac{\alpha L + T^2}{2L} + i\sigma\right)\mathcal{A} - iT\mathcal{A}_{in} = 0. \quad (4.21)$$

We have arrived at the Lugiato-Lefever equation again. From now on, we will use this mean field equation in dimensionless units (and its extensions) to treat the passive cavity, without going back to the first principle models explained before.

We will now proceed to study the solutions of the Lugiato-Lefever equation. To this end it is extremely convenient to use the scaling that is explained in [92]. Note that in that paper the authors use the fast and slow time formalism, in which the fast time plays the role of our usual dimensionless time, and the slow time t is related to our dimensionless propagation distance ξ through the group velocity, $t = \xi/v_g$. Apart from this, the losses are chosen to be 1, meaning that the fast time, detuning, and pumping power need to be rescaled accordingly. In those units the equation reads:

$$\partial_\xi\Psi = \left[-1 + i(|\Psi|^2 - \Delta) - ib_2\partial_\tau^2\right]\Psi + S, \quad (4.22)$$

where Ψ is the scaled field, Δ gives the detuning, $b_2 = \pm 1$ gives the sign of the second order dispersion and S is the normalised pump.

As simple as Equation (4.22) might look, it has a huge variety of solutions, and an impressive amount of work has been done through the years to study its mathematical properties [93–98]. The first class of solutions that can be studied are the steady state solutions, that correspond to $\partial_\xi\Psi = \partial_\tau\Psi = 0$. If we define, in accordance with [92] $X = |S|^2$ and $Y = |\Psi|^2$, the resulting equation for steady state excitations would be (when only second order dispersion is considered):

$$X = Y^3 - 2\Delta Y^2 + (\Delta^2 + 1)Y. \quad (4.23)$$

At constant pump X, and without nonlinearity, $X = (\Delta^2+1)Y$, so that the amplitude of the plane wave solution would be a Lorentzian function of the pump-resonant

mode detuning. However, the nonlinearity tilts the resonance, being the origin of the well known optical bistability [86]. This means that for some certain values of X and Δ, (4.23) will give us three solutions for the amplitude of plane waves. CW solutions exist regardless of the dispersion regime (normal or anomalous), and in both cases they can be stable, unlike in the bulk and fibre systems in which CW waves are always modulationally unstable in the anomalous dispersion regime. For the following, however, we will restrict ourselves to the case of a cavity with anomalous dispersion, since the cavity soliton solutions for which we will study the emission of resonant radiation will exist for $\beta_2 < 0$.

Despite the three possible solutions that can be found for (4.23), most of the plane waves in the system will be unstable. Some will present modulation or homogeneous instability. For any detuning between the frequencies that are called in [92] $\Delta_{MI} = 1 - \sqrt{X-1}$ and $\Delta_{\uparrow} \approx 3(X/4)^{1/3}$, when $X \gg 1$, no stable solutions exist whatsoever. For detunings below Δ_{MI} continuous wave solutions exist, but they are of no interest for us since there is only one solution to Equation (4.23). We are interested in the region of $\Delta > \Delta_{\uparrow}$, which is where three solutions (albeit only one is stable) coexist for (4.23).

As explained in [92], specially in its very clarifying figure 1, and references therein (see [72, 78, 81, 82, 86, 97–100]), there are three extremely different types of solutions: Firstly, stable continuous waves, with the stability properties discussed above. Secondly, we have MI patterns, that exist in the regime of detunings where CW solutions are not stable. Depending on the detuning, these patterns can be stable or suffer chaotic evolution. And finally, cavity solitons (CSs), which are peaked solutions nested on top of a background. This background of the CSs is a CW solution, i.e., for a CS to exist we need to be in a regime of the detuning in which the CW solution is stable (otherwise the instability of this background would lead to a MI pattern). These cavity solitons are the preferred way of generating Kerr frequency combs (KFCs), since their tall and narrow temporal profiles mean that their spectrum will be extremely wide. An exhaustive analysis of the solutions and how they appear, as well as the existence of more complicated solutions (platicons [80], super cavity solitons [101], etc.) is out of the scope of this work. Nevertheless we will, for completeness, present the time profile and evolution of the CW, MI pattern, and CS solutions of (4.22), showing both the stable and chaotic MI patterns, as well as stationary and breathing CSs. A Gaussian-distributed noise with an amplitude 50

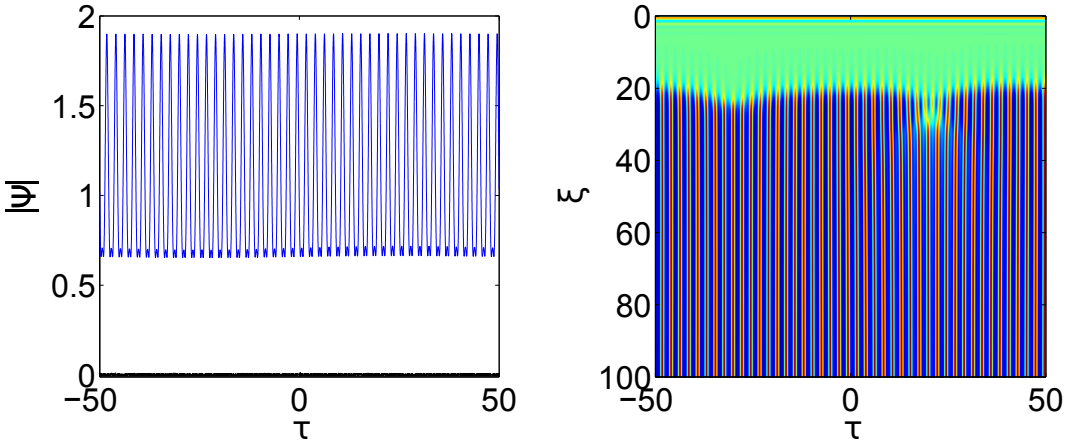

Figure 4.5: Final temporal profile (left) and evolution (right) of the field inside an initially empty cavity (except for a small noise signal) for $X = 10$ and $\Delta = -1$. The initial continuous state created by the pump is unstable and after a short transient creates a perfectly stable pattern. The total propagation distance is $\xi = 100$.

dB smaller than the initial signal is added to all the input fields in order to trigger any instabilities of the system for each set of parameters.

We start by showing in Figure 4.5 a stable MI pattern, which corresponds to $X = 10$ and $\Delta = -1$ in (4.22). Initially the cavity was empty, $\Psi_0 = 0$. As soon as the pump starts injecting energy into the system, the CW it creates starts developing oscillations due to the modulation instability, which eventually grow until a multipeak pattern is created. This transient is (relatively) short, and after the pattern is created at a propagation distance of approximately $\xi = 30$ there is no more dynamical evolution.

Now we change the detuning to $\Delta = 1$, while keeping all other parameters the same. This means that we have entered the region where the MI patterns are not stable any more. The result is shown in Figure 4.6. After the CW created by the pump suffers the MI process, patterns are constantly created and destroyed in a chaotic fashion, with the system constantly evolving in an unpredictable manner. In this case peaks of very different amplitudes might be created, and the interpulse distance might change with propagation. As it is clearly seen in the right panel, peak collisions and fission happen constantly during propagation.

In Figure 4.7 we can see the stable CW solution for $X = 10$ and $\Delta = 8$. The cavity was, excluding noise, initially empty, as in the previous cases. The pump feeds

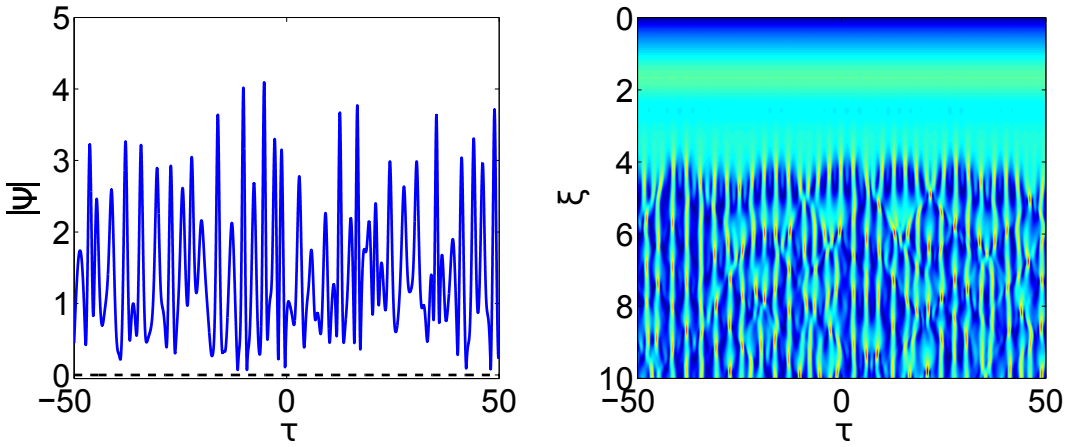

Figure 4.6: Time profile (left) and evolution (right) of a pulse after a propagation of $\xi = 10$ inside an initially empty cavity (except for a small noise signal). The other parameters are $X = 10$ and $\Delta = 1$. In this case the instability acts almost immediately and a multipeak pattern is created after a very short transient. This pattern is not stable and peaks are constantly created and destroyed.

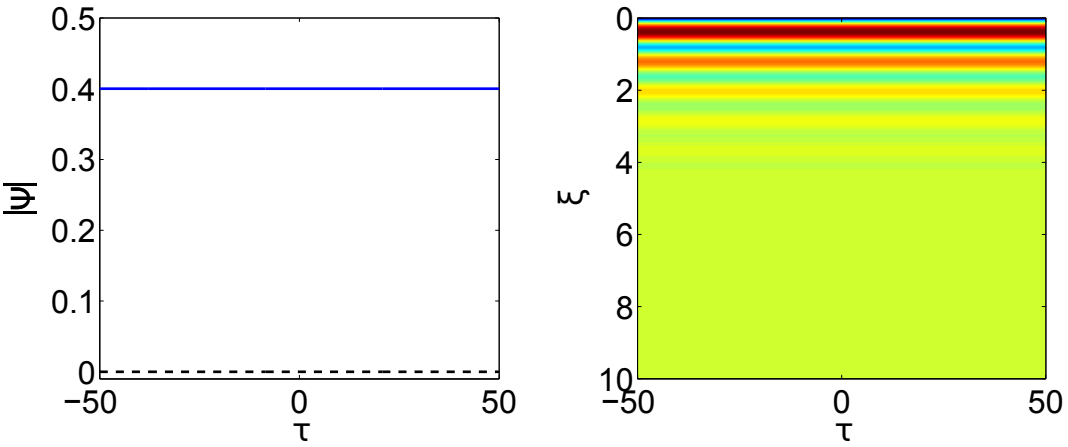

Figure 4.7: Time profile at the end of the propagation (left) and evolution (right) of the field for an initially empty cavity (except for a small noise signal) with $X = 10$ and $\Delta = 8$. The propagation distance is $\xi = 10$. For these parameters the CW solution is stable, so the pump feeds energy to the cavity and, after a transient in which the amplitude of the CW inside the cavity oscillates around the stable amplitude, it eventually stabilises at the predicted state.

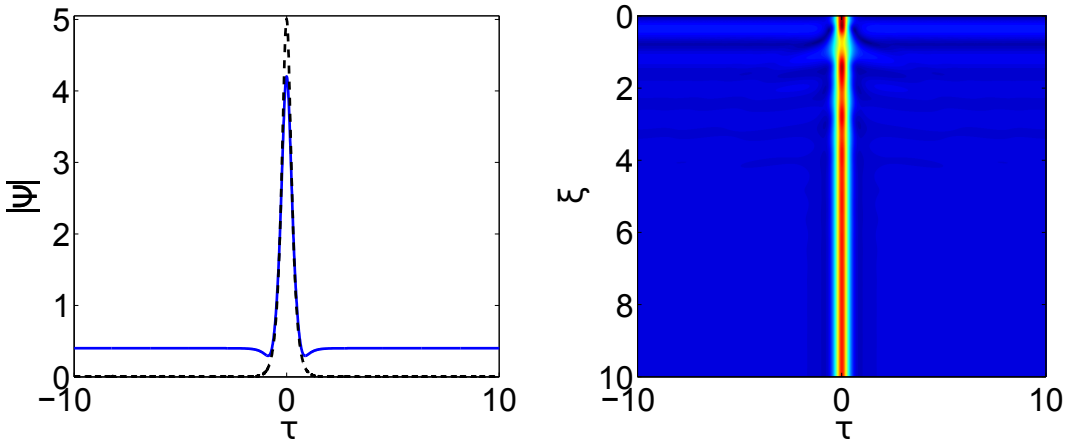

Figure 4.8: Time profile (left) and evolution (right) of an initial pulse $\Psi_0 = 5\ \mathrm{sech}\,(5\tau)$ for $X = 10$ and $\Delta = 8$. Being that the initial state had a peak of similar amplitude to the CS of the system for these parameters, the pulse evolves to form a stable soliton. After a short transient of approximately $\xi = 3$, the pulse does not change any more during the rest of the propagation (this is, $\xi = 10$). Non-vanishing tails with the amplitude of the stable CW for the parameters used are created by the pump, despite not being present in the initial state.

energy to the system until an equilibrium is reached after a short transient. Once the steady state CW solution appears no more dynamics happen in the system. This is always the final state when the cavity is initially empty and the external pump is constant, as long as the CW solution is stable.

Since all CS solutions coexist with stable CWs, we cannot excite them using a constant pumping in an empty cavity. Although this might be a problem in experimental setups, it is easy to numerically create a cavity soliton by having the initial field inside the cavity have a "soliton-like" shape. The evolution of this system when the parameters X and Δ are the same as in the previous case, but with $\Psi_0 = 5\ \mathrm{sech}\,(5\tau)$, can be seen in Figure 4.8. We find that the solution has a peak in time domain, but its tails do not decrease to zero far from this peak, as it happens in solitons of the NLSE. The fact that once this solution has been achieved the system becomes completely steady means that we have created a perfectly stable cavity soliton. The non-vanishing tails have the amplitude of the stable CW for the given values of X and Δ.

However, if we tried to create the CS state with $\Delta = 5$, we would find ourselves

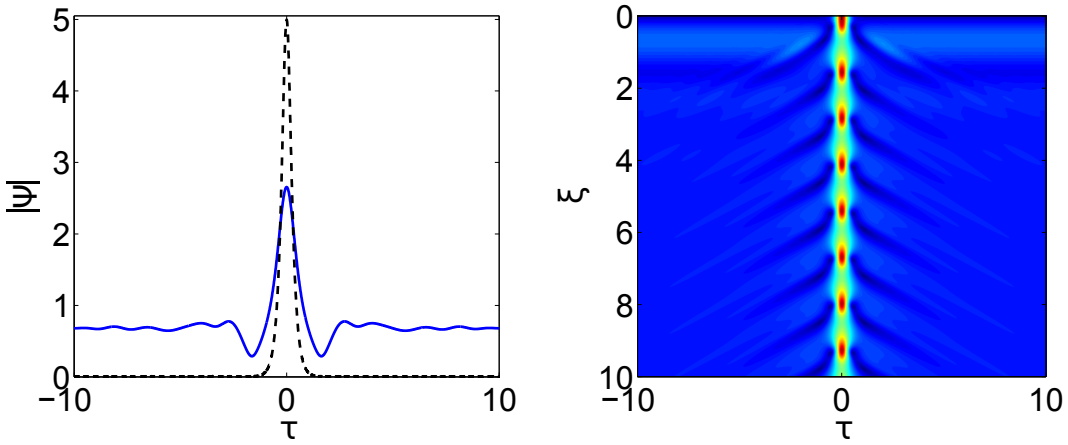

Figure 4.9: Time profile (left) and evolution (right) of an initial pulse $\Psi_0 = 5\ \mathrm{sech}\,(5\tau)$ for $X = 10$ and $\Delta = 5$. This state closely resembles the stable CS solution, but with a smaller amplitude. However, as it is evident from the contour plot, after the soliton is created it oscillates in a periodic fashion, completing several full cycles during the propagation of $\xi = 10$.

with a solution that is not completely steady, but has a periodic evolution. This is the signature of a breather solution, a class of soliton that oscillates continuously during propagation. Again, we need an initial peaked pulse in the cavity, because this type of solitons are also nested on top of a CW. After a short transient in which the tails (which were not present in the initial pulse) are created and the height of the peak moves towards that of the breather, the pulse starts evolving in a perfectly periodic fashion. This type of solution can be seen in Figure 4.9.

When we start analysing the new radiations emitted by solutions of the LLE equation when the new terms of the nonlinear polarisation are taken into account, we will be interested in the radiations emitted by the stable and deterministic solutions, i.e., cavity solitons and CW states. We have to be careful enough when choosing the parameters for the simulations, ensuring that the desired pulse is created into the cavity before analysing how it behaves under perturbations.

4.2.2 Brief introduction to RR in resonators

For now we will focus on CSs of the LLE and how they are affected by higher order dispersion, looking for some phenomenon analogous to the emission of RR in the usual NLSE.

As mentioned before, resonant radiation when a third (or higher) order dispersion term is included in the equations is a well known phenomenon in the passive cavity, and has been found experimentally on multiple occasions [71–75]. A theoretical analysis of the problem can be found in [71]. In that paper the authors do a perturbative treatment that is quite similar to the one shown in Chapter 2, and it is straightforward to adapt it to our equations. The starting point in a solution of (4.11), A_0, with a small perturbation that can be decomposed in Fourier modes: $A = A_0 + f\exp(ib(\delta)\xi - i\delta\tau) + g^*\exp(-ib(\Delta)\xi + i\Delta\tau)$. If we assume the dispersion operator is $\hat{D} = b_2/2 + b_3/6$, i.e., we only include dispersion up to third order, then linearising for small f and g leads to:

$$\begin{pmatrix} -b(\Delta) + M(\Delta) & 2A_0^2 \\ -2A_0^2 & b(\Delta) - M^*(\Delta) \end{pmatrix} \begin{pmatrix} f \\ g \end{pmatrix} = 0, \tag{4.24}$$

where the operator M is given by

$$M(\delta) = i(\Gamma + i\delta) - \frac{b_2}{2}(\partial_\tau - i\Delta)^2 - i\frac{b_3}{6}(\partial_\tau - i\Delta)^3 + 4|A_0|^2. \tag{4.25}$$

From the condition of the system having a non-trivial solution we can derive a dispersion law for the radiation. The resonance condition then reads [73]:

$$-\Gamma + i\frac{b_3}{6}\Delta^3 \pm i\sqrt{\left(2A_0^2 - \delta + \frac{b_2}{2}\Delta^2\right)^2 - A_0^4} = 0. \tag{4.26}$$

This relation shows that there will be two solutions for the frequency of the resonant radiation in the system, one for each choice of the sign before the square root. However, and since one of them is known to be significantly weaker than the other [71], we will do an approximation that will allow us to write the condition for the stronger resonance in a way that resembles the usual phase matching condition for the radiation in the NLSE, Equation (4.1). It is usually considered that, since the radiation due to higher order dispersion appears at the tails of the soliton, the amplitude of the field $|A_0|$ causing the radiation can be assumed to be the amplitude of the background over which the soliton is embedded, $|A_0| = |A_b|$. Doing this, and since the power of the background is usually small, we can neglect the second term in the square root of (4.26), which leads to a much more common form of the phase matching condition:

$$D(\Delta) \equiv \frac{b_2}{2}\Delta^2 + \frac{b_3}{6}\Delta^3 = \delta - i\Gamma - 2|A_b|^2. \tag{4.27}$$

From here it is completely straightforward to generalise the phase matching condition in resonators to higher orders of the dispersion. Being able to write this condition

for RR in a shape so similar to the well-known one for the solitons of the NLSE, only changing the nonlinear momentum for relevant parameters of the system (detuning, loss, and background amplitude), gives us a hint to what the phase matching conditions for NRR and THRR will look like. Deriving this explicitly will be our next task.

4.2.3 Extended Lugiato-Lefever equation and new resonant radiations in resonators

The first step to find NRR and THRR in the passive cavity is extending the formalism of the LLE to take into account the new couplings that appear beyond SVEA. With this, we hope to find new phase matching conditions for this system that generate radiations analogous to the NRR and THRR studied for bulk and fibre systems. This is quite straightforward in the IKeda map formalism. The only thing we need to do is to write the full nonlinear polarisation in (4.10) including the NK and THG terms. The presence of these terms does not affect the averaging procedure at all, provided their coefficients do not change much during a roundtrip, which is related to the approximation that the field will remain almost constant, and will work well in small cavities. The inclusion of the NK and THG terms leads to what was called in [102] the *extended Lugiato-Lefever equation* (eLLE):

$$i\partial_\xi A + \hat{D}(i\partial_\tau)A + i(\Gamma + i\delta)A - iP_{in} + \hat{S}(i\partial_\tau) \left[|A|^2 A + |A|^2 A^* \exp(2i\kappa\xi + 2i\mu\tau) + \frac{1}{3}A^3 \exp(-2i\kappa\xi - 2i\mu\tau)\right]_+ = 0. \quad (4.28)$$

All the scalings of the variables are as in (4.11), with κ and μ defined as usual. Once again our goal is using the method described in [77] to find the relevant phase matching conditions that will give us the frequency of the radiations emitted by cavity solitons due to all three nonlinear terms of (4.28). In analogy with the derivation we did of Equation (4.3), we decompose the field in a solution of the basic LLE Equation (4.11) and a small perturbation u. The resulting equation for the perturbation is:

$$i\left(\partial_\xi - i\hat{D}\right)u + 2g|A_b|^2 + i\Gamma g - \delta g = -\left(\hat{D} + \frac{1}{2}\beta_2\partial_\tau^2\right)A - |A_b|^2 A_b^* \exp(2i\mu\tau + 2i\kappa\xi) - \frac{1}{3}A_b^3 \exp(-2i\mu\tau - 2i\kappa\xi). \quad (4.29)$$

It is important to note that we are using the stable background solution $|A_b|$ as the one that enters the nonlinear terms (the ones that will create the NRR and THRR in the

system), since we know this background amplitude is the one responsible for resonant radiation in passive cavities. However, we have chosen to leave the full solution A in the first term, responsible for the usual RR, since in this case only the τ derivatives of the field enter the driving term. This term would therefore be trivially zero if we chose to use the CW amplitude as the solution of the unperturbed equation, A.

Although it might look like a technicality, this has a deeper physical meaning: The resonant radiation coming from the first term (which, we remember from our general analysis of (4.3), appears as a consequence of higher order dispersion acting on the solution of the equation in the SVEA limit) will only be present when the pulse inside the cavity has a non-trivial time derivative, i.e., CW solutions are always stable in the SVEA case because this driving term vanishes (they cannot emit RR). However, the other two phase matching conditions come from driving terms in which only the *amplitude* of the pulse is responsible for the driving force, so we expect to find NRR and THRR emission in CW configurations. This means that, beyond SVEA, CW solutions might not be stable any more if the phase matching conditions for the emission of NRR or THRR are satisfied. Cavity solitons, which have a non-zero time derivative around their peak, will emit all three kinds of radiations.

To find the explicit phase matching conditions we can apply the following phase shift to the perturbation field u:

$$u' = u \exp\left(-i\Delta\tau + i\left(D(\Delta) - \delta + i\Gamma + 2|A_b|^2\right)\xi\right), \tag{4.30}$$

so that the ξ derivative of u' will produce the terms necessary to cancel the extra terms in the left hand side of (4.29). This leads us to

$$i\left(\partial_\xi - i\hat{D}\right)u' = -\left(\hat{D} + \frac{1}{2}\beta_2\partial_\tau^2\right)A - |A_b|^2 A_b^* \exp(2i\mu\tau + 2i\kappa\xi) - \frac{1}{3}A_b^3\exp(-2i\mu\tau - 2i\kappa\xi). \tag{4.31}$$

The ξ dependent part of the phase on the left hand side is given by the phase of u', which is $(D(\Delta) - \delta + i\Gamma + 2|A_b|^2)$. Equating this with the phases of the three terms on the right hand side of the previous equation gives us the phase matching conditions:

$$D(\Delta) = -i\Gamma + \delta - 2|A_b|^2, \tag{4.32}$$

$$D(\Delta) = 2\kappa - i\Gamma + \delta - 2|A_b|^2, \tag{4.33}$$

$$D(\Delta) = -2\kappa - i\Gamma + \delta - 2|A_b|^2. \tag{4.34}$$

We see that these phase matching conditions closely resemble those obtained for fibres and bulk media, with the parameters of the cavity giving a constant that takes the role that the linear momentum had in the former derivation. More importantly, Equation (4.32), which gives the RR that was present already in the SVEA case, is exactly the phase matching condition derived in Equation (4.27) for the LLE in the approximation of small background amplitude. This is obviously an expected result, since finding a different phase matching condition for the RR in the model beyond SVEA would be a sign of problems in either of the two derivations. This serves as a consistency check between our model and the previous literature. However, finding the full phase matching conditions for the cavity, Equation (4.26), remains an unsolved problem for the eLLE (4.28), due to the explicit time dependence of the two new nonlinear terms.

As mentioned before, in this eLLE formalism we expect both cavity solitons and continuous wave solutions to emit resonant radiation. It is for this that we will now proceed to carefully analyse the evolution of these two types of fields in a cavity when the full nonlinear polarisation is taken into account and higher order dispersion is present in the system. The parameters we will use in our simulations are $\Gamma = 0.217$, $\delta = 0.5$, $\mu = 11$, $\kappa = 166$, and $P_{in} = 0.159$. b_2 is present in all figures, while in the ones where higher order dispersion is considered we also take $b_3 = 0.4548$. These parameters have been chosen due to their physical relevance, since, as explained in [102], they correspond to a microring cavity with a radius of $r = 30\mu m$ pumped by a CW input with a power of $P = 265$ mW and wavelength $\lambda_{in} = 1.55\mu m$. It is also assumed that $\gamma = 1(Wm)^{-1}$, the group index is $n_g = 1.5$, and the second and third order dispersion coefficients $\beta_2 = -10$ ps^2/km and $\beta_3 = -0.04$ ps^3/km.

We will start with the CW case. Although we only studied the solutions of the Lugiato-Lefever equation in anomalous dispersion, the CW solutions are stable for both normal and anomalous dispersion. A full analysis of the radiation they emit can be therefore done for both cases. As mentioned before, CW solutions will not emit the usual RR, since the driving term responsible for this radiation cancels for a flat solution. It is worth noting that, when κ is much bigger than the other parameters relevant in the phase matching conditions (4.33) and (4.34), as in the case we are analysing (since the amplitude of CW solutions is of the order of 1), the solutions for (4.33) when only second order dispersion is considered for a CW in normal dispersion are going to be extremely similar to the ones for (4.34) in anomalous dispersion.

In Figure 4.10 we plot the final spectrum of a CW when propagated for a distance

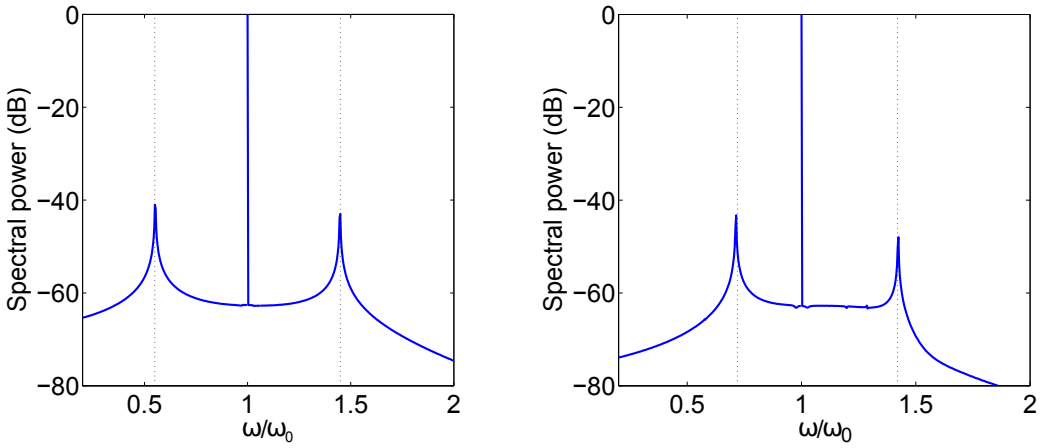

Figure 4.10: Final spectrum of a CW after a propagation of $\xi = 25$ in the normal dispersion regime. In the left plot only second dispersion is taken into account, while in the right one a third order dispersion term is included. The black lines mark the theoretically predicted frequencies for resonant radiations in the system. We can see a very good agreement in both cases. The rest of the parameters are given in the text.

of $\xi = 25$ using Equation (4.28). The left panel shows the result for b_2 only, while in the right one third order dispersion is included. For the case with only second order dispersion, as expected due to the parabolic shape of $D(\Delta)$, there are two resonant frequencies located symmetrically with respect to the pump, due to the NRR phase matching condition, since $D(\Delta) > 0$.

When third order dispersion is taken into account the situation is slightly different: one of the radiations is due to the NRR phase matching condition and the other one is THRR, since a b_3 term makes $D(\Delta)$ have different signs for big positive and big negative Δ. In particular, since $b_3 < 0$, $D(\Delta) < 0$ for Δ large and positive and $D(\Delta) > 0$ for Δ large and negative. Comparing this with the phase matching conditions (4.33) and (4.34) shows that the blue detuned peak corresponds to THRR while the red detuned one is due to NRR. This higher order dispersion is also the origin of the asymmetry in the position of the sidebands with respect to the pump. The asymmetry proves that these sidebands are indeed generated by the emission of resonant radiation and not by an usual modulation instability process, in which the new frequencies generated have the same absolute value of the detuning with respect to the original pulse.

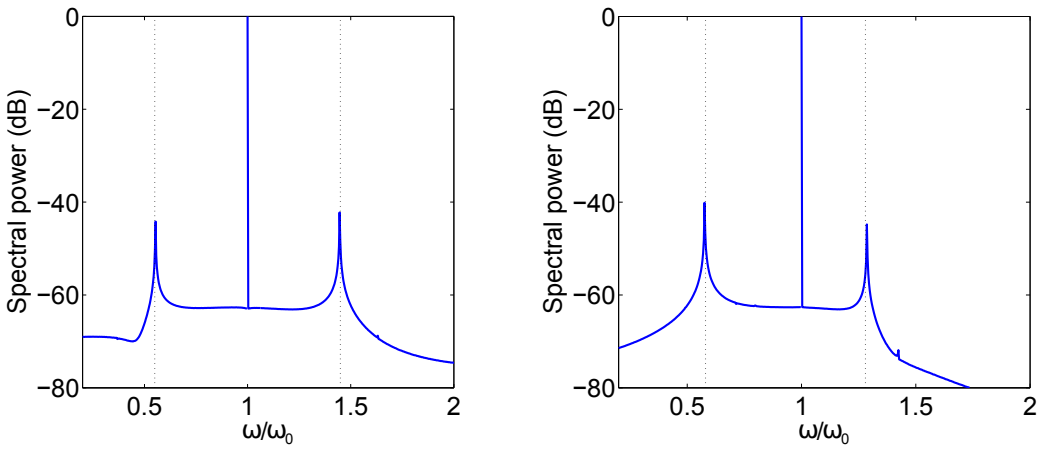

Figure 4.11: Final spectrum of a CW solution after a propagation of $\xi = 25$ in anomalous dispersion. The left panel is the case of b_2 only, while in the left one b_3 is included in our equations. The black dotted lines are the theoretical predictions for the radiation. The agreement between the theoretical and numerical positions of these radiations is very good in both cases. The value of the other parameters of the equation is as given in the text.

Figure 4.11 is as before but changing the sign of the second order dispersion. In the left panel we have again the result for b_2 only, while the plot in the right hand side is the final spectrum in the case with b_3. Since $D(\Delta) < 0$ for anomalous dispersion when no higher order terms are present, the two phase matched frequencies for which we expect radiation to be emitted come from condition (4.34). As discussed before, their position is practically the same as in normal dispersion. Introducing the third order dispersion also induces an asymmetry here. Since we did not change the sign of b_3, the behaviour is very similar to the previous case, with a blue detuned THRR peak and red detuned NRR one. The only change is that, due to the relative sign between b_2 and b_3, the THRR is less detuned than the NRR, contrary to what happened in normal dispersion.

To the best of the author's knowledge, no other instability of this kind is known to occur or has been predicted for CW solutions of the Lugiato-Lefever equation and its extensions. This new frequency generation process therefore changes qualitatively the behaviour and stability properties of these kind of solutions, and could potentially have a big impact on the propagation of light in small passive cavities.

Now all that is left is numerically simulating the propagation of a cavity soliton

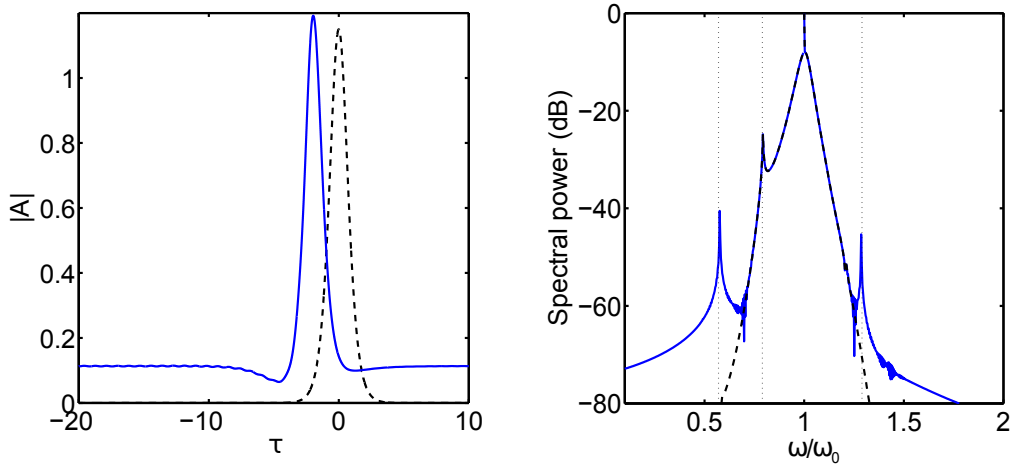

Figure 4.12: Left: Initial and final temporal profiles of pulse in the cavity when $b_3 \neq 0$. The peaked initial field generates a CS solution, which will drift and emit radiation due to the third order dispersion. Right: Final spectra for the pulse when propagated using equations (4.11) (black dashed line) and (4.28) (blue thick line). We see that the inclusion of the NK and THG terms in the equation generates two new radiation peaks in the CS spectrum, in addition to the RR peak present in the LLE. The resonant frequencies predicted by the phase matching conditions are marked by the vertical lines. The parameters used in the simulation are explained in the text.

solution under Equation (1.8). We would expect a very similar qualitative behaviour to the one seen in the bulk and fibre case, only with the frequencies of the radiation emitted given by the new phase matching conditions (4.32)-(4.34). In this case, and since a cavity soliton does have a nontrivial τ dependence, we expect to excite all three radiations when b_3 is present. It is worth insisting once again that the only difference between the simulation of a CW solution and a CS one is the initial state, which is a flat pulse for a CW, while we need a $N\text{sech}\,(N\tau)$ shape (with $N = \sqrt{2\delta}$) input field if we want to generate a CS inside the cavity [92].

In Figure 4.12 we see the result of propagating this initial seed pulse for a distance of $\xi = 25$ when the NK and THG terms of the polarisation are taken into account. The left panel shows the time profile of the intracavity field at the end of the propagation. We see that the pulse has slightly drifted due to the high order dispersion term. As before, this drifting needs to be taken into account in phase matching conditions if we want to have as precise a prediction of the resonant frequencies as possible, even though its effect here is small. We can also see that a small amplitude oscillatory pattern is starting to develop in the leading edge of the pulse, similar to the phenomenon

observed in Figure 4.2 (although in that case the oscillations appeared in the trailing edge due to the different sign of b_3).

The right panel compares the final spectra of the CS after propagation when using Equation (4.28) (blue thick line) and Equation (4.11) (black dashed line) with third order dispersion. The black vertical lines show the predicted positions of the RR, NRR, and THRR in the system, as given by (4.32)-(4.34). We see that the spectrum obtained with the usual Lugiato-Lefever equation already presents resonant radiation emission, as expected. However, the NK and THG terms of the extended Lugiato-Lefever equation are responsible for the appearance of two new radiation peaks at the exact positions where NRR and THRR are predicted. Therefore this numerical simulation supports our previous theoretical analysis of the problem and our derivation of the phase matching conditions for resonators.

With these dynamical simulations of the problem we close this section on the effect of negative frequencies on passive cavities. We have seen that striking new features appear when SVEA is broken in these systems. The instability of CW solutions could prove to be an important theoretical result, since these kind of pulses were expected to be perfectly stable before our formalism. And the emission of new resonant radiations by cavity solitons could have important consequences in the formation of Kerr frequency combs, since, as mentioned before, this type of solution is the preferred one to create these KFCs.

4.3 Super resonant radiation (SRR)

Up to now, we have found that most of the novel effects due to the extra terms that appear beyond SVEA, although qualitatively important (like the no-stability of the CW solutions in passive cavities), have a relatively small quantitative impact on the propagation of light. However, recent theoretical developments, backed by experimental results, have shown that this is not always the case, and that when working beyond SVEA some new phenomena happen that change the pulse propagation in a very noticeable way. This is the case of *super resonant radiation* (SRR) [29].

This radiation is in fact third harmonic resonant radiation that, when certain conditions are met, grows enormously with propagation, absorbing energy from the pump in a very efficient way, resulting in violent oscillations of the pulse in time

domain and a narrow, tall peak in frequency domain that can grow to have an spectral power bigger than the pump itself. Such a big modification of the behaviour of light in nonlinear media is the kind of experimentally relevant prediction that can give us further confirmation that the model based on Equation (1.8) is indeed useful, and valid to predict new features of light-matter interaction that are not present in simpler models. In fact, some experimental results suggest that this SRR has already been observed in diamond, when this material is pumped with extremely intense and short pulses.

In the following we will explain the concept of SRR from a theoretical point of view, and support our claims with numerical results. We will then proceed to briefly explain the experimental results that seem to support our hypothesis that THRR can grow enormously under certain conditions. Finally, we will explore the possibility of finding this kind of radiation in other experimental setups, as well as discussing the presence of SRR in other nonlinear equations that are relevant for fields other than optics, which suggest this phenomenon could be extremely general and applicable to a huge variety of systems.

4.3.1 Higher harmonic creation and its associated resonant radiation: Super resonant radiation

When studying resonant radiation beyond SVEA, we can see that the two different types of resonant radiations that have been experimentally identified come from the Kerr and negative Kerr terms of (1.8). In a sense, both terms have a similar effect on the propagation of a pump, since they add a nonlinear phase to intense light pulses, and the behaviour of the new resonant radiation coming from the NK term is analogous to the radiation caused by the Kerr nonlinearity. However, the THG term leaves a distinctive signature on the spectrum of a field propagated using (1.8): the generation of all odd harmonics of the signal that propagates in the material through cascaded third harmonic generation.

As mentioned earlier, third harmonic resonant radiation was not detected in the experiments that first described NRR, or even found numerically in the theoretical analysis of bulk silica performed in [25]. The authors of that last paper, being the ones that first predicted the appearance of this type of resonant radiation, explain the difficulties that they expected would make the experimental detection of THRR a real challenge.

The situation, however, took a turn recently, as reported in [29]. A numerical analysis of (1.8) has found a most striking feature of THRR that makes it stand apart from RR and NRR. The resonant radiation associated with the higher harmonic creation term of (1.8) can interact with said harmonics, growing to a level that was not expected in an effect that is mediated by a non-SVEA term.

The process can be understood as follows: the pump that propagates in a $\chi^{(3)}$ material gives energy to its third (and higher) harmonic mode. If the resonant frequency given by the phase matching condition associated with the THG term, Equation (4.6), is spectrally close to one of those high frequency modes, it will absorb the energy that was initially transferred to that specific high harmonic, concentrating it in a very narrow spectral region around the resonant frequency predicted for the THRR. The energy that was part of the input pulse is therefore transferred to a radiation mode in a two step process mediated by the odd harmonics of the pump frequency. The name "super resonant radiation" tries to emphasise this accumulation of a considerable amount of energy in an extremely narrow spectral region. This discovery could have important implications in supercontinuum generation and efficient frequency conversion.

The generation of SRR is not an easy task though: achieving phase matching between pump and THRR for a value of the resonant frequency that can interact with a high harmonic can be extremely complicated for long pulses. Shorter input fields have a much broader initial spectrum, and therefore the high harmonic peaks created by them when propagating will also have slowly decaying tails around the exact frequency of the high harmonic itself. Since, as we will see in our numerical simulations, radiation that is phase matched to a frequency that touches those tails will be promoted to SRR, we are interested in minimising the input pulse width as much as possible, so that the range of frequencies in which THRR can appear and still be converted in SRR is as broad as possible. This means that we will deal with pulses of only a few fs of temporal width, or, in our dimensionless units, a very small value of μ.

THRR also possesses another remarkable property: since for most physical systems $\kappa \gg 1/2$, the phase matching condition (4.6) will be satisfied for some detuning Δ such that $D(\Delta) < 0$. This means that for the most simple chromatic dispersion, in which only the second order term is accounted for, we will have two solutions of the phase matching conditions when we work in anomalous dispersion. We can obviously

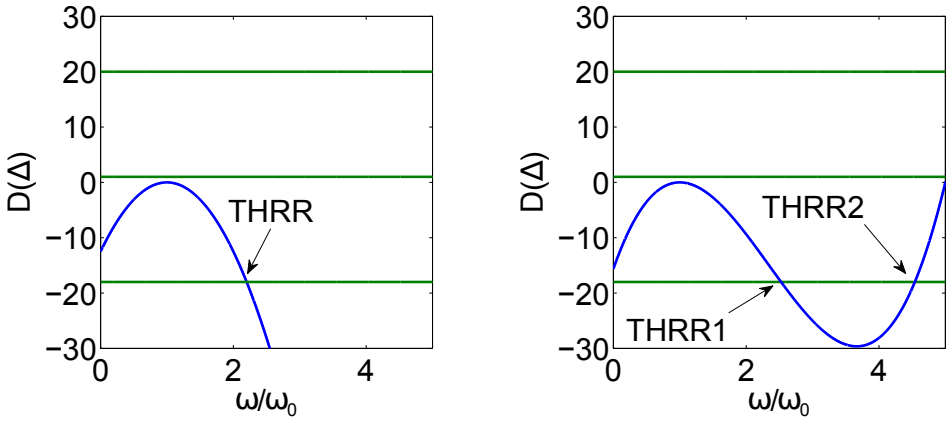

Figure 4.13: Phase matching curves for the cases of b_2 only (left) and including a $b_3 = 0.15$ term (right) for a system in which $\mu = 5$ and $\kappa = 10$. The points that satisfy the THRR phase matching condition are marked accordingly. We see that in all cases the THRR frequency will be close to the third harmonic of the pump frequency.

consider more complex scenarios with higher order dispersion terms, in which more solutions for the THRR resonant frequency can be found.

We will now explain thoroughly the analysis and results that were reported in [29]. In Figure 4.13 we see the phase matching curves for the two situations described above, this is, when only b_2 is present (left panel) and when we include a $b_3 = 0.15$ term in the equation (right panel). We have chosen the other parameters of the equation to be $\mu = 5$ and $\kappa = 10$ in both cases.

For the b_2 only case, the parabolic shape of the dispersion ensures, as we already mentioned, that there will be two solutions for the phase matching condition (4.6). Those two solutions will be symmetrically located around the pump frequency. If, as it is the case in this figure, the dimensionless detuning Δ between pump and resonant mode is bigger than 1 in units of the pump frequency μ, then the redshifted solution would have a negative frequency. As we have explained earlier, a very important part of Equation (1.8) is the filtering operator that ensures the field A will not contain any frequencies smaller than $-\mu$, so that $\mathcal{E}$ contains only positive frequencies, as it indeed should by definition. Therefore only the other, blueshifted mode can be excited.

In the case where third order dispersion is included, there are three crossings

between the dispersion curve and the THRR condition. For positive b_3 one of those solutions is again red detuned, while the other two are blue detuned and potentially close to the third harmonic. For the chosen values of μ and κ, and with $b_3 = 0.15$, the red detuned mode will be again killed by the filtering operation, whereas the other two will be around the third harmonic frequency. We therefore expect the former to be absent in the final spectrum of a pulse propagated using those parameters, while the two latter will absorb enough energy to be clearly visible as tall peaks in frequency space. As we will see later, this is indeed the result of dynamical simulations.

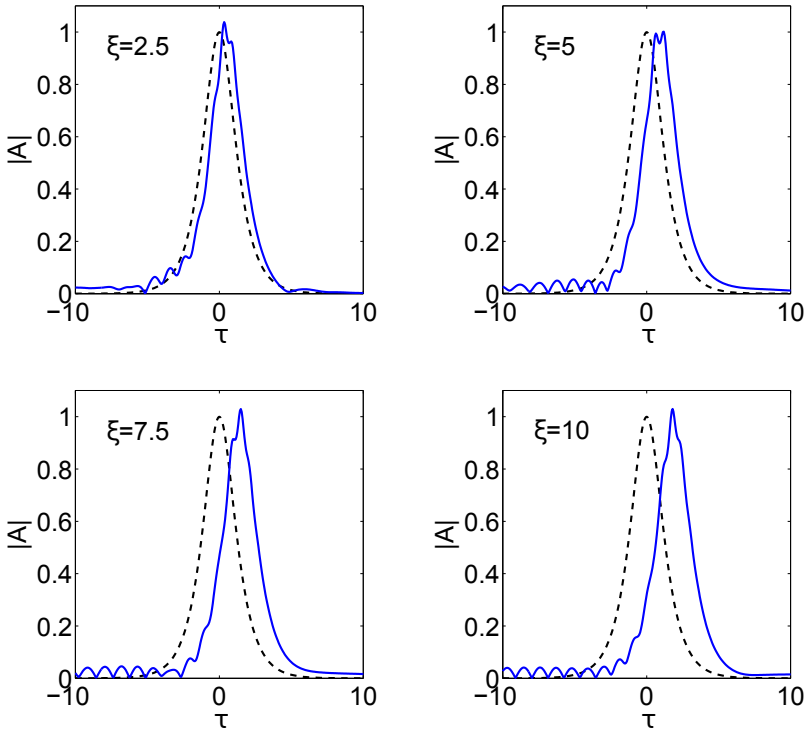

Figure 4.14: Evolution of a sech (τ) pulse under second order dispersion with $\mu = 5$ and $\kappa = 10$. We can see the violent oscillations that develop at the top of the pulse, and which are a signature of SRR. The black dashed line shows the initial profile of the soliton, and helps us see the (small) drift caused by the third order dispersion.

The importance of choosing a small value for μ is twofold: In the first place, the aforementioned slowly decaying tails of the third harmonic peak for short pulses. But a small value of this parameter also allows us to phase match the THRR to a frequency close to the third harmonic without having to use a big value for κ. This also helps maximise the effect of the radiation, since, as we know, the limit of κ and μ big is precisely the SVEA case, in which the exponentials in the NK and THG terms

oscillate so quickly that their effect in the pulse propagation averages to zero.

Now we will analyse the dynamical evolution of a sech (τ) field propagated using Equation (1.8) for the values of the parameters and the dispersion profiles that were used to generate the phase matching curves plotted in Figure 4.13. We will start with the simple case of second order dispersion only, in which the SRR phenomenon is extremely clear and easily visible, and then we will show how, although with some modifications, the main features of super resonant radiation emission are also present in the more complex scenario in which third order dispersion is included.

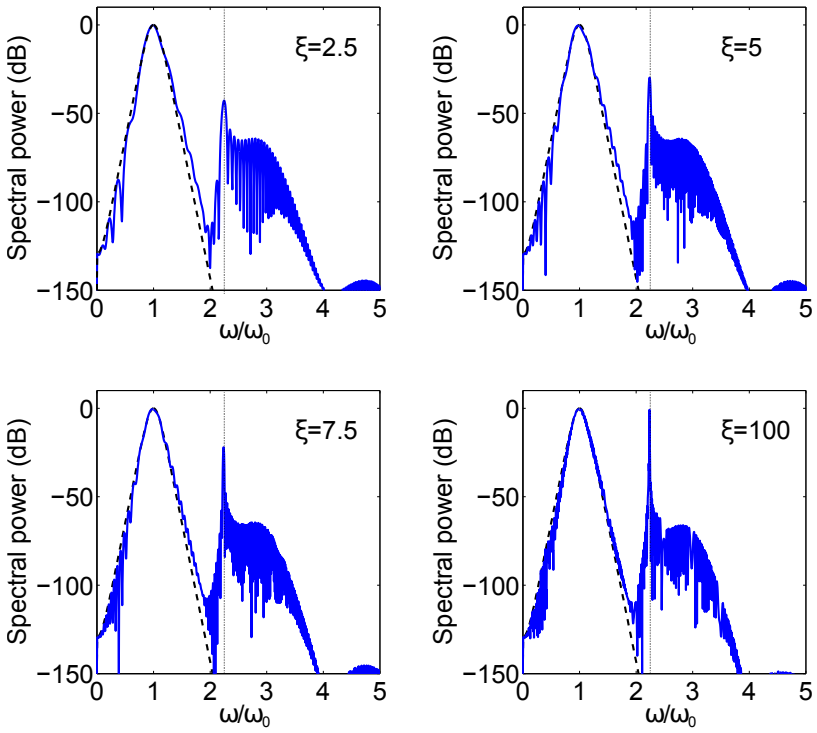

Figure 4.15: Initial and final spectrum of a sech (τ) pulse with the same parameters as in Figure 4.14. We can see the THRR peak that develops on one of the edges of the third harmonic of the pump frequency, and grows with propagation until its spectral power becomes comparable with the pump. The black dotted line shows the prediction of the position of the THRR by the phase matching conditions.

In Figure 4.14 we show the evolution of the time profile of the pulse with propagation. We can clearly see that some violent oscillations appear atop the pulse, which even visibly modify its amplitude. These oscillations then leave the pulse through its leading edge, but more radiation is being generated constantly in the pulse, as will become evident when we analyse the XFROG spectrogram of the final state. These

intrapulse oscillations in time domain are one of the signatures of SRR. We can also see that the soliton drift is small and therefore the phase matching conditions can be expected to be very precise even when the change in group velocity is not taken into account.

As for the spectrum, which is shown in Figure 4.15, we see the peak of the third harmonic resonant radiation at the position predicted by the phase matching curve in Figure 4.13. This peak starts developing shortly after the third harmonic appears, and keeps growing during propagation until its amplitude becomes comparable to the pump amplitude. We can now see clearly what we meant by the THRR being located in the tail of the third harmonic pulse: the width of the third harmonic component is such that the radiation develops on the slope of this pulse. It is due to this that the THRR is able to absorb energy from the third harmonic and become SRR.

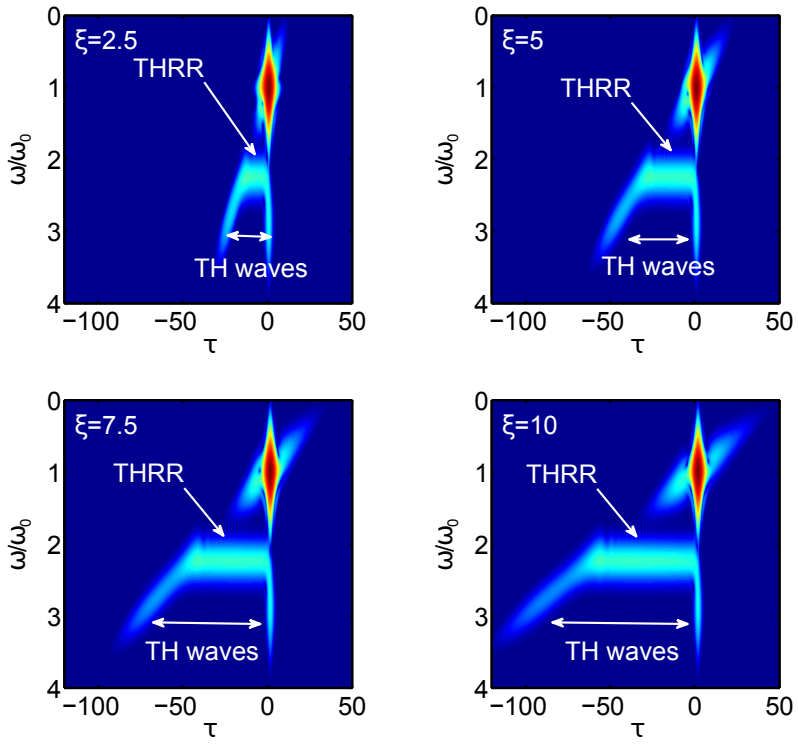

Figure 4.16: XFROG spectrogram for the pulse propagating with second order dispersion for various values of ξ. We see how the two different components of the generated third harmonic separate with propagation, and the THRR connects them. Since this last radiation is touching the third harmonic components it is emitted at a very high rate. The parameters chosen are as in Figure 4.14.

Figure 4.16 shows the XFROG spectrogram of the pulse at different stages during

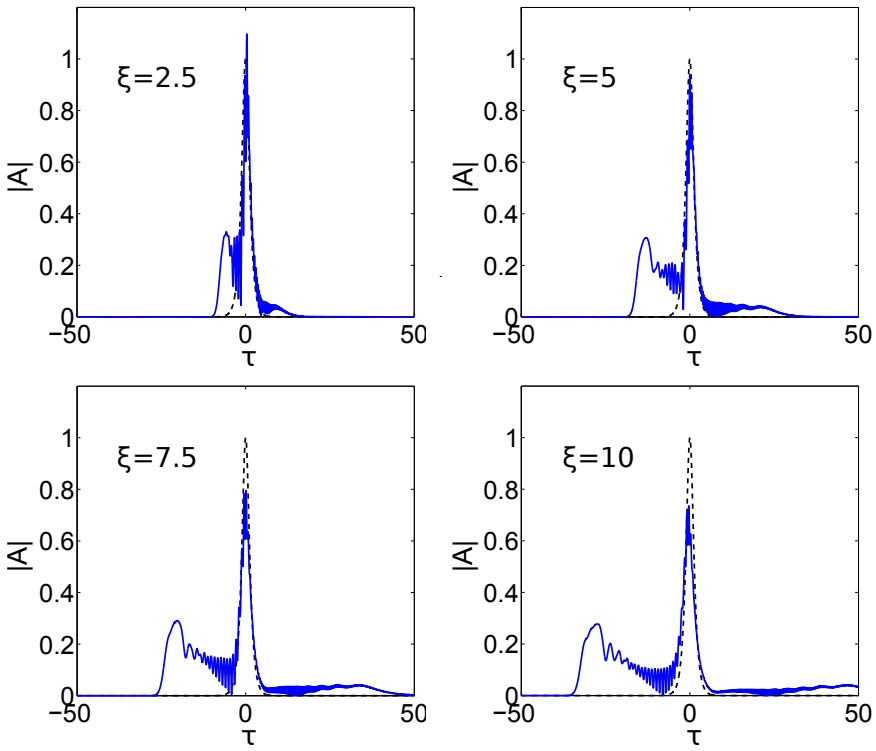

Figure 4.17: Time evolution of a sech (τ) pulse when $b_3 = 0.15$ and the rest of the parameters are kept as in Figure 4.14. We can see the two radiation tails we would expect in this case, due to the two phase matched frequencies for the THRR.

propagation. It is this figure that supports all our claims about SRR. What we see in it is that the third harmonic radiation created by the pump has two components, marked as "THG waves" in the figure. One of these components travels alongside the pulse, while the other one moves away with the group velocity that corresponds to its frequency. These two components of the third harmonic are connected by the third harmonic resonant radiation. It is because of the overlap between these two components of the third harmonic and the THRR that the rate at which this last one is emitted is greatly increased, generating SRR.

Although the nature of the phenomenon is the same when third order dispersion is included, the way it manifests in our simulations is rather different due to the complexity that the higher order dispersion adds. If we choose $b_3 = 0.15$, as we did in the phase matching curve shown in Figure 4.13, we expect to have two THRR peaks near the third harmonic of the input sech (τ) pulse. The existence of a third order dispersion also means that the group velocity will not change linearly with frequency

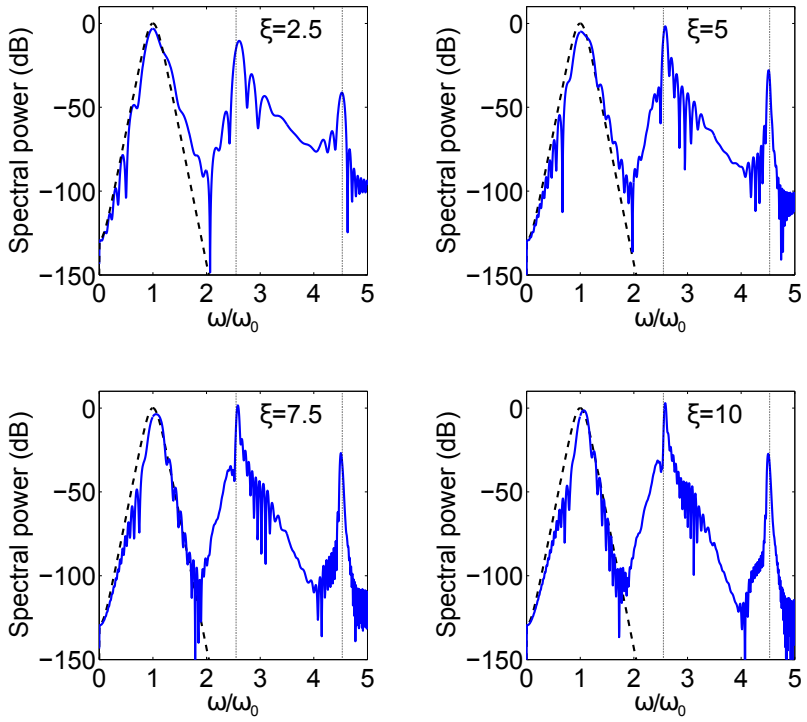

Figure 4.18: Evolution of the spectrum of the pulse shown in Figure 4.17. The black vertical lines mark the predicted positions of the THRR. We see how both peaks get much bigger than expected for a negative frequency effect (see Figure 4.4 for comparison). However, the one whose frequency is closer to the third harmonic of the input pulse is the one that gets big enough to overgrow the pump spectral power.

any more, but in a parabolic fashion. This will make the XFROG of the propagated pulse much less clear than it was in the b_2 only case.

In Figure 4.17 we have the time evolution of the pulse in time domain. As we can see, we have indeed two strong radiation tails, one in the leading edge and another one in the trailing edge of the soliton. It is the former that has a much bigger amplitude, although the latter also has a considerable amplitude for a process coming from the THG term.

The spectrum of the pulse is shown in Figure 4.18. In this case we see two peaks of THRR developing, exactly at the positions predicted by the phase matching conditions (black vertical lines). We see that both are indeed bigger than we would expect for a THRR peak, but the one that is closer to the third harmonic frequency has grown much more, surpassing the input pulse spectral power in the process. These

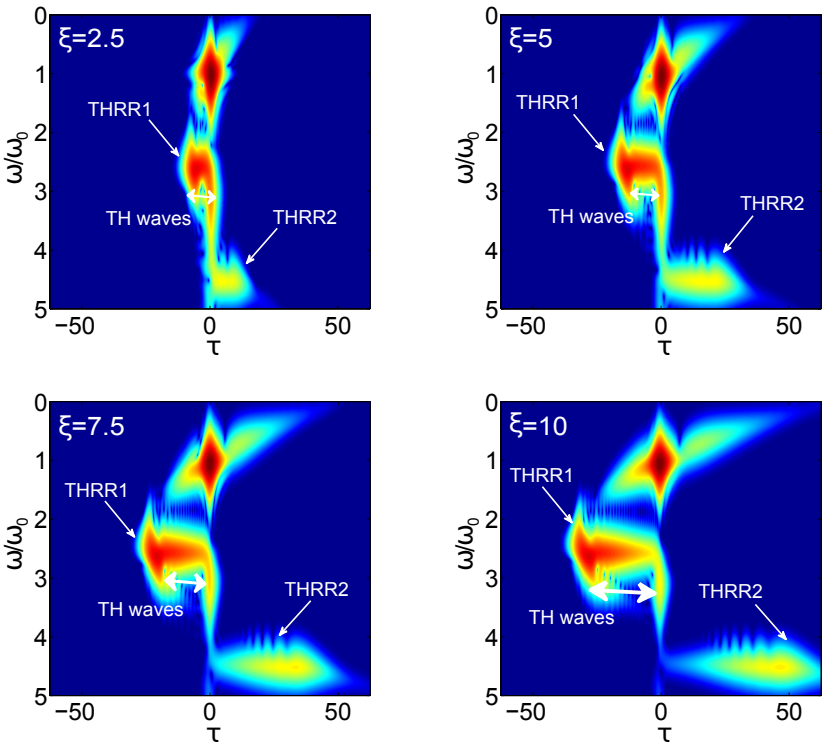

Figure 4.19: XFROG of the pulse at certain points of its evolution, with all parameters as in Figure 4.17. We see again the two components of the third harmonic, but in this case we also have two radiations due to THRR. The one closer to the third harmonic frequency is precisely the one that connects the two components of the third harmonic, being the one that is converted in SRR again.

two peaks have absorbed so much energy that, in fact, there is no distinct feature at the third harmonic frequency. All that is left of the third harmonic pulse is a small oscillation on the tail of the SRR of the system. Again, the fact that the peak closer to the third harmonic is the one that is most efficiently fed by the pump shows that the THRR becomes SRR when it is stimulated by the third harmonic pulse, in the two step process described above.

The XFROGs showing the evolution of the pulse are presented in Figure 4.19. We can see again how the third harmonic has two components, one that moves away from the soliton due to the phase velocity missmatch between the pump and the radiation at three times its frequency, and another one that stays with the pulse during propagation. In this case we have two resonant radiations due to THRR emission: One close to the third harmonic, and that once again connects the two components of the third harmonic; and another one further blue detuned, that propagates away

as given by the parabolic dependence on the frequency of the group velocity. Both of them are emitted continuously, as is clear from the spectrogram, and also overlap with the third harmonic. However, the one closest to the third harmonic waves in both frequency and time domain is the one that absorbs the most energy. Once again, this numerical results support our hypothesis of SRR being due to the THRR being stimulated by the third harmonic itself.

Up to now, we have studied SRR from a completely theoretical point of view. It is not obvious how this effect could affect experiments, since the value of the parameters used in our simulations ($\mu = 5$ and $\kappa = 10$) are very extreme and not achieved in any current experiments, to the best of the author's knowledge. It is for this that a more complex approach to SRR is needed if we want to apply it to experimentally feasible situations. We deal with this problem in the next section.

4.3.2 Experimental accesibility of SRR

In the paper that first described the phenomenon of SRR [29], there is a section devoted to the results of an experiment that achieved results compatible with the presence of SRR in the system. This experiment was performed by Thomas Roger and Daniele Faccio. We will briefly discuss the results they obtained here, and explain their relation to the numerical results explained above. After this, we will discuss the possibility of finding SRR in a completely different experimental setup, namely the fibre lasers in which the presence of a doping material in the propagation medium prevents pump depletion, which could be a serious issue for the long propagations that would allow SRR to grow to a level in which its spectral power would be comparable with the pump.

For the performed experiment 50 fs pulses were injected in a $500\mu m$ piece of bulk diamond. An amplified Ti:Sapphire laser with central wavelength $\lambda_0 = 785$ nm was used to pump an optical parametric amplifier (OPA, TOPAS-C, Light Conversion Ltd.) producing infrared light pulses whose wavelength could be tuned between 1750 and 2050 nm. The resulting pulses were produced at a repetition rate of 100 Hz and with pulse duration of 70 fs. The IR pulses were focused with an $f = 150$ mm lens to a spot radius of $\sim 36\mu m$, providing a peak intensity of $I = 28$ TW/cm^2. A single crystal diamond cut along the $\langle 100 \rangle$ axis was used to study the dynamics of the THRR as the pump wavelength is tuned. The output of the diamond crystal was imaged onto a spectrometer (Andor Shamrock 303i and iDus DU420A), providing visible spectrum

data. In order to isolate the 5th harmonic from the intense 3rd harmonic contribution and have enough dynamic range, the high frequency component ($\lambda < 510$ nm) was blocked inside the spectrometer.

The phase matching conditions in this experiment are qualitatively different from the ones presented in this thesis so far. This is because the dispersion in bulk diamond is always normal, which means temporal solitons cannot propagate in the material. In this case the resonant radiation emission is not coming from a soliton, but from the formation of a shock front [103]. This means that the shock term of the equation cannot be overlooked as in previous derivations. Note that for the theoretical explanation of the experimental results we will work with dimensional units, since they suit better the analysis of an experimental setup. The authors of reference [103] write the nonlinear momentum of an intense pulse propagating in a material as

$$D_0 = \beta(\omega_0) + \gamma P \left[1 + \frac{\Delta\omega}{\omega_0}\right], \tag{4.35}$$

whereas the linear momentum of the CW radiation with frequency ω_r is obviously given by the dispersion relation as $\beta(\omega_r) = \beta(\omega_0 + \Delta\omega)$.

With our system being bulk diamond, we know that the γP nonlinear term has to be substituted by $k_0 n_2 I$ [3], where $k_0 = \omega_0/c$, I is the intensity of the pulse, and n_2 the nonlinear refractive index (so that $n_2 I$ gives the total change in the refractive index due to nonlinear effects). Equating both momenta, and in the comoving reference frame, we have:

$$\begin{aligned}\beta_0 - \beta_1\omega_0 + k_0 n_2 I\left(1 + \frac{\Delta\omega}{\omega_0}\right) = \beta(\omega_0 + \Delta\omega) - \beta_1 \cdot (\omega_0 + \Delta\omega) \Rightarrow \\ k_0 n_2 I\left(1 + \frac{\Delta\omega}{\omega_0}\right) = \beta(\omega_0 + \Delta\omega) - \beta_0 - \beta_1\Delta\omega. \end{aligned} \tag{4.36}$$

When the condition above is satisfied we would have resonant radiation in the system. The left hand side plays the role of nonlinear momentum of the intense pump. By analogy with the usual derivation of the phase matching conditions for THRR, Equation (4.6), we can write the phase matching condition for THRR fed by a shock front in normal dispersion as

$$-2\Delta k + 3k_0 n_2 I\left(1 + \frac{\Delta\omega}{\omega_0}\right) = \beta(\omega_0 + \Delta\omega) - \beta_0 - \beta_1\Delta\omega, \tag{4.37}$$

where Δk is the dimensional version of κ, $\Delta k = \beta_1\omega_0 - \beta_0$. There is one more thing that we need to take into account if we want to predict the phase matched

frequencies as accurately as possible. As we mentioned several times before, the pump producing the resonant radiation will drift due to this radiation emission, changing its group velocity. Although this correction is small, we need to do it to achieve perfect agreement between the theoretical and experimental results. This means that we should include a small correction factor v to the group velocity term in the phase matching condition, i.e., we have to write

$$-2\Delta k + 3k_0 n_2 I\left(1+\frac{\Delta\omega}{\omega_0}\right) = \beta(\omega_0+\Delta\omega) - \beta_0 - v\beta_1\Delta\omega. \tag{4.38}$$

We discuss more about this correction factor and its value later on, when we compare this model with the experimental results.

All that is left now is using the parameters of the input pulse and the properties of bulk diamond in (4.38) to derive the phase matched frequencies. We need to know the value of the linear refractive index n (from which we can derive β as $\beta(\omega) = n(\omega)\omega/c$), and its nonlinear counterpart n_2 for diamond. These can be found in the literature (see for example [104] and references therein) to be:

$$n(\lambda) = \sqrt{1+\frac{0.3306\lambda^2}{\lambda^2-0.106^2}+\frac{4.3356\lambda^2}{\lambda^2-0.175^2}}, \tag{4.39}$$

$$n_2 = 1.26\cdot 10^{-3}\frac{\mathrm{cm}^2}{\mathrm{TW}}, \tag{4.40}$$

for λ expressed in μm. With this we have all we need to solve the phase matching condition for the THRR, Equation (4.38), and get the theoretical predictions for the position of the radiation emitted by the shock front.

Figure 4.20 shows the plot of the phase matching curves for two pump wavelengths, $\lambda_{in} = 1.85\mu m$ and $\lambda_{in} = 1.95\mu m$. The vertical lines show the position of the pump and its fifth harmonic. We can see that the first one corresponds to one situation in which the THRR emitted by the pump has a longer wavelength than the fifth harmonic, while for the second one both the THRR and the fifth harmonic are at the same position. This means that for $\lambda_{in} = 1.95\mu m$ we expect to find a peak of stimulated THRR, which will be bigger than the one found for $\lambda_{in} = 1.85\mu m$. Note that, since the left hand side of equation (4.38) has an explicit dependence in $\Delta\omega$, the value that $D(\omega_r)$ has to take to satisfy the condition is not a constant but has a ω_r dependence, therefore we do not have horizontal lines that the dispersion needs to cross any more. This is the effect of the shock term in the phase matching conditions.

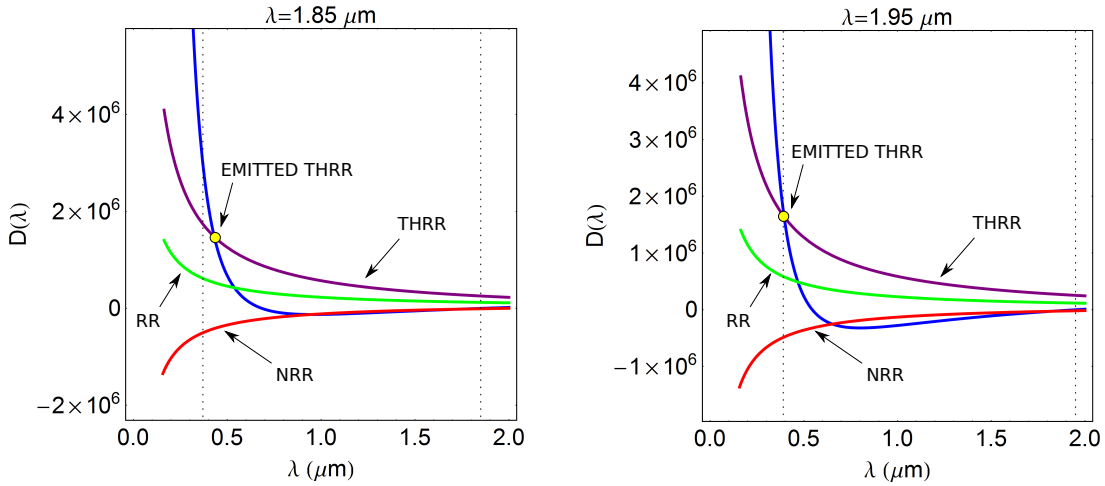

Figure 4.20: Phase matching curves for the experimental setup described in the text. The blue line represents the CW dispersion relation, while the other three lines are the phase matching conditions calculated as explained in the text. The dotted vertical lines mark the wavelengths of the pump and its fifth harmonic. We have chosen two of the pump wavelengths shown in Figure 4.21, one in which the THRR has a bigger wavelength than the fifth harmonic (left), and another one in which both have the same wavelength, and therefore the THRR becomes SRR (right).

With this discussion on how the phase matched frequency of the THRR emitted by a pulse propagating in normal dispersion is calculated, we close the theoretical analysis of the experiment reported in [29]. Now we can proceed to compare our theoretical predictions with experimental results.

Figure 4.21 shows the high-energy part of the output spectrum after a propagation of $L = 500\mu m$, while progressively varying the input pulse wavelength from 1750 nm to 2050 nm. The fifth harmonic of the pump, i.e, the wavelength that satisfies $\lambda_{5^{th}} = \lambda_{in}/5$, is marked by the red line. We can see that an additional peak is observed, which shifts towards shorter wavelengths when increasing the pump wavelength (i.e., its frequency increases as the pump frequency decreases). The position of this peak can be perfectly fitted by the black line shown, which is the prediction for the position of THRR in the system based on the phase matching conditions detailed above. We see that when the THRR and fifth harmonic peaks have similar frequencies, i.e. when the pump wavelength is $\sim$ 1960 nm, the THRR amplitude grows considerably.

To achieve this perfect agreement between the calculated position of the radiation and the experimental result, we have chosen the following value for the correction

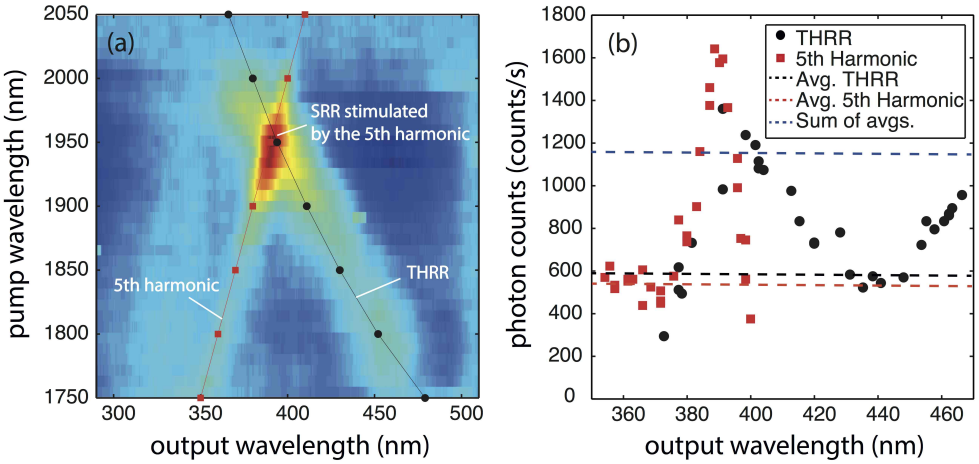

Figure 4.21: Left: Experimental result for the final spectrum in the vicinity of the fifth harmonic of a pulse as a function of the input wavelength. The position of the fifth harmonic and the the fit for the THRR are marked by red and black lines respectively. Right: Peak amplitude for the fifth harmonic and the THRR as a function of their location in the spectrum. We see that at the peak generated when both radiations are at the same spectral position the amplitude is significantly bigger than the simple addition of the amplitudes of the individual peaks. These experimental results and figure are courtesy of D. Faccio and T. Roger.

factor v:

$$v = 1.01 + 0.01\frac{\lambda_{in} - 1.75}{0.05}, \tag{4.41}$$

for λ_{in} expressed in μm. We see that this correction is a factor of $v = 1.01$ for an input wavelength of $\lambda_{in} = 1.75\mu m$, and that from there it changes linearly by ± 0.01 when we change the input wavelength by $\pm 0.05\mu m$. The input wavelengths experimentally analysed change between $\lambda_{in} = 1.75\mu m$, for which the correction factor takes the aforementioned value of $v = 1.01$, and $\lambda_{in} = 2.05\mu m$, which means $v = 1.07$. The parameter v has thus a value close to 1 for the whole range of input wavelengths studied, as would correspond to a correction factor accounting for a drift that, as we emphasized many times before, is usually small. This specific parametrisation has been chosen because it is the linear model for v that produces the most accurate predictions for the position of the THRR in the experiment.

Due to the normal dispersion of diamond, which does not allow the formation of a soliton, the propagation distance has to be short, or otherwise the pulse would disperse and its amplitude decrease to the point where nonlinear effects are negligible. This limitation of the propagation distance means that the efficiency of the conversion of

energy to SRR is not as big as in the numerical simulations presented before, although it has been stimated to be larger than 10^{-5}. Even then, these results show that the phenomenon of SRR generation is very general and relies only on the crossing of the THRR emission with a higher-order harmonic.

The right panel of the same Figure 4.21 shows the peak intensities of the fifth harmonic and THRR taken along the red and black solid lines from the left panel. There is a clear enhancement of the peaks at the point at which their emission wavelengths are overlapped ($\lambda_{in} \approx 1960$ nm). We find that the amplitude of the peak at that point is bigger than the simple addition of the amplitude we would expect both peaks to have separately by analysing their amplitude when they are separated. This is the signature of a *stimulated* process, in which the fact that the fifth harmonic and the THRR are spectrally close creates a synergy that means a bigger than expected fraction of the pump energy is transferred to radiation.

After showing how the results of this experiment can be perfectly explained by our theory, giving us a first experimental hint of the emission of super resonant radiation, we will proceed to study a different system which might be of help in the experimental search of SRR.

This completely different approach which could prove useful in finding the emission of ultra-intense SRR (and all negative frequency effects in general) is including the nonlinear non-SVEA terms in the equations modelling fibre lasers. In these systems light propagates in a doped material, which means that it will experience a gain that can compensate the losses suffered during propagation, resulting in the creation of stable pulses [105–112]. These systems are usually well described by a Ginzburg-Landau (GL) equation, but sometimes it is necessary to include refinements that make the model more realistic, see for example [110]. The most usual form of the GL equation in anomalous dispersion is:

$$i\partial_\xi A + \left(\frac{1}{2} + ib_2^{im}\right)\partial_\tau^2 A + (1 + i\gamma^{im})|A|^2 A - igA = 0, \tag{4.42}$$

The GL equation looks formally similar to the nonlinear Schrödinger equation, but including a linear term in the field A, as well as allowing the second order dispersion and the nonlinear parameters to be complex. The linear term would represent a gain in the system given by the doping and that depends on the real and positive parameter g. The complex second order dispersion coefficient b_2^{im} accounts for a

frequency dependence of the linear gain. If we only include this second order term in our equation the spectral gain would be parabolic, i.e., it would decrease around the central frequency as $-\mu^2$, becoming negative for sufficiently large detunings. Since the gain profiles in frequency domain of a doped fibre can usually be realistically modelled by a Lorentzian profile, this second order approach is valid only when the spectral width of the pulse is of the order of the gain width. An imaginary nonlinear parameter γ^{im} would account for a loss coming from two photon absorption.

This modelling based on the GL equation has several limitations. First of all, and as mentioned before, it is only valid for very spectrally narrow pulses, otherwise the approximation of parabolic gain fails to model the dynamics completely. It also shows limitations when dealing with the linear gain, which acts on arbitrarily small pulses, meaning that even the small numerical noise will be amplified. In this situation stable steady states will never be achieved. This is not the case in realistic systems, in which only pulses with a power above a certain threshold are amplified. The gain is also not constant due to saturation of the gain and the non-instantaneous response of the doping material, which will have a relaxation time, meaning that the gain coefficient g will not be a constant but have some dynamical evolution [110].

Many of these limitations can be traced back to the fact that fibre lasers are not a single piece of fibre but a complex setup in which light propagates through different materials and is affected by many different optical devices. The GL equation is just an averaged mean field model. It can be derived as a reduction of more complex models, see for example [106, 107]. Since Equation (4.42), as mentioned before, does not allow for stable perturbed solutions, we need to work with some extension of it that will not amplificate small amplitude radiative emissions that would lead to chaotic behaviours or unstable pattern formations.

Moreover, our new resonant radiations coming from negative frequency effects are usually far detuned from the pump. In the specific case of SRR, it should be near the third harmonic. We also need a pump with a broad spectrum to excite this radiation, which will break the parabolic gain approximation. We need to adapt Equation (4.42) to be valid in a range of frequencies wide enough to at least reach the third harmonic of the input pulse.

The way to solve all these problems is not trivial at all. First of all, if we want to have a power threshold for the amplification, we need a *nonlinear* gain. This means

that the parameter γ^{im} of (4.42) has to account not for the loss associated to two photon absorption, but for some nonlinear gain in the averaged system. This means that only pulses with a significant amplitude will be amplified. However, if we only changed the third order nonlinear term in this way, pulses with a big amplitude would be amplified continuously until their peak power diverges. This is a completely non-physical effect, and to regularise it we need to include a saturation of the nonlinear gain in the form of a quintic order nonlinear loss term [113]. This term arises from a power series expansion in $|A|^2$ of the gain of the system, as shown in [106,107]. As for the linear gain/loss, the correct and experimentally relevant model to use is to make the linear term account for a loss, while we add an extra gain that considers the full Lorentzian profile in the spectral domain.

About the self phase modulation terms, we will keep the three nonlinear terms we have in Equation (1.8), extending the usual formalism of GL lasers to include negative frequency effects. The fact that all other effects we are introducing in our equation are only gain and loss effects means that the phase matching conditions will not be noticeably affected, as long as these effects are small.

Once we have chosen the phenomena that our equation needs to take into account to accurately represent a realistic experiment, writing it down is an easy task. The relevant equation in our case, including all the terms discussed above, is:

$$i\partial_\xi A + \hat{D}(i\partial_\tau)A + p_{nl}[A] = i\Gamma A + i\epsilon|A|^2 A + i\nu|A|^4 A + i(G \otimes A). \tag{4.43}$$

In this equation we can choose any form of the dispersion and nonlinear polarisation we want, and we have defined three parameters Γ, ϵ, and ν, responsible for the (dimensionless) linear, cubic, and quintic gain/loss respectively. An important part of the evolution equation is the convolution represented by the last term in the right hand side of (4.43). This represents the linear gain experimented by the spectral components inside a narrow band around the pump frequency. The gain function G in frequency domain would be:

$$\tilde{G}(\Delta) = \frac{g_0}{1 + \frac{|A|^2}{E_{sat}} + \frac{\Delta^2}{\Omega^2}}. \tag{4.44}$$

This gain has the correct Lorentzian profile we need as a function of the detuning between a spectral mode and the pump, Δ, and also includes a term that kills the linear gain when the power in the system is big compared with a parameter E_{sat}. This saturation energy parameter gives the scale at which the gain due to the doping

saturates due to the intensity of the pulse in the material. For further details about the theoretical models for fibre lasers, the physical significance of our equation, or realistic values of the parameters, see [114, 115].

Now that we have the equations for our system we will do a numerical analysis to check how the gain/loss terms affect the formation of SRR. The importance of this analysis is that, up to now, we have completely ignored losses in the system, although all physical materials have some kind of absorption. These losses will affect the emission of all types of resonant radiation in two ways. On one hand, the radiation itself will be damped, causing the associated peak in the spectrum to have less amplitude than in the lossless case. On the other hand, the pump amplitude will decrease with time, meaning that less energy will be transferred to the radiation. It is because of this that fibre lasers offer an excellent opportunity to look for negative frequency effects: they allow for longer propagations due to the gain terms that compensate the material absorption.

Figure 4.22 shows the result of numerical simulations in which losses are included. We show the final time profile and spectrum of a sech (τ) pulse after a propagation of $\xi = 5$ when only second order dispersion is considered and for $\mu = 5$, $\kappa = 20$. The left panels show the result of solving Equation (1.8) when a linear loss term is included. In the right panels the equation for a fibre laser (4.43) is used. In both cases the linear loss parameter takes a value of $\Gamma = -0.05$. For the fibre laser, the rest of the parameters are $\epsilon = 0.3$ for the cubic gain, $\nu = -0.2$ for the quintic loss, $g_0 = 0.1$ for the gain around the resonance, $E_{sat} = 2$ for the saturation energy, and $\Omega = 0.25$ for the resonance width.

The results clearly show that, as expected, linear loss reduces the pump amplitude, which we can see has also a big effect on its spectral power, especially for the components that are far from the central frequency. SRR is still excited, but the peak amplitude is much smaller than in the fibre laser case. For this system we see a very sharp and clear SRR peak even for such a short propagation distance. In time domain, the pump amplitude not only does not decrease, but its maximum value has actually increased due to the nonlinear gain until a point in which an equilibrium with quintic loss is achieved. The radiation tail leading the soliton can also be seen to have a bigger amplitude, which is in line with the bigger spectral power transferred to the radiation mode. We should note that as a result of the pulse amplitude growing, the pulse power will not be $P = 1$ any more in our normalised units, which means

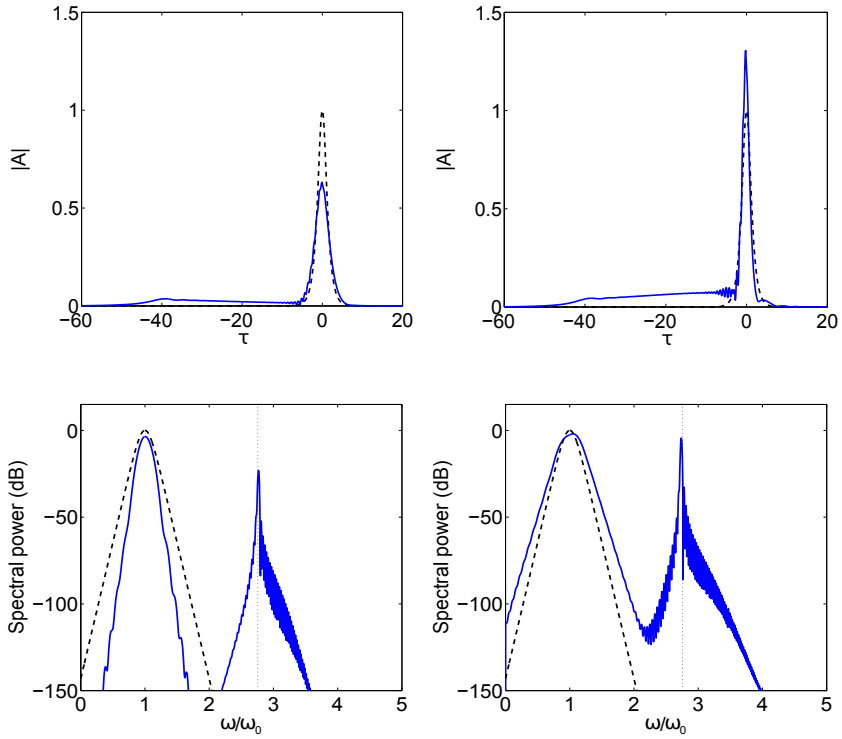

Figure 4.22: Time profile and spectrum of a sech (τ) pulse after a propagation of $\xi = 5$ in a system modelled by Equation (1.8) when linear absorption is included (left) and in a fibre laser modelled by Equation (4.43) with parameters as shown in the text (right). We see that the SRR peak is much more visible in the system in which losses are compensated. In the lossy system without gain SRR will be difficult to observe after long propagations.

there will be a slight change in the nonlinear momentum of the pump. This translates into a change in the right hand side of the phase matching condition (4.6), since q will not be equal to 1/2 any more, and the THRR peak will be slightly closer to the pump. We can see that this is indeed the case for the SRR peak in the bottom right panel of Figure 4.22.

In this simplified analysis of fibre lasers we have found that SRR would be in principle easier to find experimentally in these systems than in bulk or normal fibre media. However, we have to take into account the fact that the doping, apart from creating a narrowband gain resonance around the pump frequency, might generate absorption windows far from the gain frequency. This means that we would need to be careful when choosing a doped fibre, making sure that it is transparent at the pump, third harmonic, and SRR frequencies. From a practical point of view this

might prove to be a big challenge, given the very wide frequency window that we are dealing with when studying SRR generation.

After this study of fibre lasers and how SRR would manifest in them we close this section on the experimental feasibility of finding SRR in optical systems and move on to generalise this SRR concept to other situations.

4.3.3 Super resonant radiation beyond optics

Up to now we have studied super resonant radiation emission in Equation (1.8). However, the concepts of resonant radiation and higher harmonic creation do not apply exclusively to optics and optical fields. The idea of soliton-radiation coupling due to a perturbation can be generalised to other integrable equations [116–119]. The question is whether the same phenomenon of SRR emission can be observed or not in other systems that exhibit higher harmonic creation. One such systems is the famous *Kortweg-de Vries equation* (KdV), which has many applications in fluid and plasma physics [120–123]. To study SRR in the KdV formalism, we first need to study the phase matching conditions. Our starting point is the KdV equation with a fifth order dispersion term:

$$\partial_\xi u + \partial_\tau^3 u + k_5 \partial_\tau^5 u + 6u\partial_\tau u = 0. \tag{4.45}$$

From simple inspection of the dispersion terms we see that the dispersion relation in the previous equation is

$$b(\mu) = -\mu^3 + k_5\mu^5. \tag{4.46}$$

It is known that the modified KdV equation, an equation similar to the KdV but with a cubic nonlinearity, can be rewritten as a NLSE equation [124]. Following the same procedure in this case, if we assume an oscillatory solution of the KdV, we can cast this equation into a "NLSE-like" equation (albeit with a quadratic nonlinearity, which would correspond to a $\chi^{(2)}$ material in nonlinear optics) by doing the transformation:

$$u = \frac{1}{2}\left(A(\xi,\tau)\exp(-i\mu\tau) + A^*(\xi,\tau)\exp(i\mu\tau)\right). \tag{4.47}$$

The equation for A is then:

$$i\partial_\xi A + \hat{D}(i\partial_\tau)A + \left(1 + \frac{i}{\omega_0}\partial_\tau\right)\left[|A|^2\exp(i\phi) + \frac{1}{2}A^2\exp(-i\phi)\right]_+ = 0, \tag{4.48}$$

from where the following phase matching conditions arise

$$D(\mu) = \kappa, \tag{4.49}$$

$$D(\mu) = -\kappa + 2q. \tag{4.50}$$

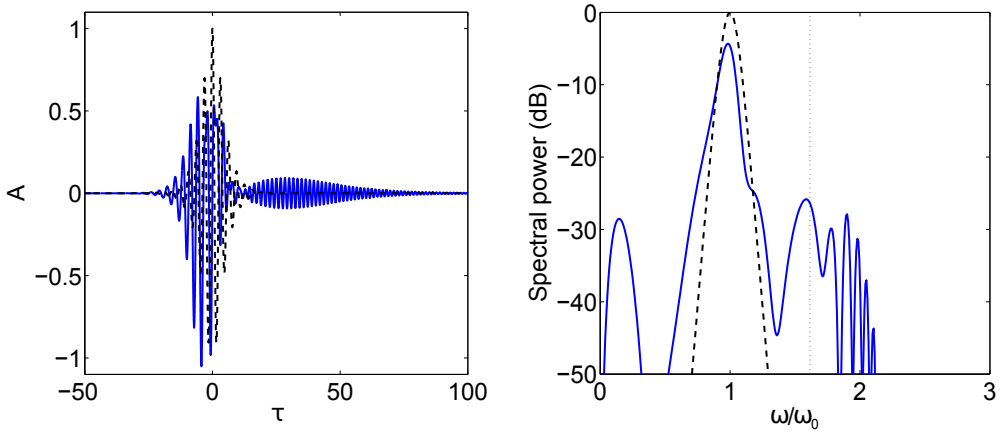

Figure 4.23: Initial (black dashed) and final (blue solid) time profiles and spectra of a pulse propagated using Equation (4.45). We see that a big radiation peak is starting to form in the position predicted by 4.50, near the second harmonic. The parameters are $\mu = 2$, $k_5 = 0.08$ and $\xi = 0.75$.

Again, q is the nonlinear momentum of our solution, which in our normalisation will have a value of $q = 1/2$. The parameter κ is calculated from the dispersion relation as $\kappa = b_1\mu - b_0$, and in this case has a value of $\kappa = -5.76$. We have used this to define the phase ϕ as $\phi = \mu\tau + \kappa\xi$. It is easy to see that these are the correct terms on the right hand side of the phase matching equations by simple comparison with the phase of the nonlinear terms in (4.48).

The second condition is the one that comes from the second harmonic generation term in the equation, so we expect this radiation to be SRR when it is phase matched to a frequency similar to that of the second harmonic. To check this fact, we have performed numerical simulations of Equation (4.45) using an input pulse of the form shown in (4.47) with $A = \mathrm{sech}\,(\tau)$.

The results can be seen in Figure 4.23. When $\mu = 2$ and $k_5 = 0.08$, we can see that after a propagation of $\xi = 0.75$ a peak is already starting to form in the position predicted by the phase matching conditions. This peak would correspond to SRR in

the system. If we found a pulse stable enough to be propagated for long distances without changing its shape significantly we would expect it to eventually outgrow the pump, as seen in the previous cases. However, the field derived from the simple $\mathrm{sech}(\tau)$ profile for A quickly collapses and loses its shape, as we can see in the plot of the temporal profile of Figure 4.23. Longer propagations are not possible without a more complex model, which is outside the scope of this work.

5 Conclusions

Here we will summarise the main findings of this thesis, explain what we have achieved so far, and discuss briefly the possibility of further research on the subject of negative frequency effects in nonlinear optics.

In recent years new light sources and optical materials have appeared that have allowed experimentalists to study nonlinear optics in regimes for which the Slowly Varying Envelope Approximation was not guaranteed to work. Despite this, the NLSE formalism and its extensions have withstood the passage of time much better than it had been anticipated, fully capturing the physics of many processes that happen for very narrow and intense pulses. However it has been proven that a more complete model is needed if we want to fully characterise the generation of new frequencies by extreme light in nonlinear media, which is a key part in, for example, understanding supercontinuum generation. In this sense, the development of models that explain the mechanism behind the generation of new frequencies by ultraintense, short pulses, is of the utmost importance.

As explained in the introduction to this work, all electromagnetic phenomena can be traced back to Maxwell's equations (1.1)-(1.4). This means that, as impractical as this might be from a computational point of view, we could numerically calculate the evolution of any general pulse in any general material with as general a polarisability as we desire. However, from a theoretical point of view, a simple numerical analysis of the problem is not satisfactory. This is why we must strive to derive simplified models that can be studied analytically and can help us give a physical meaning to the frequency conversion processes observed. It is with this idea in mind that the work of this thesis was conducted, trying to understand the physical mechanisms that are present in $\chi^{(3)}$ materials and were ignored in the NLSE. Thanks to this we can indeed explain the generation of new frequencies as the ones observed in [28] and [29] in

physical terms as a previously overlooked interaction between positive and negative frequency fields, $\mathcal{E}$ and $\mathcal{E}^*$, that are included in Equation (1.8) by means of two new nonlinear terms.

The work done in this thesis has found many significant differences between the nonlinear phenomena present in Equation (1.8) and those that were present in the NLSE and its most common extensions. Although some important effects, like the soliton self frequency shift due to the Raman scattering, were not changed significantly in the new formalism, some others were found to generate new frequencies that could not be created in a simple NLSE formalism. The energy transferred into these new frequencies is small when the spectral width of the input pulse and the energy pumped into the material are small, but become experimentally accessible for extreme pulses with intensities in the $\mathrm{TW/cm^2}$ regime and durations of a few tens of fs, which is the regime studied in our numerical simulations.

It was found that the two main processes that contribute to the generation of new frequencies by the NK and THG terms are the SPM broadening effect and resonant radiation emission. When those terms are included in our equations, the usual SPM spectral broadening is modified in a way such that new far detuned frequencies are created at the sides of the pump. And as for resonant radiation emission, which happens due to the phase matching between the pump and a CW mode, it has been found to generate frequencies that can be very far detuned from the central frequency of the initial seed. Apart from the usual RR that was present in the SVEA case, two new radiations appear in Equation (1.8), and these have been thoroughly studied throughout this thesis. It is also in relation to the emission of RR that the most striking feature of (1.8) known so far has been found: the super resonant radiation emission, or the fast exchange of energy between a pump and a resonant CW mode mediated by high harmonic generation.

As interesting as these new phenomena are, and as accurate as the theoretical description we used is, some challenges still remain that could be the starting point of future research. From a theoretical point of view, finding exact solutions (both soliton-like and CW-like) of the full Equation (1.8) would mean that a more precise analysis of the phase matching conditions for the resonant radiations would be possible, which would allow us to compute not only the frequency at which it is emitted, but also its amplitude. This would obviously be interesting in all cases analysed in this thesis, but mainly for SRR, in which having a mathematical derivation of the gain of the radiation

peak could give us further physical insight on how the energy transfer happens. It would also be extremely useful in the KFC analysis, for which we know that the phase matching conditions (4.32)-(4.34) are not complete, and we would expect to find a more general expression valid for bigger intracavity powers. Knowing the exact shape of a CS-like solution of Equation (4.28) would be the first step in finding the full phase matching conditions using a MI-like analysis. The problem of finding solutions of an equation as complex as the one we are dealing with, in which the coefficients of the nonlinear terms are not constant and have an oscillating behaviour in both space and time, is a very challenging one from the mathematical point of view.

Another possibility for further work related to what has been presented in this thesis is the extension of the formalism to new systems. Although we have studied SRR emission in an equation that would model a $\chi^{(2)}$ medium, a more exhaustive analysis could find new, unexpected results. The aforementioned fibre lasers could also lead to some interesting findings, maybe using a somehow extended version of our simple model (4.43). As explained in the body of the thesis, it seems difficult to find a compromise between the narrowband gain of these lasers and the intrinsic far detuned radiation coming from the new nonlinear interactions analysed, but the possibility of finding a way around these issues cannot be completely discarded.

As a final remark, the author would like to point out that there has been some reticence in the community towards this model due to the use of the names *negative frequencies* and *negative frequency resonant radiation*. The use of these terms traces back to the seminal paper [28], in which the NRR phase matching conditions was heuristically explained by extending the dispersion relation into the domain of $\omega < 0$. The successful analytical explanation of this radiation done in [25] showed that this radiation was indeed present in $\chi^{(3)}$ materials and that is was due to a nonlinear term that is usually ignored due to the SVEA. In line with the names originally used for this radiation, the term responsible for it was named *negative Kerr term*. The fact that the word "negative" has been explicitly introduced here does not mean that the model needs the introduction of some new, previously unknown physical magnitude. As explained throughout this thesis, the positive frequency part of the electric field $\mathcal{E}$ and its negative frequency counterpart $\mathcal{E}^*$ interact in a non-trivial way whenever there is a nonlinearity. The original Kerr nonlinearity, of the form $\mathcal{E}^2\mathcal{E}^*$, already needs the negative frequency field $\mathcal{E}^*$ to be taken into account. The success of (1.8) is not based on introducing the new concept of negative frequencies, which have

been already present in physics for many years, but finding that certain interactions between positive and negative frequencies that are usually ignored in the literature were responsible for recently observed phenomena. It is for this that the concept of negative frequencies should not be controversial at all, since no complete nonlinear optical theory could ever exist without them.

A Derivation of (3.31) and pertubation by Raman beyond SVEA

In this appendix we will derive the equation that includes the Raman effect and does not need SVEA. We will start by writing explicitly the nonlinear polarisation for a $\chi^{(3)}$ material and then see what nonlinear terms it creates for the evolution equation when the nonlinearity is allowed to have a delayed response. After this, we will try to simplify the expression as much as possible and apply the soliton perturbation techniques that are used in the SVEA case to find out how the soliton parameters evolve due to the Raman effect when SVEA is broken.

A.1 Derivation of the equation including Raman beyond SVEA

The nonlinear polarisation, when taking into account the possibility of a delayed response of the medium, is:

$$\begin{aligned} P_{NL} = \frac{\chi^{(3)}}{8}[\mathcal{E}(\tau)+\mathcal{E}^*(\tau)]\int R(\tau')[\mathcal{E}^2(\tau-\tau')+(\mathcal{E}^*)^2(\tau-\tau')+2|\mathcal{E}^2(\tau-\tau')|]d\tau' = \\ \frac{\chi^{(3)}}{8}\Big\{A\exp(-i\kappa\xi-i\mu\tau)\int R(\tau')\left[2|A|^2+A^2\exp(-2i\kappa\xi-2i\mu(\tau-\tau'))+\right. \\ \left.(A^*)^2\exp(2i\kappa\xi+2i\mu(\tau-\tau'))\right]d\tau'+ \\ +A^*\exp(i\kappa\xi+i\mu\tau)\int R(\tau')\left[2|A|^2+A^2\exp(-2i\kappa\xi-2i\mu(\tau-\tau'))+\right. \\ \left.(A^*)^2\exp(2i\kappa\xi+2i\mu(\tau-\tau'))\right]d\tau'\Big\}, \quad \text{(A.1)} \end{aligned}$$

where A is $A(\tau)$ outside the integrals and $A(\tau-\tau')$ inside.

The equation for the envelope of the analytic signal, equivalent to (1.8) but with

the Raman effect included, is therefore as follows:

$$i\partial_z A + \frac{1}{2}\partial_t^2 A + \mathrm{NL}[A] = 0, \tag{A.2}$$

where $\mathrm{NL}[A]$ is the following nonlinear term:

$$\begin{aligned}\frac{1}{3}\Big\{ A\int R(\tau')\left[2|A|^2 + A^2\exp(-2i\kappa\xi - 2i\mu(\tau-\tau'))+\right.\\ \left.(A^*)^2\exp(2i\kappa\xi + 2i\mu(\tau-\tau'))\right]d\tau' +\\ + A^*\exp(2i\kappa\xi + 2i\mu\tau)\int R(\tau')\left[2|A|^2 + A^2\exp(-2i\kappa\xi - 2i\mu(\tau-\tau'))+\right.\\ \left.(A^*)^2\exp(2i\kappa\xi + 2i\mu(\tau-\tau'))\right]d\tau'\Big\}. \end{aligned}\tag{A.3}$$

Doing the expansions $A^2(\tau-\tau') = A^2(\tau) - \tau'\partial_\tau A^2$, $|A|^2(\tau-\tau') = |A|^2(\tau) - \tau'\partial_\tau|A|^2$, and $(A^*)^2(\tau-\tau') = (A^*)^2(\tau) - \tau'\partial_\tau(A^*)^2$, and also the decomposition of the response function as $R(\tau) = (1-f_R)\delta(\tau) + f_R h(\tau)$, (A.3) becomes

$$\begin{aligned}\frac{1}{3}[&(3-f_R)A|A|^2 + (3-f_R)A^*|A|^2\exp(2i\kappa\xi + 2i\mu\tau)\\ &+ A^3(1-f_R)\exp(-2i\kappa\xi - 2i\mu\tau) + (A^*)^3(1-f_R)\exp(4i\kappa\xi + 4i\mu\tau)\\ &- 2\tau_R A\partial_\tau|A|^2 - 2\tau_R A^*\partial_\tau|A|^2\exp(2i\kappa\xi + 2i\mu\tau)\\ &- f_R A\partial_\tau(A^*)^2(\tilde{th})(-2\mu)\exp(2i\kappa\xi + 2i\mu\tau)\\ &- f_R A\partial_\tau A^2(\tilde{th})(2\mu)\exp(-2i\kappa\xi - 2i\mu\tau)\\ &- f_R A^*\partial_\tau(A^*)^2(\tilde{th})(-2\mu)\exp(4i\kappa\xi + 4i\mu\tau)\\ &- f_R A^*\partial_\tau A^2(\tilde{th})(2\mu)\\ &+ f_R A|A|^2\tilde{h}(2\mu) + f_R A^*|A|^2\tilde{h}(-2\mu)\exp(2i\kappa\xi + 2i\mu\tau)\\ &+ f_R A^3\tilde{h}(2\mu)\exp(-2i\kappa\xi - 2i\mu\tau)\\ &+ f_R(A^*)^3\tilde{h}(-2\mu)\exp(4i\kappa\xi + 4i\mu\tau)],\end{aligned}\tag{A.4}$$

where $\tilde{f}(y)$ is the Fourier transform of $f(x)$ evaluated at y,

$$\tilde{f}(y) = \int_{-\infty}^{\infty} dx f(x)\exp(iyx). \tag{A.5}$$

Setting $f_R = 0$ (which also implies $\tau_R = 0$, with τ_R as defined for the usual Raman effect in the SVEA case) we recover the original Equation (1.8) with the conjugate Kerr effect and the THG, as well as the term $(A^*)^3$ that will be killed by the filtering.

We find ourselves with a nonlinear equation with many and extremely convoluted nonlinearities. If we want to be able to do some analytical work with this result we

must do some simplifications. This will be ignoring the terms with Fourier transforms of h and th. In principle, since these Fourier transforms are evaluated at 2μ and -2μ, we assume that they will affect only parts of the spectrum far detuned from the pump. The difference in the frequency shift for the central frequency of the pulse between the SVEA and non-SVEA case should then be given by terms without these transforms. In this approximation we find the following nonlinearity, after rescaling:

$$A|A|^2 + A^*|A|^2\exp(2i\kappa\xi + \mu\tau) + \\ \frac{1}{3}A^3\exp(-2i\kappa\xi - 2i\mu\tau) - \tau_R A\partial_\tau|A|^2 - \tau_R A^*\exp(2i\kappa\xi + 2i\mu\tau)\partial_\tau|A|^2. \quad \text{(A.6)}$$

Now that we have a more simple nonlinear term we finally write the equation for Raman beyond SVEA:

$$i\partial_\xi A + \frac{1}{2}\partial_\tau^2 A + \Big[A|A|^2 + A^*|A|^2\exp(2i\kappa\xi + 2i\mu\tau) + \\ \frac{1}{3}A^3\exp(-2i\kappa\xi - 2i\mu\tau) - \tau_R A\partial_\tau|A|^2 - \tau_R A^*\exp(2i\kappa\xi + 2i\mu\tau)\partial_\tau|A|^2\Big]_+ = 0. \quad \text{(A.7)}$$

A.2 Perturbation of solitons and evolution of their parameters due to Raman effect beyond SVEA

If we only consider the terms coming from the Raman effect (the terms with a derivative) to be the perturbation we have

$$i\epsilon = T_R A\partial_\tau|A|^2 + T_R A^*\partial_\tau|A|^2\exp(2i\kappa\xi + 2i\mu\tau) \Rightarrow \\ \epsilon = -iT_R A\partial_\tau|A|^2 - iT_R A^*\partial_\tau|A|^2\exp(2i\kappa\xi + 2i\mu\tau). \quad \text{(A.8)}$$

As in the SVEA case, we can assume that our solution will be of the shape given by (3.22), and use equations (3.24)-(3.27) to find the evolution of its parameters. Due to the contribution of the new term, which is in general complex due to the phase $\exp(2i\kappa\xi + 2i\mu\tau)$, the pulse amplitude A_0 will not be constant any more and the delay will have a contribution coming directly from the perturbation. We already know how the first part of the perturbation affects the three quantities we are interested in. In the following we will derive how the extra term modifies the evolution of those parameters.

A.2.1 Change in the amplitude

Given by (3.24), the change in the amplitude due to the new term contributing to the Raman effect is:

$$\frac{\partial_\xi A_0}{\tau_R} = \mathrm{Re}\left[\int_{-\infty}^{\infty} d\tau(-i|A|^2\partial_\tau|A|^2 - i(A^*)^2\partial_\tau|A|^2\exp(2i\kappa\xi + 2i\mu\tau))\right]. \tag{A.9}$$

Again, the first term will be purely imaginary and therefore will not contribute to the change in ξ. Plugging the assumed solution for A in the other one we find the following expression:

$$\begin{aligned}\frac{\partial_\xi A_0}{\tau_R} = \mathrm{Re}\Big[-i \int d\tau (A_0^2 \mathrm{sech}\left(A_0(\tau-\tau_c)\right)^2 \exp[2i(\kappa\xi-\phi)] \\ \partial_\tau(A_0^2\mathrm{sech}\left(A_0(\tau-\tau_c)\right)^2)\exp[2i(\delta+\mu)\tau])\Big] = \\ \mathrm{Re}\Big[2iA_0^5\exp[2i(\kappa\xi-\phi)] \\ \int d\tau \mathrm{sech}\left(A_0(\tau-\tau_c)\right)^4\tanh\left(A_0(\tau-\tau_c)\right)\exp[2i(\delta+\mu)\tau]\Big].\end{aligned} \tag{A.10}$$

The integral is a Fourier transform from τ to $2(\mu+\delta)$. Performing this transform, and using the property

$$\mathcal{F}[f(ax-b)] = |a|^{-1}\tilde{f}\left(\frac{y}{a}\right)\exp(-iyb/a), \tag{A.11}$$

we find the following expression for the derivative of the amplitude:

$$\begin{aligned}\partial_\xi A_0 = -\tau_R \mathrm{Re}\Big[\frac{4\pi}{3}\exp[2i(\kappa\xi-\phi)](A_0^2+(\delta+\mu)^2)(\delta+\mu)^2 \\ \mathrm{csech}\left[\frac{\pi(\delta+\mu)}{A_0}\right]\exp[2i(\delta+\mu)\tau_c]\Big].\end{aligned} \tag{A.12}$$

A.2.2 Change in the frequency shift

The change in frequency shift is controlled by (3.25). We already know how the usual Raman term of the polarisation affects the frequency shift δ, so we will focus only on the other one. We start with

$$\begin{aligned}\frac{\partial_\xi\delta}{\tau_R} = \mathrm{Im}\left[i\int_{-\infty}^{\infty} d\tau(A^*)^2\partial_\tau|A|^2\tanh(A_0(\tau-\tau_c))\exp(2i\kappa\xi+2i\mu\tau)\right] = \\ \mathrm{Re}\Big[-2\int d\tau A_0^5\mathrm{sech}\left(A_0(\tau-\tau_c)\right)^4\tanh\left(A_0(\tau-\tau_c)\right)^2 \\ \exp[2i(\kappa\xi-\phi)+2i(\delta+\mu)\tau]\Big].\end{aligned} \tag{A.13}$$

We find ourselves again with an integral similar to the one we had in the previous case. Using the same property and performing the transform we can write the new contribution to the detuning evolution as

$$\partial_\xi \delta = -\tau_R \mathrm{Re}\Bigg[\exp[2i(\kappa\xi - \phi)] \left(\frac{8\pi A_0^3}{15}(\delta+\mu) - \frac{8\pi}{15A_0}(\delta+\mu)^5 \right) \operatorname{csech}\left(\frac{\pi(\delta+\mu)}{A_0} \right) \exp[2i(\delta+\mu)\tau_c] \Bigg]. \quad \text{(A.14)}$$

A.2.3 Change in the delay

To calculate the delay we need Equation (3.26). If we ignore the contribution from the detuning, and remembering that the usual Raman term did not produce any direct change in the delay, we have that the evolution equation for τ_c is

$$\frac{\partial_\xi \tau_c}{\tau_R} = A_0^{-1}\mathrm{Re}\left[\int_{-\infty}^{\infty} d\tau(\tau - \tau_c) - i(A^*)^2 \partial_\tau |A|^2 \exp(2i\kappa\xi + 2i\mu\tau) \right] = 2iA_0^4 \mathrm{Re}\Bigg[\exp[2i(\kappa\xi - \phi)] \int_{-\infty}^{\infty} d\tau \operatorname{sech}\left(A_0(\tau-\tau_c)\right)^4 \tanh\left(A_0(\tau-\tau_c)\right) [A_0(\tau-\tau_c)] \exp[2i(\delta+\mu)\tau] \Bigg]. \quad \text{(A.15)}$$

Once again we have to solve a Fourier transform evaluated at $2(\delta+\mu)$. The result of this is

$$\partial_\xi \tau_c = \tau_R \mathrm{Re}\left[2iA_0^2 \exp[2i(\kappa\xi - \phi)] \exp[2i(\delta+\mu)\tau_c] f_\tau\left(\frac{2(\delta+\mu)}{A_0} \right) \right], \quad \text{(A.16)}$$

where we have defined a new function $f_\tau(x)$ as

$$f_\tau(x) = -\frac{1}{48}\sqrt{\frac{\pi}{2}} x \left(-8(2+x^2) + \pi x(4+x^2) \operatorname{ctanh}\left(\frac{\pi x}{2} \right) \right) \operatorname{csech}\left(\frac{\pi x}{2} \right). \quad \text{(A.17)}$$

A.2.4 Change in the phase

Although we are not interested in the value of the phase at each point as a magnitude in itself, the value of ϕ enters explicitly the evolution equations of the other parameters, and therefore we need to calculate it if we want to have an accurate estimate of how those other parameters evolve with ξ. The full evolution of the phase is given

by (3.26), and for our perturbation is:

$$\partial_\xi\phi = \frac{1}{2}(A_0^2-\delta^2) + \tau_c\partial_\xi\delta - \tau_R\mathrm{Im}\left[i\int_{-\infty}^{\infty} d\tau|A|^2\partial_\tau|A|^2(A_0^{-1}-(\tau-\tau_c)\tanh[A_0(\tau-\tau_c)])+ i\int_{-\infty}^{\infty} d\tau(A^*)^2\partial_\tau|A|^2(A_0^{-1}-(\tau-\tau_c)\tanh[A_0(\tau-\tau_c)])\exp(2i\kappa\xi+2i\mu\tau)\right]. \quad (A.18)$$

The first term adds the contribution of the usual nonlinear phase and a phase due to the detuning with the soliton's assumed central frequency. The second one is also due to a detuning that causes a delay. The third term is the contribution to the phase from the usual Raman effect in the SVEA case, and the fourth one is the new contribution that we find when we include the negative frequency terms. Since the terms inside the parentheses of the second term are both even in $\tau-\tau_c$, the function to integrate will have the parity of $|A|^2\partial_\tau|A|^2$, which is odd. This means that the integral will be zero and the usual Raman effect will not explicitly affect the phase (although it will do through a modification of δ and τ_c). Thanks to this we only need to calculate the second integral, which once more is a Fourier transform of hyperbolic trigonometric functions. The final evolution equation for ϕ then reads

$$\partial_\xi\phi = \frac{1}{2}(A_0^2-\delta^2) + \tau_c\partial_\xi\delta + \tau_R\mathrm{Im}\left[2iA_0^3\exp[2i(\delta+\mu)\tau_c]\exp[2i(\kappa\xi-\phi)]\left(\phi_1\left[\frac{2(\delta+\mu)}{A_0}\right]-\phi_2\left[\frac{2(\delta+\mu)}{A_0}\right]\right)\right], \quad (A.19)$$

with the functions $\phi_1(x)$ and $\phi_2(x)$ defined as

$$\phi_1(x) = \frac{i}{24}\sqrt{\frac{\pi}{2}}x^2(4+x^2)\mathrm{csech}\left(\frac{\pi x}{2}\right), \quad (A.20)$$

$$\phi_2(x) = -\frac{i}{240}\sqrt{\frac{\pi}{2}}\left(32-10x^4+\pi x(x^4-16)\mathrm{ctanh}\left(\frac{\pi x}{2}\right)\right)\mathrm{csech}\left(\frac{\pi x}{2}\right). \quad (A.21)$$

B Conventions and units

In this appendix we will explain the conventions for certain definitions and operations used throughout this work, as well as a brief summary of the relation between the dimensionless units we use in the text and dimensional units.

First of all, we define the Fourier transform of a function $f(x)$ to be

$$\mathcal{F}[f(x)] \equiv \tilde{f}(y) = \int_{-\infty}^{\infty} f(x) \exp(iyx) dx, \tag{B.1}$$

and therefore the inverse Fourier transform is given by

$$\mathcal{F}^{-1}[\tilde{f}(y)] \equiv f(x) = \frac{1}{2\pi} \int_{-\infty}^{\infty} \hat{f}(y) \exp(-iyx) dy. \tag{B.2}$$

Unless explicitly stated otherwise, all dynamical simulations of partial differential equations are performed using a split-step Fourier method. For an equation of the form $\partial_x f(x,y) = A(\partial_y) f(x,y) + B(x,y,f) f(x,y)$, this method is implemented by separating the contribution of operators A and B to the evolution of f. Schematically, we could assume that the change in f produced by an increase of h in the variable x would have two contributions, $\Delta f = \Delta f_A + \Delta f_B$, where:

$$\Delta f_A = hA(\partial_y) f, \tag{B.3}$$

$$\Delta f_B = hB(x,y,f) f(x,y). \tag{B.4}$$

Solving both these equations is quite simple, since the first one can be solved exactly in Fourier space and the second one is an ordinary differential equation. This method assumes that the operators A (that plays the role of a dispersion operator) and B (where we account for nonlinearities and effects explicitly dependent in the variables of f) act independently, since we are approximating $f(x+h,y) = \exp(h(A+B)) f(x,y) \approx \exp(hA)\exp(hB) f(x,y)$, which is only true if A and B commute. This is not the case

for the relevant equations of this work, like (1.8) or (4.28). To reduce the error associated with the splitting, a different ordering of the operations can be done, by means of the approximation

$$f(x+h,y) = \exp(h(A+B))f(x,y) \approx \exp(hA/2)\exp(hB)\exp(hA/2)f(x,y). \quad \text{(B.5)}$$

Here, instead of letting the dispersion and nonlinearity act independently, half of the nonlinearity is applied to the initial field, then the full nonlinear contribution to the evolution is added, and finally we apply the remaining dispersion part. This method is more accurate than the simple splitting explained before [125, 126].

For ordinary differential equations $\partial_x f(x) = C(x,f)$, including the integration of the nonlinear part of partial differential equations through the split-step Fourier method, we use a fifth order Runge-Kutta algorithm given by [127]:

$$k_1 = C(f,x), \quad \text{(B.6)}$$

$$k_2 = C(f + 4k_1/11, x + 4h/11), \quad \text{(B.7)}$$

$$k_3 = C(f + (9k_1 + 11k_2)/50, x + 2h/5), \quad \text{(B.8)}$$

$$k_4 = C(f + (-11k_2 + 15k_3)/4, x + h), \quad \text{(B.9)}$$

$$k_5 = C(f + ((81+9\sqrt{6})k_1 + (255-55\sqrt{6})k_3 + (24-14\sqrt{6})k_4)/600, \\ x + (6-\sqrt{6})h/10), \quad \text{(B.10)}$$

$$k_6 = C(f + ((81-9\sqrt{6})k_1 + (255+55\sqrt{6})k_3 + (24+14\sqrt{6})k_4)/600, \\ x + (6+\sqrt{6})h/10), \quad \text{(B.11)}$$

$$f(x+h,y) = f(x,y) + h\frac{(4k_1 + (16+\sqrt{6})k_5 + (16-\sqrt{6})k_6)}{36}. \quad \text{(B.12)}$$

All throughout this thesis dimensionless units are used. Unless explicitly stated when defining the relevant variable, the distances are scaled so that the dispersion length $L_D = t_0^2/|\beta_2|$ corresponds to $\xi = 1$. t_0 is the width of the input pulse, and we use it as the scale of time, i.e., in dimensionless units $\tau = 1$ is the width of the pulse. For convenience, we normalise the power/amplitude of pulses so that the fundamental soliton of the NLSE is $\mathrm{sech}\,(\tau)$, i.e., it has an amplitude of 1. By absorbing the nonlinear coefficient γ of the system under consideration in a rescaling of the field amplitude we will have that the nonlinear momentum of the soliton, which would be $q = \gamma P/2$ in dimensional units, is simply $q = 1/2$. This corresponds to a transformation from the usual scaling of the pulse envelope A in dimensional units, normalised so that $|A|^2$ is the pulse power in Watts, to a dimensionless version

$A \to A' = \sqrt{\gamma L_D} A$, which is a dimensionless quantity. The n-th order coefficient of the dispersion is normalised as $b_i = \beta_i/(|\beta_2| t_0^{i-2})$.

The advantage of these units is two-fold: on the one hand, all the relevant quantities reduce to small numbers in this framework, instead of having magnitudes that might have numerical values differing by orders of magnitude. For example, propagation distances might be a few tens or hundreds in ξ units, while the temporal profiles of the pulses and all the changes they experience happen in a few units of τ; amplitudes of waves will also be in the range between 0 and a few units. For short pulses the dimensionless frequency $\omega_0 t_0$ will also be small. This is easier to handle numerically for a computer than simulations that include magnitudes of the order of 10^{15} (like the dimensional frequency) or 10^{-20} (values that the dispersion or nonlinear coefficients can reach), since making the machine precisions of all the numbers compatible can be a challenge. On the other hand this makes the simulations more general, since the results do not only apply to one specific experimental setup with certain parameters, as we can scale the results to apply to many different systems.

As a quick note on the last sentence, it has to be specified that there are two new parameters in the model (1.8) that were not present in Equation (1.6): μ and κ. The first one is the dimensionless frequency μ, which was not explicitly present in the NLSE. This means that we lose one degree of freedom in our dimensionless analysis: in the NLSE all dimensionless results can be scaled back to dimensional units by choosing an appropriate pulse duration; after this, we can still choose the pulse frequency freely, since there is no assumed value for its dimensionless value. Any result we get from (1.8), however, will have a μ dependence. In this case, when we want to scale back to dimensional units, we can only choose either the pulse duration or its frequency freely, since once we fix one the value of the other will be given by $\omega_0 t_0 = \mu$. This means that, unlike in the NLSE, for which any simulated result can be applied to any experimental setup by choosing the appropriate scaling, the numerical solutions of (1.8) are only valid for experimental systems with a compatible value of μ. It is important to take this into account when trying to adapt our model to specific experiments. The other parameter, $\kappa = (\beta_1 \omega_0 - \beta_0) L_D$, is fixed by the dispersion coefficients of a material at the relevant frequency. Once again, this means that the simulations with a correct value of κ must be chosen when trying to scale the results back to the dimensional units relevant for an experiment.

Lastly, it is worth mentioning that all our results are calculated in a frame of

reference that moves with the soliton. As such, a solitonic solution of our equations would always be centred at $\tau = 0$. If the pulse gains any delay during propagation this will be given directly by the value of τ for any propagation distance. The boost that transforms from laboratory to rest frame is $t \to t + \beta_1 z$.

When plotting the spectrum of pulses, the spectral power is given in dBs. For a field A this calculated as:

$$SP(dBs) = 20 \log \left(\frac{\mathcal{F}[A]}{max(\mathcal{F}[A_{in}])} \right), \tag{B.13}$$

where A_{in} is the input pulse.

When studying the SRR phenomenon we make use of the XFROG technique [3, 128]. This is an extension of the Frequency Resolved Optical Gating technique in which a pulse to be studied is correlated with a different reference pulse. In our case we define a magnitude $S(\tau, \Delta)$ as:

$$S(\tau, \Delta) = \left| \int_{-\infty}^{\infty} A(\xi, \tau) A_{in}(\tau) \exp(i(\mu + \Delta)\tau) d\tau \right|^2. \tag{B.14}$$

This allows us to see at the same time the features in time and spectral domain of a pulse $A(\xi, \tau)$ using the input pulse as the reference, as seen in figures 4.16 and 4.19.

References

[1] J. C. Maxwell, Philosophical Magazine (Taylor & Francis) **90**, 11 (1861).

[2] J. C. Maxwell, Philosophical Transactions of the Royal Society of London **155**, 459 (1865).

[3] G. P. Agrawal, *Nonlinear Fiber Optics* (4th ed., Academic Press, San Diego, 2007).

[4] D. J. Griffiths, *Introduction to Electrodynamics* (3rd ed., Prentice-Hall, New Jersey, 1999).

[5] J. D. Jackson, *Classical Electrodynamics* (John Wiley & Sons, Chichester, 1962).

[6] F. M. Mitschke and L. F. Mollenauer, Opt. Lett. **11**, 659 (1986).

[7] J. P. Gordon, Opt. Lett. **11**, 662 (1986).

[8] R. H. Stolen and C. Lin, Phys. Rev. A **17**, 1448 (1978).

[9] A. Hasegawa and F. Tappert, Appl. Phys. Lett. **23**, 142 (1973).

[10] P. Andrekson, Laser Focus World **35** (5), 145 (1999).

[11] V. E. Zakharov and A. B. Shabat, Sov. Phys. JETP **34**, 62 (1972).

[12] N. Akhmediev and M. Karlsson, Phys. Rev. A **51**, 2602 (1995).

[13] A. V. Husakou and J. Herrmann, Phys. Rev. Lett. **87**, 203901 (2001).

[14] F. Biancalana, D. V. Skryabin, and A. V. Yulin, Phys. Rev. E **70**, 016615 (2004).

[15] D. V. Skryabin, F. Luan, J. C. Knight, and P. St.J. Russell, Science **301**, 1705 (2003).

[16] H. Leblond and D. Mihalache, Physics Reports **523**, 61 (2012).

[17] P. Kinsler, Phys. Rev. A **81**, 013819 (2010).

[18] G. Genty, P. Kinsler, B. Kibler, and J. M. Dudley, Opt. Express **15**, 5382 (2007).

[19] J. C. A. Tyrrell, P. Kinsler, and G. H. C. New, J. Mod. Opt. **52**, 973 (2005).

[20] M. Kolesik, P. Townsend Whalen, and J. V. Moloney, IEEE J. Sel. Top. Quantum Electron. **18**, 494 (2012).

[21] Sh. Amiranashvili, U. Bandelow, and N. Akhmediev, Phys. Rev A **87**, 013805 (2013).

[22] Sh. Amiranashvili and A. Demircan, Adv. Opt. Technol. **2011**, 989515 (2011).

[23] M. Conforti, F. Baronio, and C. De Angelis, IEEE Photonics **2**, 600 (2010).

[24] M. Conforti, F. Baronio and C. De Angelis, Phys. Rev. A **81**, 053841 (2010).

[25] M. Conforti, A. Marini, T. X. Tran, D. Faccio, and F. Biancalana, Opt. Express **21**, 31239 (2013).

[26] J. M. Dudley, G. Genty, and S. Coen, Rev. Mod. Phys. **78**, 1135 (2006).

[27] J. A. Armstrong, N. Bloembergen, J. Ducuing, and P. S. Pershan, Phys. Rev. **127** 1918 (1962).

[28] E. Rubino, J. McLenaghan, S. C. Kehr, F. Belgiorno, D. Townsend, S. Rohr, C. E. Kuklewicz, U. Leonhardt, F. König, and D. Faccio, Phys. Rev. Lett. **108**, 253901 (2012).

[29] C. Redondo Loures, T. Roger, D. Faccio, and F. Biancalana, *submitted*.

[30] Sh. Amiranashvili and A. Demircan, Phys. Rev. A **82**, 013812 (2010).

[31] J. Yang, *Nonlinear waves in integrable and nonintegrable systems* (SIAM, Philadelphia, 2010).

[32] M. E. Peskin and D. V. Schroeder, *An Introduction to Quantum Field Theory* (Addison-Wesley Publishing Company, 1995).

[33] A. Nahata and T. F. Heinz, Opt. Lett. **23**, 67 (1998).

[34] N.G. Vakhitov and A.A. Kolokolov, Radiophys. Quantum Electron. **16**, 783 (1973).

[35] D. E. Pelinovsky, Y. S. Kivshar, and V. V. Afanasjev, Physica D **116**, 121 (1998).

[36] D. J. Kaup, Phys, Rev. A **42**, (1990).

[37] P. Dirac, Proceedings of the Royal Society A **114**, 243 (1927).

[38] E. Fermi, *Nuclear Physics* (University of Chicago Press, 1950).

[39] D. J. Griffiths, *Introduction to Quantum Mechanics* (Prentice-Hall, New Jersey, 1995).

[40] F. Shimizu, Phys. Rev. Lett. **19**, 1097 (1967).

[41] R. R. Alfano and S. L. Shapiro, Phys. Rev. Lett. **24**, 592 (1970).

[42] Y. R. Shen and M. M. T. Loy, Phys. Rev. A **3**, 2099 (1971).

[43] C. Redondo Loures, A. Armaroli, and F. Biancalana, Opt. Lett. **40**, 613 (2015).

[44] S. C. Pinault and M. J. Potasek, J. Opt. Soc. Am. B **2**, 1318 (1985).

[45] J. Botineau and R. H. Stolen, J. Opt. Soc. Am. **72**, 1592 (1982).

[46] J. C. Butcher, *Numerical Methods for Ordinary Differential Equations* (2nd ed., John Wiley & Sons, Chichester, 2008).

[47] M. R. Spiegel, S. Lipschutz, and J. Liu, *Handbook of Formulas and Tables* (3rd ed., Schaum's outlines McGraw Hill, 2009).

[48] H. Nakatsuka, D. Grischkowsky, and A. C. Balant, Phys. Rev. Lett. **47**, 910 (1981).

[49] W. J. Tomlinson, R. H. Stolen, and C. V. Shank, J. Opt. Soc. Am. B **1**, 139 (1984).

[50] M. J. Potasek and G. P. Agrawal, Phys. Rev. A **36**, 3862 (1987).

[51] J. M. Hickmann, J. F. Martino-Filho, and A. S. L. Gomes, Opt. Commun. **84**, 327 (1991).

[52] G. Yang and Y. R. Shen, Opt. Lett. 9, 510 (1984).

[53] C. V. Raman, Indian J. Phys. **2**, 387 (1928).

[54] A. Smekal, Naturwissenschaften **11**, 873 (1923).

[55] E. M. Dianov, A. Y. Karasik, P. V. Mamyshev, and A. A. Fomichev, JETP Lett. **41**, 294 (1985).

[56] F. M. Mitschke and L. F. Mollenauer, Opt. Lett. **11**, 659 (1986).

[57] J. P. Gordon, Opt. Lett. **11**, 662 (1986).

[58] G. P. Agrawal and C. Headley III, Phys. Rev. A **46**, 1573 (1992).

[59] K. J. Blow and D. Wood, IEEE J. Quantum Electron. **25**, 2665 (1989).

[60] R. H. Stolen, J. P. Gordon, W. J. Tomlinson, and H. A. Haus, J. Opt. Soc. Am. B **6**, 1159 (1989).

[61] P. V. Mamyshev and S. V. Chernikov, Opt. Lett. **15**, 1076 (1990).

[62] R. H. Stolen and W. J. Tomlinson, J. Opt. Soc. Am. B **9**, 565 (1992).

[63] A. Bonderson, M. Lisak, and D. Anderson, Physica Scripta **20**, 479 (1979).

[64] D. Anderson and M. Lisak, Phys. Rev. A **27**, 1393 (1983).

[65] M. Erkintalo, G. Genty, and J. M. Dudley, Opt. Lett. **35**, 658 (2010).

[66] J. N. Elgin, T. Brabec, and S. M. J. Kelly, Opt. Commun. **114**, 3221 (1995).

[67] M. Durand, A. Jarnac, A. Houard, Y. Liu, S. Grabielle, N. Forget, A. Durécu, A. Couairon, and A. Mysyrowicz, Phys. Rev. Lett. **110**, 115003 (2013).

[68] M. Durand, K. Lim, V. Jukna, E. McKee, M. Baudelet, A. Houard, M. Richardson, A. Mysyrowicz, and A. Couairon, Phys. Rev. A **87**, 043820 (2013).

[69] T. Roger, D. Majus, G. Tamosauskas, P. Panagiotopoulos, M. Kolesik, G. Genty, I. Grazuleviciute, A. Dubietis, and D. Faccio, Phys. Rev. A **90**, 033816 (2014).

[70] M. Conforti, F. Baronio, and S. Trillo, Phys. Rev. A **89**, 013807 (2014).

[71] C. Millian and D. V. Skryabin, Opt. Express **22**, 3732 (2014).

[72] S. Coen, H. G. Randle, T. Sylvestre, and M. Erkintalo, Opt. Lett. **38**, 37 (2013).

[73] J. K. Jang, M. Erkintalo, S. G. Murdoch, and S. Coen, Opt. Lett. **39**, 5503 (2014).

[74] M. R. E. Lamont, Y. Okawachi and A. L. Gaeta, Opt. Lett. **38**, 3478 (2013).

[75] Y. Okawachi, K. Saha, J. S. Levy, Y. H. Wen, M. Lipson, and A. L. Gaeta, Opt. Lett. **36**, 3398 (2011).

[76] S. Malaguti, M. Conforti, and S. Trillo, Opt. Lett. **39**, 5626 (2014).

[77] D. V. Skryabin and A. V. Yulin, Phys. Rev. E **72**, 016619 (2005).

[78] T. J. Kippenberg, R. Holzwarth and S. A. Diddams, Science **332**, 555 (2011).

[79] T. Herr, V. Brasch, J. D. Jost, C. Y. Wang, N. M. Kondratiev, M. L. Gorodetsky, and T. J. Kippenberg, Nat. Photonics **8**, 145 (2014).

[80] V. E. Lobanov, G. Lihachev, T. J. Kippenberg, and M.L. Gorodetsky, Opt. Express **23**, 7713 (2015).

[81] Y. K. Chembo and N. Yu, Phys. Rev. A **82**, 033801 (2010).

[82] A. B. Matsko, A. A. Savchenkov and L. Maleki, Opt. Lett. **37**, 4856 (2012).

[83] A. B. Matsko, W. Liang, A. A. Savchenkov, and L. Maleki, Opt. Lett. **38**, 525 (2013).

[84] K.Ikeda, Opt. Commun. **30**, 257 (1979).

[85] K. Ikeda, H. Daido, and O. Akimoto, Phys. Rev. Lett. **45**, 709 (1980).

[86] M. Haelterman, S. Trillo and S. Wabnitz, Opt. Commun. **91**, 401 (1992).

[87] M. Haelterman, S. Trillo and S. Wabnitz, Opt. Lett. **17**, 745 (1992).

[88] L. A. Lugiato and R. Lefever, Phys. Rev. Lett. **58**, 2209 (1987).

[89] P. Parra-Rivas, D. Gomila, M. A. Matías, S. Coen, and L. Gelens, Phys. Rev. A **89**, 043813 (2014).

[90] A. Coillet, J. Dudley, G. Genty, L. Larger, and Y. K. Chembo, Phys. Rev. A **89**, 013835 (2014).

[91] Y. K. Chembo and C. R. Menyuk, Phys. Rev. A **87**, 053852 (2013).

[92] S. Coen and M. Erkintalo, Opt. Lett. **38**, 1790 (2013).

[93] P. Parra-Rivas, D. Gomila, M. A. Matías, P. Colet, and L. Gelens, Opt. Express **22**, 30943 (2014).

[94] P. Parra-Rivas, D. Gomila, F. Leo, S. Coen, and L. Gelens, Opt. Lett. **39**, 2971 (2014).

[95] D. Gomila, A. J. Scroggie, and W. J. Firth, Physica D **227**, 70 (2007).

[96] C. Godey, I. V. Balakireva, A. Coillet, and Y. K. Chembo, Phys. Rev. A **89**, 063814 (2014).

[97] F. Leo, L. Gelens, P. Emplit, M. Haelterman, and S. Coen, Opt. Express **21**, 9180 (2013).

[98] I. V. Barashenkov and Y. S. Smirnov, Phys. Rev. E **54**, 5707 (1996).

[99] F. Leo, S. Coen, P. Kockaert, S. P. Gorza, P. Emplit, and M. Haelterman, Nat. Photonics **4**, 471 (2010).

[100] A. B. Matsko, A. A. Savchenkov, V. S. Ilchenko, D. Seidel, and L. Maleki, Phys. Rev. A **85**, 023830 (2012).

[101] T. Hansson and S. Wabnitz, J. Opt. Soc. Am. B **32**, 1259 (2015).

[102] C. R. Lourés, D. Faccio, and F. Biancalana, Phys. Rev. Lett. **115**, 193904 (2015).

[103] T. Roger, M. F. Saleh, S. Roy, F. Biancalana, C. Li, and D. Faccio, Phys. Rev. A **88**, 051801 (2013).

[104] M. J. Weber, *Handbook of Optical Materials*, (CRC Press, 2003).

[105] I. S. Aranson and L. Kramer, Rev. Mod. Phys. **74**, 99 (2002).

[106] E. Ding and J. N. Kutz, J. Opt. Soc. Am. B **26**, 2290 (2009).

[107] A. Komarov, H. Leblond, and F. Sanchez, Phys. Rev. E **72**, 025604 (2005).

[108] P. Grelu and N. Akhmediev, Nature Photonics **6**, 84 (2012).

[109] A. Komarov, H. Leblond, and F. Sanchez, Phys. Rev. A **71**, 053809 (2005).

[110] A. Zaviyalov, P. Grelu, and F. Lederer, Opt. Lett. **37**, 175 (2012).

[111] S. M. J. Kelly, K. Smith, K. J. Blow, and N. J. Doran, Opt. Lett. **16**, 1337 (1991).

[112] N. R. Pereira and L. Stenflo, Physics of Fluids **20**, 1733 (1977).

[113] R. J. Deissler, J. Stat. Phys. **54**, 1459 (1989).

[114] J. N. Kutz, SIAM Rev. **48**, 629 (2006).

[115] P. Grelu (editor), *Nonlinear Optical Cavity Dynamics: From Microresonators to Fiber Lasers* (Wiley-VCH, Weinheim, 2016).

[116] V. I. Karpman, Phys. Rev. E **47**, 2073 (1993).

[117] V. I. Karpman, Phys. Lett. A **186**, 303 (1994).

[118] V. I. Karpman, Phys. Lett. A **210**, 77 (1996).

[119] V. I. Karpman, Phys. Lett. A **284**, 238 (2001).

[120] L. V. Wijngaarden, Annual Review of Fluid Mechanics **4**, 369 (1972).

[121] A. R. Osborne and T. L. Burch, Science **208**, 451 (1980).

[122] Y. Nakamura, H. Bailung, and P. K. Shukla, Phys. Rev. Lett. **83**, 1602 (1999).

[123] K. R. Helfrich and J. A. Whitehead, Geophys. Astrophys. Fluid Dynamics **51**, 35 (1990).

[124] V.E. Zakharov and E.A. Kuznetsov, Physica D **18**, 455 (1986).

[125] J. A. Fleck, J. R. Morris, and M. D. Feit, Appl. Phys. **10**, 129 (1976).

[126] G. M. Muslu and H. A. Erbay, Mathematics and Computers in Simulation **67**, 581 (2005).

[127] H. A. Luther and H. P. Konen, SIAM Review **7**, 551 (1965).

[128] S. Linden, J. Kuhl, and H. Giessen, Opt. Lett. **24**, 569 (1999).